University of Granada
Faculty of Sciences
Department of Optics

Application of Optical Methods for the Evaluation of Human Tissues Generated by Tissue Engineering

PhD Thesis

Ana-Maria-Andreea Ionescu
Bachelor's Degree in Physics
Master in Advanced Methods and Techniques in Physics

Granada, 2013

Editor: Editorial de la Universidad de Granada
Autor: Ana Maria Andreea Ionescu
D.L.: GR 1889-2013
ISBN: 978-84-9028-590-9

Editor: Editorial de la Universidad de Granada
Autor: Julia Molero Jurado
D.L.: En trámite
ISBN: En trámite

Universidad de Granada
Facultad de Ciencias
Departamento de Óptica

Aplicación de Métodos Ópticos para la Evaluación de Tejidos Humanos Generados mediante Ingeniería Tisular

Tesis Doctoral

Ana-Maria-Andreea Ionescu
Licenciada en Física
Máster en Métodos y Técnicas Avanzadas en Física

Granada, 2013

Universidad de Granada
Facultad de Ciencias
Departamento de Óptica

Application of Optical Methods for the Evaluation of Human Tissues Generated by Tissue Engineering

Memoria que presenta la Licenciada en Física
y Máster en Métodos y Técnicas Avanzadas en Física
Ana-Maria-Andreea Ionescu
para aspirar al título de Doctor Internacional.

Fdo.: Ana-Maria-Andreea Ionescu

Universidad de Granada
Facultad de Ciencias
Departamento de Óptica

Application of Optical Methods for the Evaluation of Human Tissues Generated by Tissue Engineering

Los doctores María del Mar Pérez Gómez, Catedrática de Escuela Universitaria y Enrique Hita Villaverde, Catedrático de Universidad, ambos pertenecientes al Departamento de Óptica de la Universidad de Granada, y Miguel Alaminos Mingorance, Profesor Titular de Universidad y perteneciente al Departamento de Histología de la Universidad de Granada.

Certifican:

Que el trabajo de investigación que recoge esta Memoria de Tesis Doctoral, titulada **"Application of Optical Methods for the Evaluation of Human Tissues Generated by Tissue Engineering"**, presentada por la Licenciada en Física y Máster en Métodos y Técnicas Avanzadas en Física Dña. Ana-Maria-Andreea Ionescu, ha sido realizada bajo nuestra dirección en el Departamento de Óptica y el Departamento de Histología de la Universidad de Granada.

Vº Bº La Directora de Tesis	**Vº Bº El Director de Tesis**	**Vº Bº El Director de Tesis**
Fdo. Dr. María del Mar Pérez Gómez *Catedrática de Escuela Universitaria* *Departamento de Óptica* *Universidad de Granada*	***Fdo. Dr. Miguel Alaminos Mingorance*** *Titular de Universidad* *Departamento de Histología* *Universidad de Granada*	***Fdo. Dr. Enrique Hita Villaverde*** *Catedrático de Universidad* *Departamento de Óptica* *Universidad de Granada*

Universidad de Granada
Facultad de Ciencias
Departamento de Óptica

Application of Optical Methods for the Evaluation of Human Tissues Generated by Tissue Engineering

La doctoranda Ana Maria Andreea Ionescu y los directores de la tesis María del Mar Pérez Gómez, Miguel Alaminos Mingorance y Enrique Hita Villaverde, garantizamos, al firmar esta tesis doctoral, que el trabajo ha sido realizado por la doctoranda bajo la dirección de los directores de la tesis y hasta donde nuestro conocimiento alcanza, en la realización del trabajo, se han respetado los derechos de otros autores a ser citados, cuando se han utilizado sus resultados o publicaciones.

Granada, 13.02.2013

Directores de la Tesis:

María del Mar Pérez Gómez

Miguel Alaminos Mingorance

Enrique Hita Villaverde

Doctoranda:

Ana Maria Andreea Ionescu

Bunicilor mei,

Familiei mele,

“I wouldn't have missed a single minute of it,

Not for the whole world.”

(Stephen King)

AGRADECIMIENTOS

Al Ministerio de Ciencia e Innovación de España por ayudarme a concluir mis estudios académicos de posgrado por medio de la concesión, por un periodo de cuatro años, de la Beca de Formación del Profesorado Universitario (FPU).

A la Dra. Maria del Mar Pérez Gómez, directora de esta tesis, por toda su ayuda y sabios consejos. Le agradezco que me haya abierto hace ya cinco años las puertas de su grupo de investigación, dándome la oportunidad de tener una visión más amplia del mundo de la investigación y descubrir cuánto me motiva. Agradezco también a los otros dos directores, el Dr Miguel Alaminos Mingorance por introducirme en el mundo maravilloso de la biología y ayudarme a entenderlo y Dr.Enrique Hita Villaverde, por su disponibilidad, apoyo y colaboración en este trabajo.

A los directores del Departamento de Optica, Manolo Rubiño y Rosario Gonzalez por permitirme hacer parte de su grupo, sentirme una compañera más durante todo el desarrollo de esta Tesis y, no por último, permitirme utilizar las instalaciones del Departamento.

A todos los miembros del Departamento de Optica por su amistad y buen trato.

A Ana Yebra y María José Rivas por su apoyo, amistad y cariño.

Nuevamente, y de manera muy especial, a María del Mar, porque además de directora de esta Tesis, ha sido también mi amiga, confidente, y a veces, incluso madre. Por abrirme la puerta de su casa y compartir tantos momentos inolvidables, siempre alrededor de una buena comida internacional.

A mis compañeros y, antes de todo, amigos, Juancho, Oscar y Laura, por todo el ánimo, toda la paciencia, por confiar y creer en mí, por ser como unos hermanos y sobre todo por su valiosa amistad. A Juancho, por brindarme su apoyo, ánimo y colaboración en todo momento y sobre todo cuando más necesitaba de ellos, sin poner nunca peros o darme negativas, sino todo lo contrario. A Oscar por

provocarme a descubrir la cocinera que llevo dentro, por compartir conmigo los secretos de la extraordinaria cocina peruana, por animarme a viajar y despertar en mi la curiosidad de descubrir nuevos lugares ("a la aventura chico!!!"). A Laura por ser una verdadera amiga con la que comparto secretos "de chicas", por dejarme hacer parte de su familia y por brindarme mi primer "sobrinito".

A Luis Javier por ser un buen amigo y por ayudarme a entender que la informática te puede hacer la vida mucho más fácil una vez aprendido su idioma.

A Monica por ser una bellísima persona, por toda su amistad, cariño y apoyo.

A Luis por haber compartido tanto tiempo el laboratorio 126 y haberme enseñado que un color verdoso del aceite de oliva no significa un aceite mejor.

A mis compañeros del Departamento de Histologia, Ingrid, Miguel 'chico', Ana Celeste y Giuseppe por ayudarme con la preparación de las muestras utilizadas en esta Tesis, por introducirme en el maravilloso mundo de las células, por su amistad y apoyo.

Al Dr. Juan de Díos García López Durán del Departamento de Física Aplicada por su ayuda con las medidas reológicas utilizadas en esta Tesis, por su colaboración y disponibilidad.

To professor Scott Prahl from the University of Oregon, USA for helping me with the experimental setup used in this Thesis and for sharing his valuable knowledge and expertise during the time he spent with us in Granada. To Anne, his wife, for being such a beautiful and kind person, always with a smile on her face, for her friendship and care.

To professor Che Connon for receiving me in his Laboratory in Reading, UK , but most importantly, for making me feel like another member of his group. For his unconditional support, good advices, constant intellectual challenges and for helping me to professionally develop.

To James for sharing his time and knowledge with me, and of course, for his unbelievably efficient "Tissue culture short course". To Roanne and Ricardo for their friendship and support during my stage in Reading. To, Chris, Vasco, and

Steve for making from my stay in Reading such a great experience. To all of them, for converting Reading into a place worth returning to.

Doamnei profesoare Gabriela Iacobescu, pentru sprijinul necondiționat în aventura academicã întreprinsã departe de casã, pentru cuvintele de încurajare şi prietenia oferite.

Anei pentru cã a fost punctul meu de sprijin din prima zi în care am ajuns în Granada şi de atunci, de forma continua e incondicional, m-a ajutat mereu, gata oricând sã îmi dea un sfat atunci când lo necesitaba; por ser una muy buena amiga y por aguantarme en los últimos instantes de la redacción de esta Tesis.

A mis amigos de Dilar, Edi, Mariluz, Jesus, David y Mariluz, por hacerme sentir como en casa, por permitirme hacer parte de su familia y compartir tantos momentos agradables.

Familiei Ghinea, pentru sprijinul şi dragostea acordate pe întreaga duratã a realizãrii acestei Teze Doctorale.

Familiei mele, mami şi tati, pentru dragostea imensã, încrederea şi sprijinul oferite necondiționat, pentru educația oferitã, pentru cã m-au fãcut sã simt cã întotdeauna voi avea pe cineva care sã fie alãturi de mine indiferent de deciziile luate, bune sau rele.

Surioarei mele Ozzy pentru cã indiferent de situație, şi oricât de mare este distanța dintre noi, e mereu lângã mine, pentru cã are grijã de cei de acasã, pentru cã mã iubeşte emorm, mã înțelege şi crede în mine. Lui Octav, pentru cã are grijã de 'mi hermanita', pentru sprijinul şi increderea acordate, pentru cã ştiu cã pot conta oricând pe el. Amândurora pentru cã împreunã ne vom împlini visul vieților noastre.

Ție, prietenului meu cel mai bun, confidentul meu, celui care mã acceptã aşa cum sunt, cu bune şi cu rele, care îmi oferã o iubire nesfârşitã şi alãturi de care mã simt şi mã voi simți mereu respectatã, protejatã şi fericitã. Pentru cã împreuna am început o aventurã personalã şi profesionalã care nu se poate termina decât cât se poate de bine. Lucrarea aceasta e atât a mea cât şi a ta pentru cã datoritã

ție sunt ceea ce sunt azi. Răzvan, îți multumesc por estar ahí SIEMPRE que lo necesito y por ser el amor de mi vida.

CONTENTS

LIST OF FIGURES

LIST OF TABLES

ABBREVIATIONS

CC1	*1 minute compressed collagen gel*
CC3	*3 minutes compressed collagen gel*
CTF	*Contrast Transfer Function*
DMEM	*Dulbecco's Modified Eagle Medium*
DSF method	*Direct Summation of Fields method*
DSLR camera	*Digital Single Lens Reflex camera*
ECM	*Extracellular Matrix*
EGF	*Epidermal Growth Factor*
ESCs	*Embryonic Stem Cells*
FCS	*Fetal Calf Serum*
GAGs	*Glucosaminoglycans*
He-Ne	*Helium-Neon*
IAD method	*Inverse Adding-Doublin method*
iad program	*Inverse Adding Doubling program*
IOP	*Intraocular Pressure*
KPros	*Keratoprostheses*
K-W	*Kruscal-Wallis statistical test*
LCD	*Liquid Cristal Display*
LSCs	*Limbel Stem Cells*
MSCs	*Mesenchymal Stem Cells*
M-W	*Mann-Whitney statistical test*
NCCs	*Nanostructured Corneal Constructs*
N-NCCs	*Non Nanostructured Corneal Constructs*
PBS	*Phosphate Buffered Saline*
PGs	*Proteoglycans*
SEM	*Scanning Electron Microscopy*
VAF	*Variance Accounting For*
VLR	*Viscoelastic Linear Region*

Dacă cineva nu a greşit niciodată,

înseamnă că nu a încercat să facă nimic nou.

(Albert Einstein)

1. INTRODUCTION

The knowledge of the histological structure as well as their physical properties is of critical importance for the evaluation of human tissues. In the field of the regenerative medicine, prior to the clinical use of the human tissue generated by tissue engineering, it is essential to determine their fundamental characteristics, as part of the characterization process and quality control. Therefore, Chapter 1 of this Thesis is divided in three sections, each one describing one of the above mentioned of these items.

LIGHT PROPAGATION IN TISSUE

Understanding how ultra-violet, visible and infra-red radiation propagates in biological tissues represents a real need in both diagnostic and therapeutic medicine, due to the increasing use over the past years of these radiations for the development of therapeutic techniques and as well as for the quantitative analysis of diagnostic measurements (Ansari and Mohajerani, 2011; Wilson and Patterson, 2008; Patterson et al., 1991). For example, the local tissue temperature is of prime importance in laser surgery and depends on the spatial distribution of the incident radiation.

Diagnostic methods use fluorescent, scattered or transmitted light to measure parameters such as drug concentration and blood oxygenation. Therefore, detailed information about the propagation of the excitation and observed light is required. The general problem of the light propagation in tissue is represented by a tissue of arbitrary geometry, whose optical properties may be functions of position and time, is irradiated by external and/or internal sources of light. In order to solve this problem, three basic requirements are needed:

(1) a mathematical description of the interaction of optical radiation with tissue;
(2) information about the optical properties of the irradiated tissue (usually provided by experiment) and;
(3) Workable solutions of the mathematical equations to provide sufficiently accurate calculations under circumstances of biomedical interest (Patterson et al., 1991).

Numerous models that predict fluence rates in tissue or reflection and transmission of light by tissue have been developed. The accuracy of these models ultimately depends upon how well the optical properties of the tissue are known. Optical parameters are usually obtained by converting measurements of observables quantities (e.g. reflection) into parameters which characterize light propagation in tissue. The conversion process is based on a particular theory of light transport in tissue (Bashkatov et al., 2011; Cheong et al., 1995).

In past years, many investigators have reported values of the total attenuation coefficient, the effective attenuation coefficient, the effective penetration depth, the absorption and scattering coefficients and the scattering anisotropy factor for a variety of tissues at a variety of light wavelengths. Specifically, Sardar and collaborators performed a comprehensive study on optical properties of ocular tissues, in the visible and near-infrared wavelength spectrum (Yust et al., 2012; Sardar et al., 2009; Sardar et al., 2007). Additionally, the authors present a brief description of the radiative transport equation, which is the basis for all light propagation models and its associated parameters and also show how optical properties can be determined by using different measurements.

Light which enters a tissue can be scattered and absorbed. The optical properties of the tissue are wavelength dependent and, in the next paragraphs, we will consider them time invariant and independent of the light field. In most problems in tissue optics, multiple light scattering is important and any useful theory must account for this (Ansari and Mohajerani, 2011; Patterson et al, 1991).

Multiple scattering electromagnetic theory (Andrews and Philips 2005; Ishimaru, 1978) can be used to describe the propagation of light in tissue. Tissue could be considered as a random medium whose permittivity, $\varepsilon(r)$, fluctuates with position about some mean value ε_1, so that

$$\varepsilon(r) = \varepsilon_1 + \varepsilon_2(r) \qquad (1.1)$$

where $\varepsilon_2(r)$ is a random process whose important characteristics (i.e. variance and correlation length) are known. The statistical behaviour of the electric field can then be described using Maxwell's equations. Although physically appealing, this formalism has not found application in tissue optics due to its complexity, the lack of readily applied solutions and the lack of information about $\varepsilon_2(r)$ (Patterson et al., 1991).

The usual approach is called radiative transfer theory. According to this theory, the radiance $L(r,s)$(Wm^{-2}sr^{-1}) of light at the position r travelling in a direction of the unit vector s is decreased by absorption and scattering but is increased by light that is scattered from s' directions into the direction s. The radiative transport equation which describes this light interaction is

$$s \cdot \nabla L(r,s) = -(\mu_a + \mu_s)L(r,s) + \mu_s \int_{4\pi} p(s,s')L(r,s')d\omega' \qquad (1.2)$$

where μ_a(m^{-1}) is the absorption coefficient and represents the probability per infinitesimal path length that a photon will be absorbed by the tissue, μ_s(m^{-1}) is the scattering and represents the probability per infinitesimal path length that a photon will be scattered by the tissue, μ_t(m^{-1}) is the attenuation coefficient, $d\omega'$ is the differential solid angle in the direction s' and $p(s,s')$ is the phase function. The total attenuation coefficient is

$$\mu_t = \mu_a + \mu_s \qquad (1.3)$$

The phase function describes the angular distribution for a single scattering event. For tractability, the phase function is usually assumed to be a function only of a angle between s and s'. If the integral of the phase function is normalized to equal one, then $p(s,s')$ is the probability density function for scattering from direction s' to direction s,

$$\int_{4\pi} p(s,s')d\omega' = 1 \qquad (1.4)$$

Usually the form of the phase function is not known. In these cases the phase function is characterized by a single parameter g called the average cosine of the phase function g,

$$g = \int_{4\pi} p(s, s')(s \cdot s')d\omega' \qquad (1.5)$$

This parameter is also known as the anisotropy coefficient. It is a measure of the asymmetry of the single scattering pattern. g approaching 1, 0 and -1 describes extremely forward, isotropic, and highly backward scattering, respectively (Cheong, 1995).

Formulation of the transport equation assumes that each scattering particle is sufficiently distant from its neighbours to prevent interactions between successive scattering effects. In theory, these scatterers and absorbers must be uniformly distributed throughout the medium. Fluorescence and polarization events are neglected. Most tissue optics studies considered only steady-state (time independent) transport of light (Ansari and Mohajerani, 2011; Cheong, 1995).

The knowledge of the absorption and scattering coefficients, as well as the phase function, is required for the calculations of light distribution based on the radiative transport equation. To arrive to these parameters, one must first have a solution of the radiative transport equation. Because of the difficulty of solving the transport equation exactly, several approximations have been made regarding the representation of the radiance and/or of the phase function.

Two simple solutions of the transport equation provide the expressions for the unscattered transmission and for asymptotic fluence rate deep in a bulk tissue (far from light sources and boundaries) (Cheong, 1995; Cheong et al, 1990).

Unscattered Transmission. Unscattered light is attenuated exponentially following the Beer's law. For light passing through a slab of tissue with thickness x and having no reflections at the surface, the transmission is given by:

$$T_C = e^{-\mu_t x} \qquad (1.6)$$

where T_C is the unscattered transmission (also named collimated or primary transmission). Therefore, the total attenuation coefficient of a tissue sample can be calculated using:

$$\mu_t = -\frac{1}{x}\ln T_C \qquad (1.7)$$

If measurements of T_C are made when surface reflections are present (e.g. in air) corrections are required for the reflections at all mismatched surfaces. For a tissue sample placed between glass or quartz slides, the collimated beam is reflected at the air-slide, slide-tissue, tissue-slide and slide-air interfaces. If the sample is only a few optical depths thick, multiple internal reflections must be considered. A net reflection coefficient for an air-glass-tissue layer is given by:

$$r = \frac{r_g + r_t - 2r_g r_t}{1 - r_g r_t} \qquad (1.8)$$

where the Fresnel reflections at the air-glass and glass-tissue interfaces are r_g and r_t respectively. The measured transmission T is

$$T = \frac{(1-r)^2}{1 - r^2 T_C^2} T_C \qquad (1.9)$$

This last equation (1.9) is first solved for T_C, before using (1.7) to calculate μ_t.

Asymptotic fluence rate. In tissue regions far from light source and boundaries, the fluence rate (Wm^{-2}) decays exponentially. This is the dominant mode of propagation in an unbounded medium (Garcia de Abajo, 2007; van de Hulst, 1980) and is often called the diffusion mode. The rate of decay is called the effective attenuation coefficient (μ_{eff}) or the diffusion exponent. An expression for this asymptotic fluence rate is

$$\Phi(z) \sim (constant) e^{-\mu_{eff} z} \qquad (1.10)$$

where μ_{eff} refers to the measured rate of decay of the fluence in this diffusion region. The approximate relation for the effective attenuation coefficient in

terms of the absorption, scattering and anisotropy scattering coefficients is described by the diffusion theory.

Diffusion theory. The radiance in (1.2) can be divided into unscattered and scattered components:

$$L(r,s) = L_c(r,s) + L_d(r,s) \qquad (1.11)$$

The unscattered portion (L_c) contains all the light that has not interacted with the tissue and satisfies the Beer's law and transmission equation (1.6). The scattered portion (L_d) contains all the light that has been scattered al least once and can be expressed with an infinite sum of Legendre polynomials. Nevertheless, the diffusion approximation simplifies this sum to the first two terms (an isotropic and a slightly-forward directed term) in order to have a more tractable transport equation (Rogers et al., 2009; Andrews and Philips, 2005; Ishimaru, 1978):

$$(\nabla^2 + \kappa^2)\Phi(r) = -Q_0(r) \qquad (1.12)$$

where $\Phi(r)$ is the total scattered fluence rate given by

$$\Phi(r) = \int_{4\pi} L_d(r,s)d\omega \qquad (1.13)$$

The source term $Q_0(r)$ is generated by scattering of collimated normal irradiation

$$Q_0(r) = -3\mu_s[\mu_a + \mu_s(1-g) + \mu_t g](1-r_s)F_0(r)\exp(-\mu_t z) \qquad (1.14)$$

Here F_0 is the irradiance (Wm^{-2}). When absorption is dominated by scattering, the constant κ in (1.12) is an approximation of the actual measured effective attenuation coefficient μ_{eff}.

$$\kappa^2 = 3\mu_s[\mu_a + (1-g)\mu_s] \qquad (1.15)$$

For diffuse irradiances, Q_0 is typically set to zero because the diffuse incidence is introduced in the boundary conditions. The accuracy of the diffusion equation is affected by the ratio of scattering to absorption, the

scattering anisotropy and the distance from light sources and boundaries (Star, 1989).

The solution of the diffusion equation (1.2) for the total fluence rate in a finite parallel slab is (Andrews and Philips, 2005)

$$\Phi_{total}(z) = a_1 \exp(\kappa z) + a_2 \exp(-\kappa z) + a_3 \exp(-\mu_t z). \qquad (1.16)$$

For a finite slab under plane collimated irradiation, Ishimaru provides values for a_1, a_2, a_3 (Ishimaru, 1978) for matched boundaries. In the case of a semi-infinite slab a_1 must equal zero; values for a_2 and a_3 have been evaluated by Prahl, based on the delta-Eddington approximation, for a uniform collimated irradiance F_0 for matched and mismatched boundary conditions (Prahl, 1988).

In a semi-infinite slab, the dominant term in (1.16) yields the next approximate relation for the measured effective attenuation coefficient

$$\mu_{eff} \approx \kappa \qquad \text{if} \quad \mu_a \ll \mu_s. \qquad (1.17)$$

The accuracy of this relation decreases with decreasing ratios of scattering to absorption and increasing anisotropy and fails completely when absorption dominates scattering.

Cheong (Cheong et al., 1990) gives the following expressions for light flux solutions of the diffusion equation (1.12)

$$F_+(z) = \frac{a_1}{4}[1 - h\kappa]e^{\kappa z} + \frac{a_2}{4}[1 + h\kappa]e^{-\kappa z} + \left\{\frac{a_3}{4}[1 + h\mu_t] + \frac{\mu_s g(1 - r_s)F_0}{2[\mu_a + (1 - g)\mu_s]}\right\} e^{-\mu_t z} \qquad (1.18a)$$

$$F_-(z) = \frac{a_1}{4}[1 + h\kappa]e^{\kappa z} + \frac{a_2}{4}[1 - h\kappa]e^{-\kappa z} + \left\{\frac{a_3}{4}[1 - h\mu_t] - \frac{\mu_s g(1 - r_s)F_0}{2[\mu_a + (1 - g)\mu_s]}\right\} e^{-\mu_t z} \qquad (1.18b)$$

$$F_d(z) = F_+(z) - F_-(z) \qquad (1.18c)$$

$F_+(z)$ and $F_-(z)$ are the forward and backward diffuse fluxes, respectively and $F_d(z)$ is the net scattered flux along the direction of irradiation. The coefficient h is

$$h = 2/3[\mu_a + \mu_s(1-g)] \qquad (1.19)$$

For a semi-infinite slab, both the fluence rate and the fluxes have the same exponential behaviour for large z:

$$F_{\pm}(z) \sim \frac{a_1}{4}[1 \pm h\kappa]e^{-\kappa z} \qquad \text{if} \quad \mu_a \ll \mu_s \qquad (1.20)$$

Consequently, for high scattering biological tissue, interstitial measurements of either fluence rate by isotropic detectors or flux by flat cut fibers placed deep inside the tissue permits evaluation of κ as suggested by (1.16) and (1.20) (Svaasand et al, 1981; Doiron et al., 1983; Preus et al., 1982; Wilson et al., 1986).

Knowing the diffuse reflection (R), total transmission (T_t) and unscattered transmission (T_c) allows the determination of three optical properties: absorption coefficient (μ_a), scattering coefficient (μ_s) and anisotropy coefficient (g). The reflection and transmission of a slab of thickness x with index matched boundaries in the diffusion approximation are given by (Welch and Gardner, 2002; Dam et al., 2000; Prahl, 1988; Jacques and Prahl, 1987; van Gemert et al., 1987):

$$R = -\frac{\mu_s g}{[\mu_a+(1-g)\mu_s} + \frac{h}{2}\{a_1\kappa - a_2\kappa - a_3\kappa\} \qquad (1.21a)$$

$$T = \frac{\mu_s g}{[\mu_a+(1-g)\mu_s]} e^{-\mu_t x} - \{a_1\kappa e^{\kappa x} - a_2\kappa e^{-\kappa x} - a_3\mu_t\kappa e^{-\mu_t x}\} \qquad (1.21b)$$

The total transmission is $T_t = T + T_c$, where T_c is given by (1.6).

However, if only the diffuse reflection and total transmission measurements are available, only absorption (μ_a) and reduced scattering ($\mu'_s = \mu_s(1-g)$) coefficients can be calculated. The anisotropy coefficient has been included in the μ'_s by the similarity relations: $\mu'_a = \mu_a$ and $\mu'_s(1-g') = \mu_s(1-g)$. Anisotropic scattering is reduced to isotropic scattering by setting

$g' = 0$ and so, $\mu'_s = \mu_s(1-g)$ (Teran et al., 2010; Garcia de Abajo, 2007; van de Hulst, 1980; Yoon et al., 1989).

There are some diffusion models that incorporate index mismatched boundaries, scattering anisotropy and tissue layers with varying optical properties, but these models lead to complicated relations for reflection and transmission and the optical properties cannot be expressed directly in terms of reflection and transmission. In order to determine the optical properties, iterative methods must be used in such models.

Table 1 shows some models proposed by different authors for modelling the propagation of laser light in tissue and the optical parameters required by each model.

Table 1.1. Conversion Formulas relating Kubelka-Munk to Transport Coefficient

Author	η	χ or χ′[1]	Restrictions [2]
Klier[3]	$\frac{(1-\varphi)(1-a)}{(1+\varphi)\xi}$	$-\frac{a}{2\xi}\left\{1-\frac{1}{\varphi}\right\}$	*Isotropic scattering*
van Gemert& Star[4]	$\frac{(1-\varphi)(1-a')}{(1+\varphi)\xi}$	$-\frac{a'}{2\xi}\left\{1-\frac{1}{\varphi}\right\}$	*Anisotropic scattering; delta-isotropic phase function*
van Gemert& Star	$\frac{1}{2}+\frac{1}{4}(1-a')$	$\frac{4}{3}+\frac{38}{45}(1-a')$	*Anisotropic scattering; assumes* $\mu_s >> \mu_a$
Meador & Weaver	$\frac{1}{2}+\frac{1}{4}(1-a)$	$\frac{4}{3}+\frac{38}{45}(1-a)$	*Isotropic scattering; Delta-Eddingtonphase function (4 moments)*
Meador & Weaver	$\frac{1}{2}$	$\frac{4}{3}+\frac{20}{45}(1-a)$	*Isotropic scattering; Delta-Eddingtonphase function (2 moments)*
Brinkworth	$\frac{1}{2}$	$\frac{4}{3}+\frac{80}{45}(1-a)$	*Isotropic scattering; Eddingtonphase function*

[1] χ for isotropic and χ' for anisotropic scattering; $a = \mu_s/(\mu_s+\mu_a)$ and $a' = \mu_s(1-g)/[\mu_s(1-g)+\mu_a]$

[2] All formulas assume index matched boundaries

[3] $(\varphi^2-1)/2\varphi = (1+R^2-T^2)/2R$, and $\varphi = [\xi + ln(1-\xi)]/[\xi - ln(1-\xi)]$

[4] $(\varphi^2-1)/2\varphi = (1+R^2-T^2)/2R$, and $\mu_s(1-g)/[\mu_s(1-g)+\mu_a] = [\xi + ln(1-\xi)]/[\xi - ln(1-\xi)]$

In particular, when one-dimensional geometry is a reasonable representation, the adding-doubling method (Liu and Weng, 2006; Riu and Ruprecht, 1996; Prahl, 1995) provides an accurate solution of transport equation for any phase function. It allows modelling of anisotropically scattering, internally reflecting and arbitrarily thick layered media with relatively fact computations (Teran et al., 2010). The adding-doubling approximation is one simple method and it has been successfully used to determine the optical properties of turbid media, such as biological tissues (Yust et al., 2012; Sardar et al., 2009).

The principle of the *adding method*, as first proposed by van de Hulst (1963) is illustrated in Figure 1.1. For a very thin slab, one can write the radiance at the two surfaces from knowledge of the phase function, since the multiple scattering is negligible. If an identical slab is added, the radiance of the final thicker slab can be calculated by considering the successive scattering back and forth between the component layers. Computation for thicker slabs can be carried out by adding other thin layers or, more efficiently, by doubling the total thickness with each iteration.

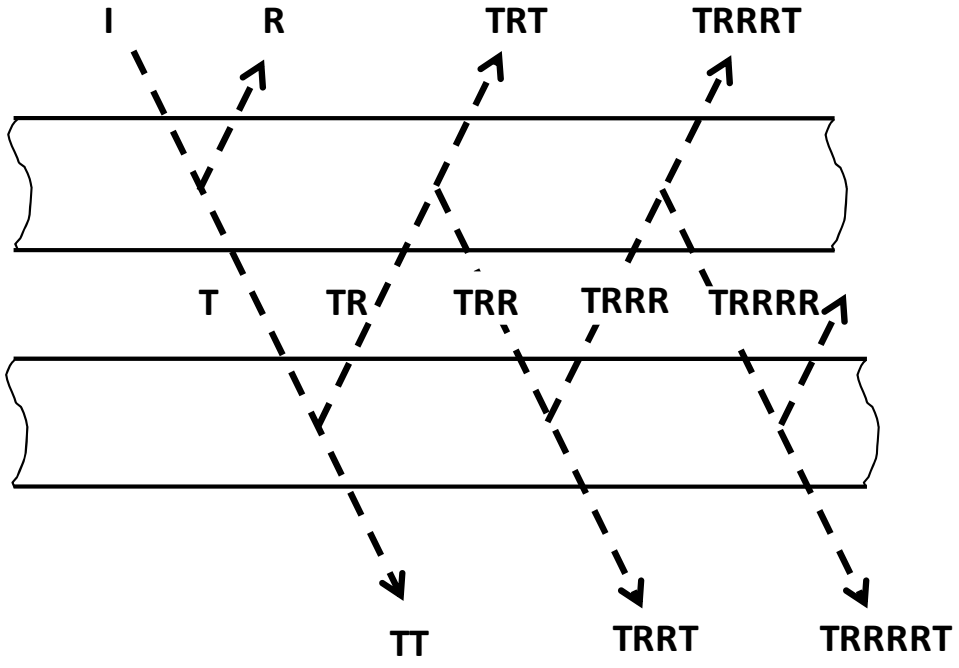

Figure 1.1. Schematic representation of the adding-doubling approximation method

Prahl (Prahl et al., 1993) proposed a method for determining the optical properties of turbid media based on the adding-doubling approximation, called inverse adding-doubling (IAD): inverse implies a reversal of the usual process of calculating reflection and transmission from optical properties, and adding-doubling indicates the method used to resolve the radiative transport equation. The adding-doubling method is sufficiently fast that iterated solutions are possible on current microcomputers and sufficiently flexible that anisotropic scattering and internal reflection at boundaries may be included (Madsen and Wilson, 2013). Complete details of the IAD method will be described in Chapter 5.

Nevertheless, there are also other solutions for the radiative transfer equation which are not direct solutions. Among them, numerical evaluations and particle simulations are of great interest. While numerical integration could be used to evaluate the scattering integral in the radiative transfer equation (1.2), particle simulations represent the great majority of *Monte Carlo applications* in radiative transfer. The term "Monte Carlo method" refers to both numerical evaluations and particle simulations based on random sampling from appropriate probability distributions (Kienle and Patterson, 1996; Patterson et al., 1991), but, in the further discussion only particle simulations will be considered when describing the Monte Carlo applications.

In the simplest algorithm, photons are injected into the medium one-by-one and their history is traced until they are either absorbed or permanently scattered out of the region of interest. Parameters such as injection position, path-length between interactions and scattering angle are randomly sampled from probability distributions based on the known physics of the problem. Quantities of interest, such as absorbed energy are scored at desired locations. The data required (for example μ_a, μ_s, g) are identical to those required for solution of the radiative transfer equation (Patterson et al., 1991).

The Monte Carlo particle simulation displays a simple concept and allows direct handling of complex geometries and optical inhomogeneities. A limiting consideration is that the accuracy of scored quantities increases only with the square root of the number of photon histories. This fact makes the Monte Carlo particle simulation a computationally expensive method. However, this technique is finding increased application as computing power becomes more cheaply available. Various authors have applied it to tissue optics (Tuchin, 2007; Palmer and Ramajuan, 2006; Palmer et al., 2006; Marchesini et al., 1994).

Techniques to improve the accuracy of Monte Carlo simulations, known as variance reduction methods have been developed. One very useful method, particularly applicable to situations where scatter dominates absorption, is survival weighting. In this method, simulated photons are never totally absorbed but rather are transported through the medium with an associated weight, as shown in Figure 1.2a. At each interaction, the fraction μ_a/μ_t of a photon's weight represents deposited energy, while the remaining fraction, μ_s/μ_t, is the factor by which the photon's weight is reduced (Patterson et al., 1991).

Two other common variance reduction techniques are splitting and Russian roulette. Splitting involves increased sampling in regions or directions that are likely to contribute to scoring, while roulette involves decreased sampling for unfavourable photons, such as those that are poorly located, directed or have a very low weight. In the splitting technique, a favourably located or directed photon is split into n 'sub-photons', each of weight n^{-1}, thereby increasing the number of trajectories while conserving total photon weight. Likewise, Russian roulette involves random sampling that terminates an unfavourable photon with a probability $1 - n$ $(0 < n < 1)$, so that the photon survival probability of n is accompanied by a compensating weight increase factor of n^{-1}. A simulation involving splitting and roulette is shown in Figure 1.2b (Kienle and Patterson, 1996; Patterson et al., 1991).

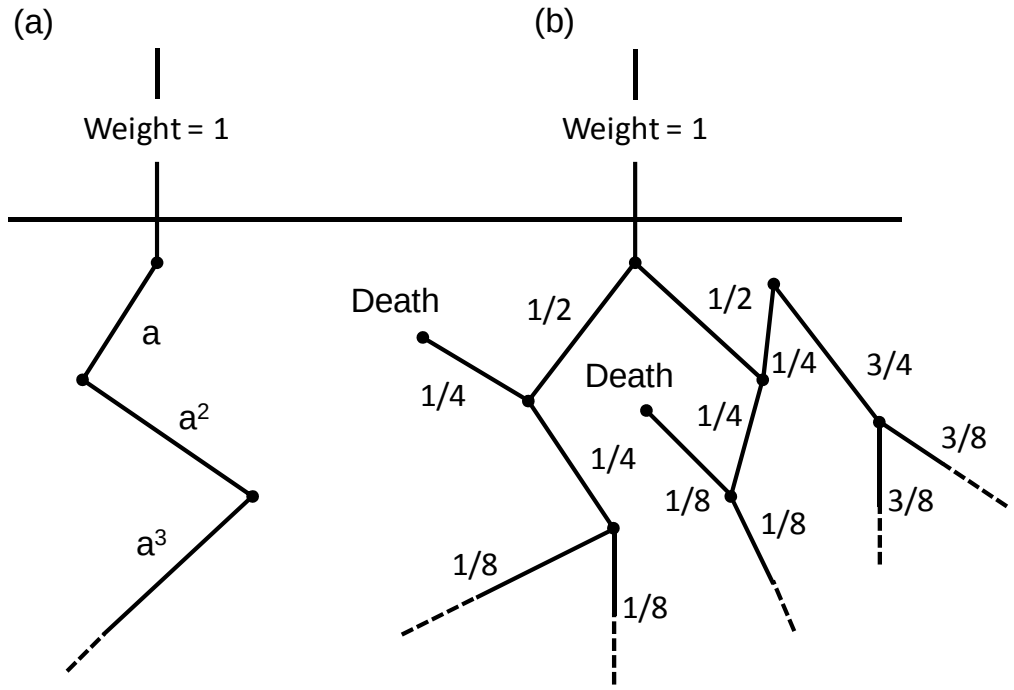

Figure 1.2. Schematic representation of variance reduction techniques used in Monte Carlo particle transport simulation. (a) Survival weighting with factor $\alpha = \mu_s/\mu_t$. b) Splitting of forward directed photons with parameter n_{split}=2, and rouletting of reverse directed photons with parameter $n_{roulette}$=1/3. Note that only one in three reverse directed photons survives but that its weight is tripled.

While other variance reduction methods exist, the above methods are simple and effective to use in order to reduce computation time.

In this first sub-chapter, we have described the light propagation in biological tissue in which the optical properties do not depend on the local electromagnetic field and the effects of multiple scattering are important. These particular conditions apply to many important uses of light in medicine (Ansari and Mohajerani, 2011). Although a mathematical description to this situation in terms of Maxwell's equation is theoretically possible, ultimately, it is the radiation transfer theory, the formalism used to describe all the experimental results. This theory formulates an equation in terms of absorption and differential scattering coefficients.

However, the only method capable of dealing with 3D geometries (such as biological tissues geometries) is the Monte Carlo simulation. It is a conceptually simple method that requires substantial computer resources for precise calculations. Nowadays, these resources are becoming more and more available and tissue optics is following the trend seen in other fields of radiation physics, where the simulation studies are prevalent. Nonetheless, as stated before, in order to calculate the light field in tissue, information about the optical properties of the irradiated tissue is required.

In the second section of this Chapter, we will describe the main optical properties of biological tissues and some of the methods used to measure them.

OPTICAL PROPERTIES OF TISSUE

The main processes that light suffers when travelling throughout a tissue are absorption and scattering.

Absorption. The overall effect of absorption is a reduction in the intensity of the light beam traversing the medium. A relationship between the absorption of light in a purely absorbing medium and the thickness of the medium was first determined in 1729 by Bouguer (1729). Some years later Lambert (1760) derived the following mathematical expression for the relationship, known as the Lambert-Bouguer law

$$\frac{dI}{I} = \mu_a dx \qquad (1.22)$$

which describes how each successive layer dx of the medium absorbs the same fraction dI/I of the incident intensity I for a constant μ_a, the latter known as the absorption coefficient with units of inverse length (usually mm^{-1}). For an incident intensity I_0, therefore, the transmitted intensity I through a distance x will be

$$I = I_0 e^{-\mu_a x} \qquad (1.23)$$

The absorption coefficient μ_a can thus be interpreted as the probability that a photon will be absorbed by the medium per unit length. The reciprocal of the absorption coefficient, known as the absorption length, is the distance required for the intensity of the beam to fall to $1/e$ of the initial intensity. When (1.23) is expressed in base 10 logarithms

$$I = I_0 10^{-Kx} \qquad (1.24)$$

then the constant K is known as the extinction coefficient. The absorbance of the medium is defined as the log_{10} ratio of the incident and transmitted intensities

$$A = log_{10}\left(\frac{I_0}{I}\right) = Kx \qquad (1.25)$$

where the unit of absorbance is the 'optical density' (OD).

In 1852, Beer determined that the absorption coefficient of a compound is linearly related to its concentration c diluted in a non-absorbing medium (Beer, 1852)

$$\mu_a = \alpha c \qquad (1.26)$$

where α is known as the specific absorption coefficient. Substituting for μ_a in the Lambert-Bouguer law gives what is known as the Lambert-Beer law

$$I = I_0 e^{-\alpha c x} \qquad (1.27)$$

Expressing the Lambert-Beer law in log_{10} gives

$$I = I_0 10^{-\varepsilon c x} \qquad (1.28)$$

where ε is the specific extinction coefficient. In a solution containing a mixture of n absorbing compounds, the total absorbance is the sum of the individual extinction coefficients multiplied by the distance x

$$A = (K_1 + K_2 + \cdots + K_n)x = (\varepsilon_1 c_1 + \varepsilon_2 c_2 + \cdots + \varepsilon_n c_n)x \qquad (1.29)$$

The Lambert-Beer law is only valid under certain limited conditions: the light entering the medium must be monochromatic and perfectly collimated, and the medium itself must be purely and uniformly absorbing. Therefore, certain errors will arise when applying the law to practical measurements, since, for example, even lasers are not perfectly monochromatic, and also biological media are not uniformly absorbing media (Hollis, 2002).

In biological tissues, there are many compounds which absorb light radiation such as proteins, haemoglobin, melanin etc. It is worth noting that it is expected that in the ultraviolet region of the wavelength spectrum, μ_a would be very large due to the high UV absorption characteristics of many biomolecules such as proteins and nucleic acids. As the wavelength increases, this absorption falls off and absorption due to specific chromophores such as haemoglobin, myoglobin, bilirubin and melanin dominates. Therefore, large differences in μ_a among different tissues are expected in this wavelength range as their chromophores content will vary considerably. For wavelengths higher than 1000nm, infrared absorption by water becomes the dominant mechanism and it is probable that the absorption coefficient of most tissues would be largely water-like. For reference, the absorption spectra of melanin, haemoglobin and water are shown in Figure 1.3.

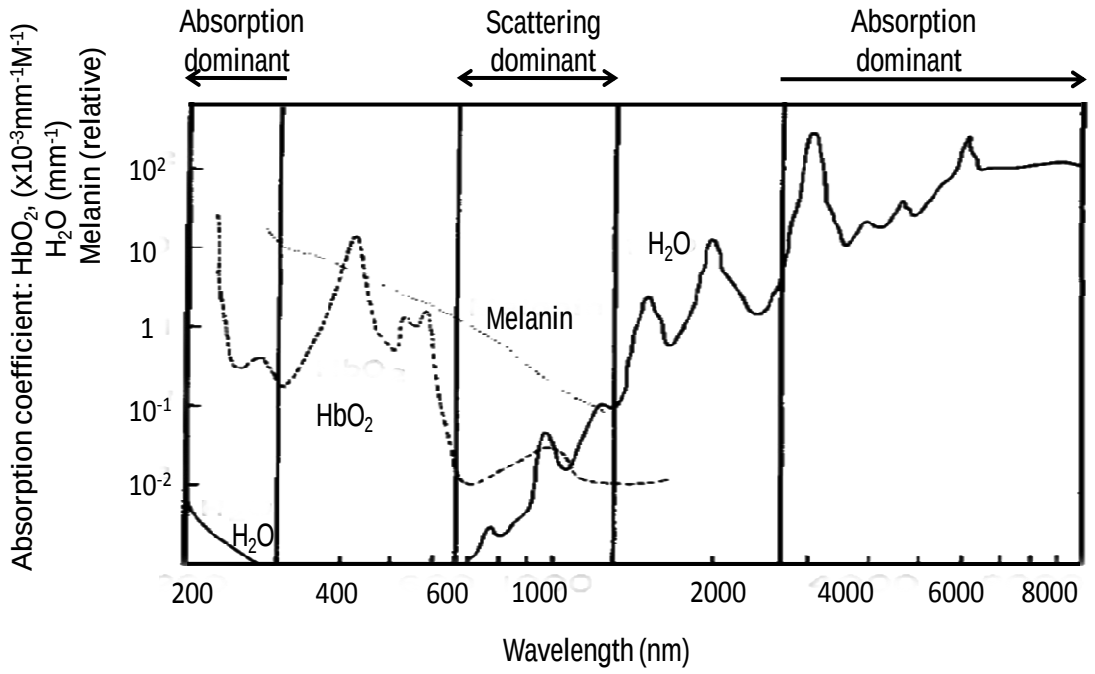

Figure 1.3. The absorption spectra of water, oxyhaemoglobin and melanin (after Boulnois (1986) and Hale and Querry (1973)). Also shown are approximate boundaries of regions where absorption is dominant or scattering is dominant for light propagation in soft tissue (Patterson et al., 1991)

Scattering. Elastic scattering of light occurs when charged particles in a medium are set into oscillatory motion by the electric field of the incident wave, and re-emit (as opposed to absorb) light of the same frequency as the primary wave. Scattering occurs at non-resonance frequencies, hence the scattered intensities are relatively weak, since the forced vibrational amplitudes of the particles are much smaller than those at natural resonances. In most solids and liquids, however, intermolecular interactions broaden the absorption frequencies such that both scattering and absorption of light occur at all wavelengths. As a result of scattering, the velocity of light in all matter is less than it is *in vacuo*. In an optically dense or homogeneous medium, i.e. one in which the molecular separation is much smaller than the wavelength of the incident light, individual atoms or molecules in a medium will scatter the incident radiation in all directions. The phase difference of the scattered light relative to the primary wave will depend on the frequency of the primary wave. In any direction the total scattered field is then a superposition of all the scattered wavelets propagating in that direction. The scattered waves will interfere with the incident wave, modifying its phase and hence the velocity of the light through the medium.

The refractive index of a medium is given by

$$n = \frac{c}{v} \qquad (1.30)$$

where c is the speed of light *in vacuo* and v the speed of light in the medium.

The refractive index depends on the number of molecules per unit volume and their polarisability, since the total scattered wave that interferes with the incident wave depends on the amplitudes of, and phase relations between, the individual scattered wavelets. Furthermore, the refractive index for a given medium changes with the frequency of the incident light. This phenomenon is known as dispersion and is due in part to the frequency-dependence of the relative phase change between the incident and scattered waves. Theory has shown, however, that to explain dispersion in real media

over a broad spectrum, including the resonance frequencies, the absorption of light must also be considered. Thus, the complex refractive index is defined as

$$N = n + ik \qquad (1.31)$$

where the real part, n, as defined in (1.31), determines the speed of the wave and the imaginary part, k, determines the absorption of the wave as it propagates through the medium. From Maxwell's equations k can be related to the absorption coefficient, as follows

$$k = \frac{\mu_a \lambda}{4\pi} \qquad (1.32)$$

where λ is the wavelength of the incident light.

Scattering of light in tissue is caused by the size and shape of the tissue constituents (cells, fibers) and their refractive indices. The scattering arises due to a relative refractive index mismatch at the boundaries between two such structures, e.g. between the extracellular fluid and the cell membrane.

In particular, the refractive index of the fibrils, the refractive index of the extrafibrillar material, and the ratio of these two refractive indices, all play a major role in determining the extent of light scattered by the tissue.

The simplest model considers that all tissue components have a uniform refractive index. This essentially means that light cannot distinguish between fibrils and the material between them, hence it can propagate directly through the tissue unscattered. This model is generally rejected, partly because it fails to explain two important properties of tissues, such as birefringence and, in some cases, transparency loss when the structure is distorted. Also, recent X-ray diffraction data have unambiguously confirmed earlier evidence for a difference in the refractive indices of the fibrils and of the extrafibrillar material. Most modern models are based on the lattice theory put forward by Maurice (Maurice, 1957). By approximating the fibril to perfect, infinitely long cylinders, an estimate of the scattering from an individual fibril can be calculated. The refractive index difference between the

fibrils and interfibrillar matrix means that each fibril scatters a small amount of light. However, if the fibrils are packed in a lattice arrangement, correlation in their relative positions leads to destructive interference of light scattered away from the forward direction, all the light energy going into the constructive interference in the forward direction. The Direct Summation of Fields (DSF) method has been used to predict transmission by an arbitrary short range order distribution of different-sized fibrils. It is a statistical technique in which the scattering from each individual fibril is computed, and the effects of interference are included and summed for the whole tissue using a method called ensemble averaging (Meek et al.,2003) The DSF method has been tested and found to give reliable results in a number of situations (Rawe et al., 1997; Leonard DW, 1996; Freund et al., 1991). It has been demonstrated that light scattering in tissues will increase if: (1) order in the spatial arrangement of the fibrils is destroyed; (2) fibril diameters increase; (3). fibril number density increases; (4) there is an increased refractive index imbalance between the hydrated fibrils and the extrafibrillar matrix; (5) tissue thickness increases. (Meek et al., 2003)

As mentioned before, beside fibrils the tissue consists also of cells, which play an important part in the scattering of the incident light on tissue. The cells vary greatly in size, from blood platelets of approximately 4 μm to nerve cells as much as a metre in length. Figure 1.4 shows a 'generalised' cell (Marieb, 1995), i.e. it represents the basic components found in many human cells, but no cell type in particular. However, all cells consist of three main components: the cell membrane, the cytoplasm and the nucleus. The cell membrane, which constitutes the outer boundary of the cell, is made up of a phospholipid bilayer, approximately 8nm in thickness, with numerous proteins embedded in it. The cytoplasm is the intracellular 'matrix' held within the bounds of the cell membrane. It consists of the cytosol, a water-based fluid within which the other constituents are suspended, the organelles, each of which have a special function in the cell mechanism, and non-functioning units known as inclusions, which include lipid droplets in fat cells and melanin granules in certain skin cells. Cells receive their energy

supply from organelles called mitochondria, the number of which reflects a cell's need for energy. The mitochondria, approximately 1-4 μm by 0.3-0.5 μm in size (Palade, 1972), are surrounded by a double layer of membrane similar to the outer cell membrane. The nucleus is the largest organelle in the cell and constitutes its control centre. The size of the nucleus varies with cell type, with an average diameter in the order of 5 μm (Marieb, 1995). The nucleus, like the mitochondria, is surrounded by a double-layered phospholipid membrane.

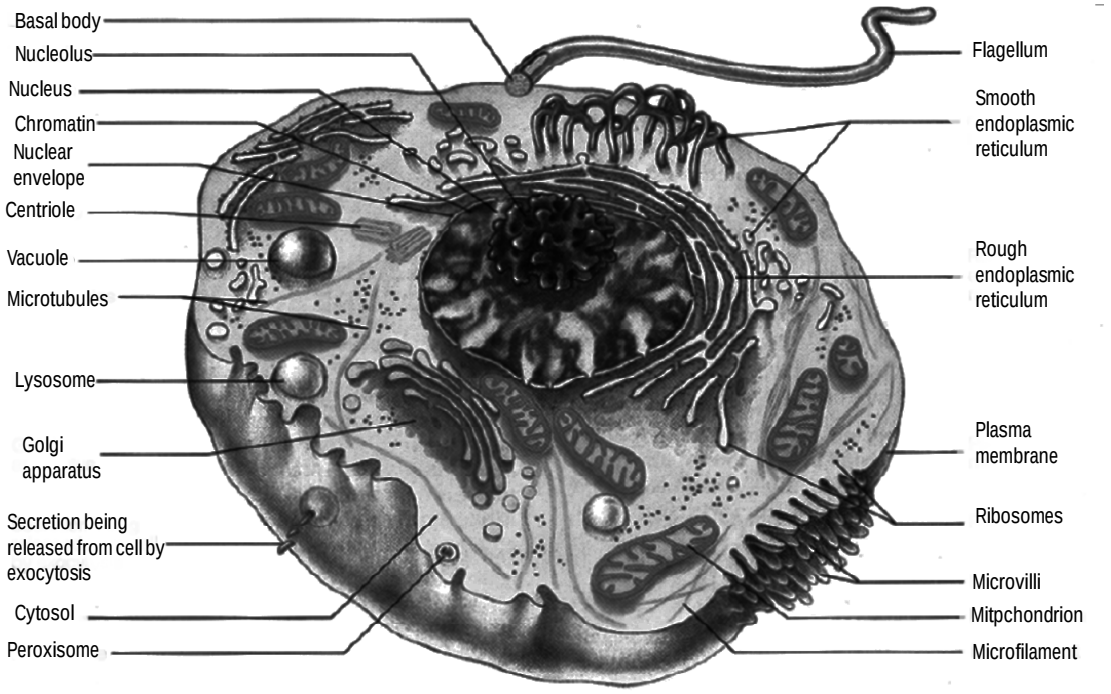

Figure 1.4. A 'generalised' human cell. (Marieb, 1995)

In order to understand how light is scattered in tissue it is helpful to study the structures responsible for scattering on a microscopic, i.e. cellular or sub-cellular, level. Each microscopic scattering particle or object will give rise to its own scattering phase function, which depends on the physical properties of the object. A single scattering event in tissue can be considered to arise from an 'averaged scattering object', representing a distribution of scattering objects with an averaged phase function. The contribution of each type of object to the averaged scattering properties in tissue will depend on their individual scattering properties and their relative concentrations.

Mourant et al (1998) studied suspensions of mammalian cells in order to determine the dominant scattering centres in tissue. Comparing their measurements of the transport scattering coefficient μ_s and the anisotropy factor g with predictions from Mie theory, they determined that the observed scattering was due to particles with a distribution of sizes, equivalent to spheres with diameters ranging from about 0.2 to at least 1μm. They also measured the phase functions of isolated cell nuclei and mitochondria and compared them to the phase function measured for the cells. The authors concluded that the majority of light scattering from a cell at small angles is due to the nucleus, the smaller organelles such as the mitochondria being responsible for scattering at larger angles. In another study, Mourant et al. (2000) determined that approximately 55% of scattering from cells at angles greater than 40º was due to the internal cellular structures. By comparing scattering from cells and nuclei at different growth phases they concluded that the nucleus and its sub-structures are responsible for a maximum of approximately 40% of the scattering at any angle and that, as confirmed by the known change in mitochondrial content with growth phase, other organelles in the cytoplasm must also contribute significantly to the observed high-angle scatter.

In the previous sections we have discussed the physical basis for the absorption and scattering of light radiation, and the components of biological tissue responsible for these. The theories discussed in Section "Light propagation in tissue" can describe light propagation by both large and small particles (relative to the wavelength of the illuminating light) assuming a small enough collection of particles, or one in which the particles are far enough apart, such that their individual scattered fields do not significantly perturb one other. Also, we have discussed what happens in biological tissue, where the scattering particle density is such that the interaction of scattered waves between neighbouring particles cannot be ignored and multiple scattering can occur. In the next section, we will briefly describe some of the methods used to measure the absorption and scattering properties of biological tissues.

Methods of measurement of optical properties. Many methods have been proposed for the measuring the optical properties of tissue. They can be divided in two categories: *direct* and *indirect* methods. The direct methods use nothing more than the Lambert-Beer's law to find the optical properties. Also in the same category are included unscattered transmission measurements, effective attenuation measurements, and goniophotometric measurements of the single scattering phase function (Fernández-Oliveras et al., 2012; Ansari and Mohajerani, 2011). In the indirect methods, the optical properties are explicitly given in terms of the measured quantities (*noniterative*) or implicitly related to the measured quantities (*iterative*). The last ones are the most cumbersome to use, but the optical model used is more sophisticated than the noniterative methods.

A schematic representation of all the methods that can be used to measure the optical properties of tissues is given in Figure 1.5 (Cheong et al., 1990).

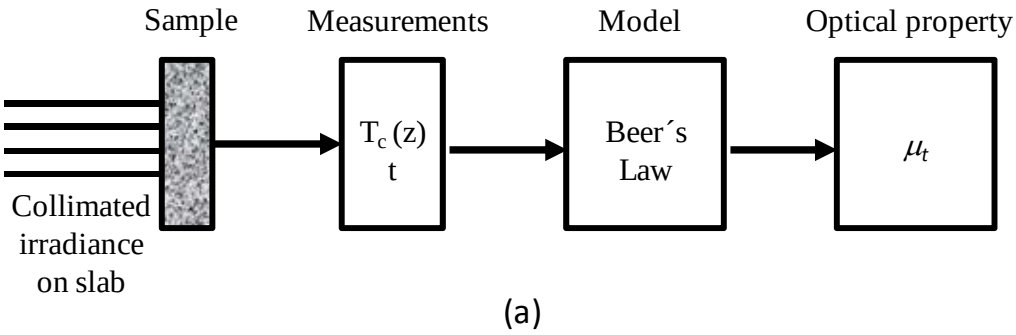

Figure 1.5a. Measured values from the unscattered transmission T_c through a sample of thickness x are analyzed using Beer's law to provide estimates of the total attenuation coefficient (μ_t).

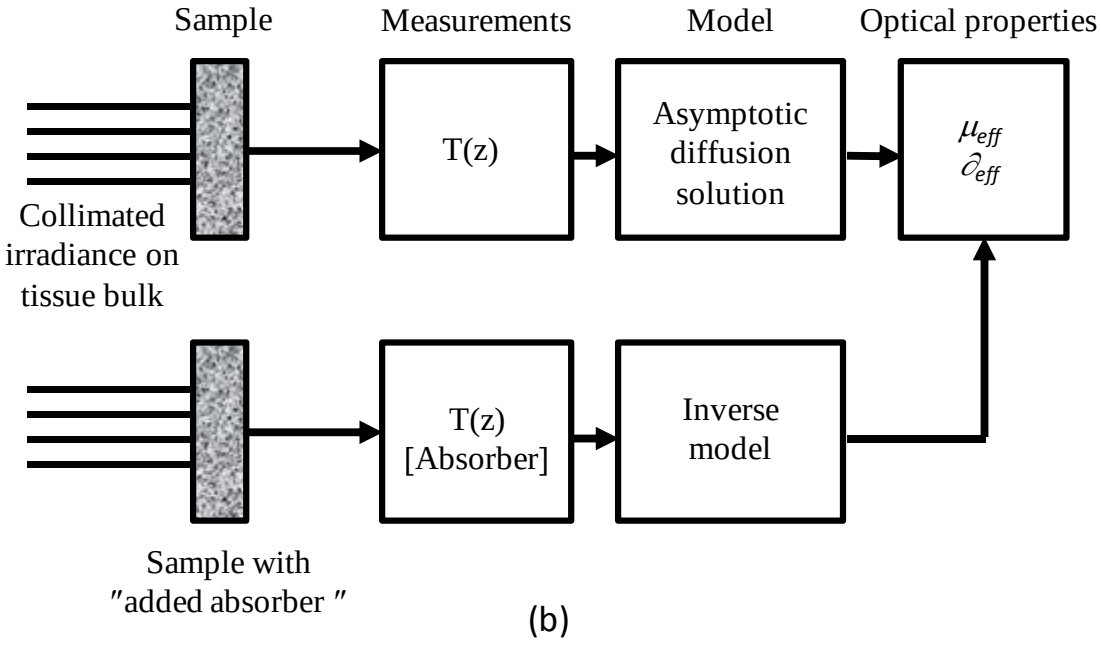

Figure 1.5b. Interstitial measurements of fluence rate (or flux) inside a sample with or without an added absorber yield an estimate of the effective attenuation coefficient (μ_{eff}) or the effective penetration depth ($\partial_{eff} = 1/\mu_{eff}$)

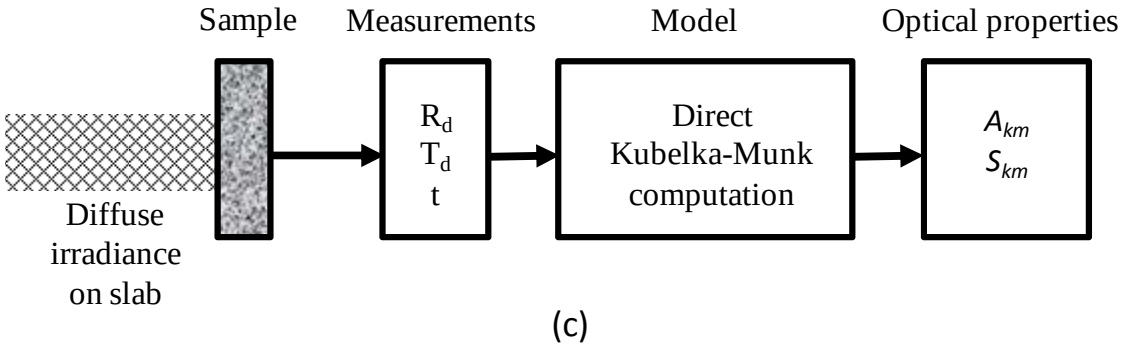

Figure 1.5c. Measurements of diffuse reflection R_d and diffuse transmission T_d and sample thickness x for diffuse irradiance are used in

$$R = \frac{\sinh(S_{KM} yt)}{x\ cosh(S_{KM} yt) + y\ sinh(S_{KM} yt)} \qquad T = \frac{\mathrm{y}}{x\ cosh(S_{KM} yt) + y\ sinh(S_{KM} yt)}$$

to compute Kubelka-Munk absorption $A_{KM}$and scattering S_{KM} coefficients.

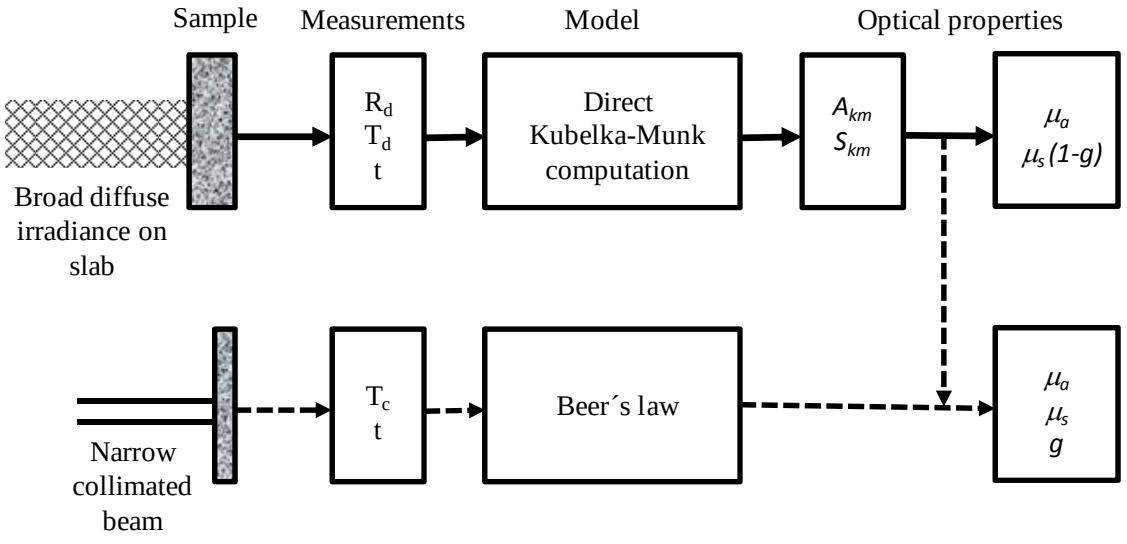

(d)

Figure 1.5d. Measurements of diffuse reflection and transmission for diffuse irradiance lead to Kubelka-Munk coefficients; these are then converted to transport parameters. When collimated transmission is available, μ_a, μ_s and g can be calculated.

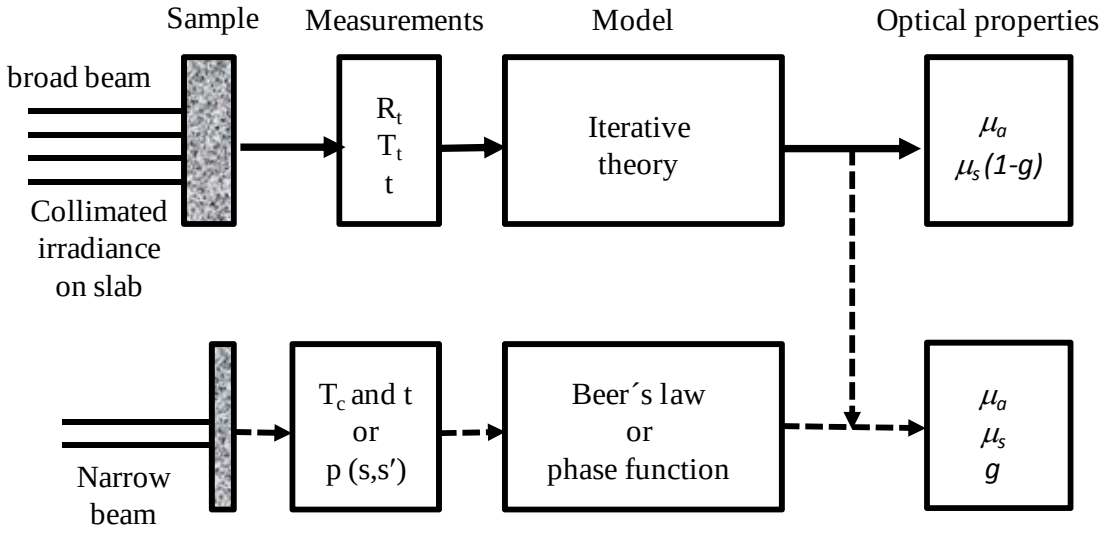

(e)

Figure 1.5e. If only total reflection and transmission are available, the absorption coefficient μ_a and reduced scattering coefficient $\mu_s(1-g)$ can be determined with an iterative light transport model. An additional measurement (collimated transmission or the phase function) permits separate estimation μ_a, μ_s and g

In the present Thesis, we will use the iterative method shown in Figure 1.5e when evaluating the optical properties of native and artificial tissues developed by tissue engineering for corneal and oral mucosa applications. In order to understand the characteristics of these tissues, in the next section we will describe the principles of tissue engineering and the morfo-functional aspects of the native tissue that will be mimicked.

TISSUE ENGINEERING OF HUMAN CORNEA AND ORAL MUCOSA

The term "tissue engineering" is thought to have been officially coined and defined in its modern sense by Robert Nerem in 1988 at the Lake Granlibakken NSF workshop on the topic of engineering tissue (Viola et al., 2003). However, the concept was brought to wide spread attention and formalized in a review paper in Science in 1993 (Langer and Vacanti, 1993) which paraphrased the definition: *Tissue engineering is an interdisciplinary field that applies the principles of engineering and the life sciences toward the development of biological substitutes that restore, maintain or improve tissue function.*

In the subsequent years since the field of tissue engineering was formalized, there has been an enormous scientific effort to produce tissue constructs for clinical use (Vacanti, 2006). The success of the approach has thus been modest in relation to the expenditure of time and resources (Nerem, 2006) with few tissue engineered constructs approved for clinical use (the most successful of these being artificial skin). The myriad limitations of current tissue engineering methods are enumerated by Dr.Vacanti in an article in the journal Tissue Engineering (Vacanti, 2006). Nonetheless, tissue engineering in general does hold great promise and the potential for producing tissue engineered replacements for diseased or injured tissues in the reasonably near term does exist. One of the most engineered tissues is the cornea. This is because corneal tissue is reasonably "simple", thin and avascular (Ko et al., 2007). However, all tissues are extremely complex at some level (in the cornea it is at the level of matrix molecule organization).

The term "engineering" as it relates to tissue engineering. An engineer is defined as "One who contrives, designs, or invents" (first definition, OED second edition 1989). In the sense of this definition, the term "tissue engineering" seems a perfectly reasonable description for what has been attempted in the field since its inception. However, in practice, the gerund "engineering" carries the implication that a particular task can be accomplished given the currently available knowledge base, adequate funding and adequate manpower. Indeed, tissue engineering has the potential to address the transplantation crisis caused by the shortage of donor tissues and organs. It is through the imitation of nature that tissue engineering is able to address the patient need; nevertheless, a number of challenges need to be faced. In a review book on the principles of tissue engineering, Robert Nerem explains these challenges of imitating the nature faced by tissue engineers (Nerem, 2000). He believes that in the area of cell technology, the challenge includes cell sourcing, the manipulation of cell function and the effective use of stem cell technology. Next are those aspects that are part of construct technology, such as the design and engineering of tissue like constructs and the manufacturing technology required to provide off-the-shelf availability to the clinician. Finally, there are the issues concerning the integration of a construct into the living system, with the most critical issue being the engineering of immune acceptance (Nerem, 2000). Only if these issues are overcome, the tissue engineering of the most vital of organs can be addressed and the crisis in transplantation can be confronted.

It is this challenge of imitating nature that has been accepted by those who are providing leadership to this new area of technology called tissue engineering (Nerem and Sambanis, 1995; Langer and Vacanti, 1993). To imitate nature, it is required, in first place, the understanding of the basics of biology of the tissues of interest; with this, methods can be developed for the control of these biologic processes, and finally, based on the ability to control, strategies can be developed either for the engineering of living tissue substitutes or for the fostering of tissue repair or remodelling.

Cell technology. *Cell sourcing*. The starting point for any attempt to engineer a tissue or organ substitute is a consideration of the cells to be employed. Not only a sufficient quantity is needed, but it is has to be ensured that it will be free of pathogens and contamination of any type whatsoever. In addition, the source that will be employed has to be able to provide autologous, allogeneic, or xenogeneic cells. As indicated in Table 1.2, there are both advantages and disadvantages to each of these.

Type	Comments
Autologous	*Patient's own cells; immune acceptable, does not lend itself to off-the-shelf availability*
Allogeneic	*Cells from other human sources; lends itself to off-the-shelf availability, but may require engineering immune acceptance*
Xenogeneic	*From different species; not only requires engineering immune acceptance, but must be concerned with animal virus transmission*

Table 1.2. Cell Source (Nerem, 2000)

Cell function and genetic engineering. Once the cell types to be employed have been selected, the next issue to be addressed relates to the manipulation of the functional characteristics of a cell, so as to achieve the behaviour desired. This can be performed either by manipulating a cell's extracellular environment (e.g. its matrix), the mechanical stresses to which it is exposed, or its biochemical environment, or by manipulating a cell's genetic program. This last possibility can be used together with tissue engineering in a variety of ways that include the alteration of matrix synthesis, inhibition of the immune response, enhancement of non-thrombogenicity, engineering the secretion of specific biologically active

molecules (e.g. a specific insulin secretion rate in response to a specific glucose concentration) or the alteration of cell proliferation (Nerem, 2000).

All these possibilities are related to the creation of a cell-seeded construct that can be implanted as a tissue or organ substitute; nonetheless, the fostering of the repair or remodelling of tissue also represents tissue engineering. In this case, the use of genetic engineering might take the form of gene therapy, such as the introduction of growth factors to foster the repair of bone defects. By using a gene therapy approach to tissue engineering only a transient expression will be required. Because of this, the use of gene therapy as a strategy in tissue engineering may become viable prior to its employment in treating genetically related diseases (Nerem, 2000).

Stem cell technology. To what cell selection is concerned, a considerable interest has been shown in the use of stem cells, the "mother" cells within the body, as a primary source for therapies based on cell and tissue replacement (Solter and Gearhart, 1999). The excitement about stem cells reached a new level when the isolation of the first lines of human embryonic stem cells was reported in two articles in 1998 (November 6, issue of Science). Vogel, in 1999, summarized the types of human stem cells that had been isolated (Table 1.3) (Vogel, 1999). The embryonic stem cells are of most interest. They are pluripotent (capable of differentiating into many cell types), and perhaps are even totipotent (capable of developing into all cell types).

Type	Source/daughter tissue
Embryonic	*Embryo or fetal tissue/ all types*
Hematopoietic	*Adult bone marrow/blood cells*
Neuronal	*Fetal brain/neurons, glia*
Mesenchymal	*Adult bone marrow/muscle, bone, cartilage, tendon*

Table 1.3. Human stem cells that have been isolated (Vogel, 1999)

Laboratory investigations of stem cells in regenerative medicine have determined that, in the case of cornea, the corneal epithelium is derived from an adult stem cell type resident within the cornea. These cells, known as limbal stem cells (LSC's), have been widely investigated for their ex-vivo culture and subsequent transplantation efficacy, with some techniques already enjoying limited clinical application. Thus far however, only preliminary evidence currently exists to suggest that there is a population of adult stem cells which gives rise to stromal keratocytes or to the corneal endothelium. A handful of reports have discussed studies in which non-LSC adult stem cells such as mesenchymal stem cells (MSCs) or embryonic stem cells (ESCs) are being applied to corneal regeneration (McIntosh Ambrose et al., 2010). Another tissue of interest in tissue engineering is the oral mucosa. In this case, investigators from the University of Tel-Aviv, Israel showed that the highly regenerative capacity of the human adult oral mucosa suggests the existence of a robust stem cell population in its lamina propia. These results showed that the lamina propia of adult oral mucosa harbors a primitive stem cell population with a distinct primitive neural-crest like phenotype (Marynka-Kalmani et al., 2010).

It is necessary to understand how a stem cell differentiates into a tissue-specific cell in order to take full advantage of stem cell technology. This requires knowledge not just about the molecular pathways of differentiation, but even more importantly the identification of the combination of signals leading to a stem cell becoming a specific type of differentiated tissue cell.

Construct technology. Construct design and engineering. After selecting the source of stem cells, the next aspect to be considered is the development of a model in which these cells are organized in a three-dimensional architecture and with functional characteristics such that a specific tissue is mimicked. The design and engineering of a tissue-like substitute is a challenge on its own right (Nerem, 2000).

Table 1.4 summarizes the many possible approaches to obtain this tissue-like substitute. The cell-seeded polymeric scaffold is an approach

pioneered by Langer and his collaborators (Langer and Vacanti, 1993, Cima et al., 1991) and considered the classic tissue engineering approach. There is also the approach of a cell-seeded collagen gel pioneered by Bell in the late 1970s and early 1980s (Bell at el., 1979; Weinberg and Bell, 1986) and used mainly for skin substitutes.

Auger proposed an intriguing approach (Heureux et al, 1998; Auger et al., 1995,), referring to it as a cell self-assembly. It involves a layer of cells secreting their own matrix which becomes a sheet after a period of time. First it was developed as part of a skin substitute research but afterwards its use was extended to other applications such as blood vessel by simply rolling up one of these cell self-assembled sheets into a tube.

One important approach in the construct technology is the acelullar approach. Although in tissue engineering the end result should include functional cells, there is also the strategy where the implant is without cells (i.e. acellular) and the cells are then recruited from the recipient or host. One result of this approach is to, in effect, bypass the cell sourcing issue, and replace this with the issue of cell recruitment, i.e., the recruiting of cells from the host in order to populate the construct. Because these are the patient's own cells, there is no need for any engineering of immune acceptance.

Approach	Commets
Acellular matrix	*Recquires the recruitment of host cells*
Cell-seeded collagen gels	*Initially used in a skin substitute; has other potential applications*
Cell-seeded polymeric scaffolds	*Initially used in a skin substitute; has other potential applications*
Cell self-assembly	*Based on the cells synthesizing their own matrix*

Table 1.4. Possible approaches to the engineering of constructs that mimic tissue.

Whatever the approach, in order to achieve any success in the generation of a tissue-like substitute, the engineering of architecture and of functional characteristics that allow a specific tissue to be mimicked is critical. In fact, because of the interrelationship of structure and function in cells and tissues, it would be unlikely to have the appropriate functional characteristics without the appropriate three-dimensional architecture (Nerem, 2000).

Manufacturing technology. Mimicking a specific tissue does not stop with the design and engineering of a tissue-like construct. It should also take into account the manufacturing processes. The main focus in the manufacturing technology has been placed on the bioreactor technology. A bioreactor simply represents a controlled environment – both chemically and mechanically – in which a tissue-like construct can be grown (Nerem, 2000). Although it is generally recognized that a construct, once implanted in the living system will undergo remodelling, it is equally true that the environment of a bioreactor can be tailored to induce the *in vitro* remodelling of a construct so as to enhance characteristics critical to the success achieved following implantation (Seliktar et al., 1998). Thus, the manufacturing process can be used to influence directly the final product and is part of the overall process leading to the imitation of nature.

Integration into the living system. The final issue to be addressed is the incorporation of a tissue engineering product concept into the living system. Here one starts with animal experiments. Despite the fact that a variety of animal models have been developed for the study of different diseases, there is a lack of good animal models for use in the evaluation of a tissue-engineered implant. The existing models are still somewhat unproved, at least in many cases, when it comes to their use in evaluating the success of a tissue-engineered implant (Nerem, 2000).

In addition, there is a significant need for the development of methods to evaluate quantitatively the performance of an implant. This is not only the case for animal studies, but is equally true for human clinical trials. In regard

to this last one, it may not be enough to show efficacy and long term patency, it may also be necessary to demonstrate the mechanism(s) that lead to the implanted tissue substitute's success. Furthermore, it is not just in clinical trials that there is a need for more quantitative tools for assessment: it also would be desirable to have available technologies to assess periodically the continued viability and functionality of a tissue substitute after implantation (Nerem, 2000).

The success of any tissue engineering approach depends also on the immune acceptance and biocompatibility. This comes naturally with the use of autologous cells, but if one moves to non-autologous cell systems, then the challenge of engineering immune acceptance is critical to the achieving success in the imitation of nature.

Tissue engineering has been applied in many medical fields, such as ophthalmology and dentistry in order to overcome the complications raised by tissue transplantation and/or the shortage of donor tissues.

In ophthalmology, the supply of good-quality donor tissue does not meet the demand since more than 10 million people worldwide suffer from vision loss due to corneal damage (disease or injury) whose treatment often is corneal transplantation (Zerbe et al., 2006). Therefore, a cornea substitute as a donor tissue replacement is in urgent demand (Yang et al., 2001; Ma, 2004).

In dentistry, different surgical procedures carried out in the oropharyngeal region frequently result in large tissue defects (Schultze-Mosgau, 2004). Reconstruction of these defects is challenging and oral and maxillofacial surgeons are often confronted with a shortage of oral mucosa to replace the excised tissues (Song et al., 2004). Although it has been demonstrated that primary reconstruction of large oral defects is always more advantageous than secondary reconstructions, primary surgical closure of large oral defects is extremely difficult. In these cases, various types of skin-bearing flaps have been proposed as autologous substitutes of the oral mucosa (Baumann et al., 1996). In some patients, however, the use of skin-bearing

flaps is often associated to complications, such as the presence of adnexal structures causing hair growth on the implanted graft or excessive keratinisation of the reconstructed tissue (Toftet al., 2000). All these disadvantages sometimes cause a significant morbidity and aesthetic and functional limitations for the patients submitted to these techniques. Construction of biological substitutes of the human oral mucosa by tissue engineering could contribute to solve these problems and complications (Sanchez-Quevedo et al., 2007)

As mentioned before, the success of any tissue engineered substitute depends on the proper understanding of the morphological and functional characteristics of the native tissue to be mimicked.

Human cornea.

Corneal anatomy. The cornea is the first ocular tissue that light encounters when entering the eye. It comprises a highly structured membrane bound but relatively acellular, transparent collagenous tissue that joins the more disorganized and opaque sclera at the limbus. The diameter of the human cornea is about 12mm and the average radius of curvature of the central anterior surface is 7.8mm. The cornea is roughly 474µm thick at the centre and 607µm thick in the periphery (Hjortdal, 1996). It is bounded anteriorly by a stratified squamous epithelium and posteriorly by an actively pumping monolayer of non-proliferative cells which are referred to as the corneal endothelium. The main tissue of the cornea is the stromal tissue which comprises 90% of the total thickness where the three principal functions of the cornea (protection, transmission and refraction) are simultaneously satisfied by the long- and short-range extracellular matrix organization. (Ruberti and Zieske, 2008)

Microscopic anatomy. Figure 1.6 shows the three major functional layers of he cornea: the epithelium, stroma and endothelium.

Epithelium. The corneal epithelium is a 50µm thick, “tight”, stratified, squamous, multilaminar epithelium comprising three distinct cellular strata.

The stratum germinatum is the most posterior layer and the only epithelial cell layer capable of undergoing mitosis (Hanna and O'Brien, 1960). The middle layer comprises daughter and wing cells which are pushed anteriorly during epithelial desquamation. The surface layer of squamous cells forms the complete tight junctions which generate the primary chemical and antigen protective barrier in the cornea. This continual desquamation of the corneal epithelium depends on a stable supply of stem cells which reside in limbal niches at the junction between the sclera and the cornea (Schermer et al., 1986). A healthy epithelium has 5-7 layers of cells and rests on a basement membrane comprising laminin, type IV collagen, and identifiable hemidesmosomes and anchoring fibrils.

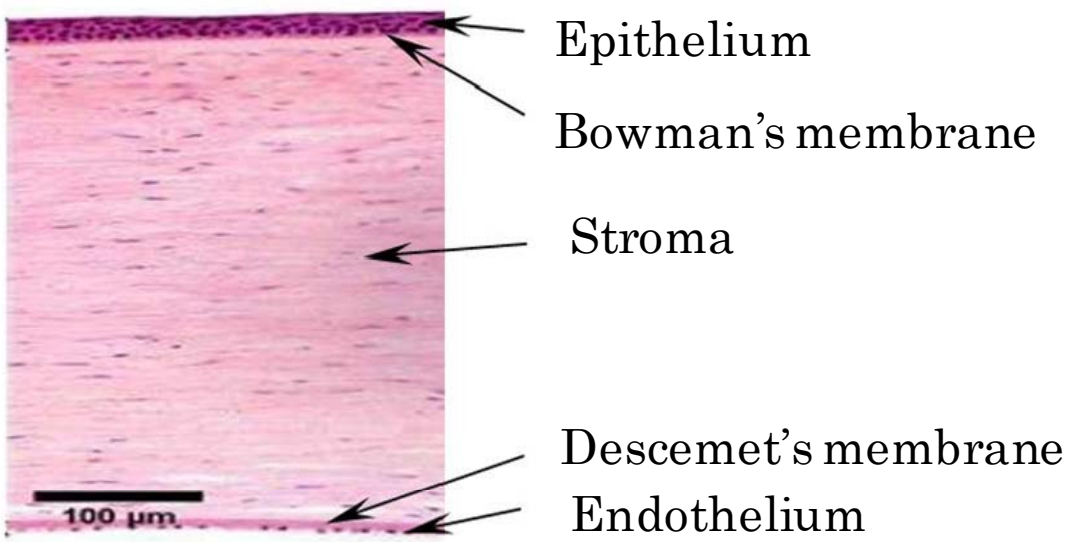

Figure 1.6. Histological section of a human cornea

That the cornea requires a functional epithelium is demonstrated by pathological conditions which chronically disrupt the ocular surface mucosa (ocular cicatricial pemphigoid, Stevens-Johnson syndrome, etc.), disrupt tear production (Sjogren's) or by injuries which destroy the stem cells niches in the limbus (severe chemical or alkali burns). Losing the epithelial barrier typically results in corneal opacity and the loss of the surface air/tear

interface for refraction. Natural or tissue engineered grafts cannot succeed without a functional epithelium. (Ruberti and Zieske, 2008).

Nonetheless, Ruberti and Zieske (2008) assert that the epithelium is there to protect the stroma from invasion (and to maintain the tear/air interface). It is the stromal architecture that produces the necessary aberration-free curvature to generate the refractive power. In addition, given the significant advances in corneal epithelial culturing onto various substrates (Zieske et al., 1994), and the fact that donor corneas (which are de-epithelized) gain epithelial coverage from the host, the epithelium is currently a critical concern for corneal tissue engineers. It is important to mention the fact that there is a considerable effort to innervate engineered corneal constructs (Li et al., 2003, 2005). The rationale for this approach is derived from data which suggest that denervation of the corneal stroma leads to poorly formed epithelium without proper cellular stratification (Alper, 1975).

Endothelium. The corneal endothelium is a transporting monolayer of about 400000 hexagonal cells, 20µm across and 4-6µm in height. The endothelium maintains the corneal transparency by keeping the corneal stroma in a state of relative deturgescense via a complex pump-leak mechanism ((Maurice, 1972) for pump discovery and (Bonanno, 2003) for extensive review of endothelial ion transport). Without the endothelium the cornea has a natural tendency to imbibe fluid which can cause swelling, opacity and blindness. This dehydration mechanism is part of a sophisticated corneal transport system which includes both limiting layers and is described in detail in Ruberti and Klyce (2002). As with the epithelium, an engineered construct that is perfectly mimetic of the natural stroma could not function without a patent, active endothelial layer. However, it may be quite possible for a collagen based cornea that does not swell by incorporating an analog to sutural fibners in the dogfish (Smelser, 1962). Nonetheless, an endothelium is a far greater concern for tissue engineers than the epithelium, as it has been refractory to expansion in culture and the host endothelium will not

effectively repopulate and deturgesce a bare donor stromal graft. Recently, untransformed endothelial cells have been cultivated and multiple times expanded in a specialized culture medium (McAlister et al., 2005; Joyce and Zu, 2004; Engelmann et al., 2004; 1999). Due to these relative successful efforts associated with culturing and expanding endothelial cells *in vitro*, the endothelium does not appear to present a "significant" hurdle to corneal tissue engineering effort at this time (Ruberti and Zieske, 2008). Ultimately, many efforts to expand primary endothelial cells in culture will be critical to the success of engineered corneas.

Stroma. The adult human stroma is approximately 500µm thick, relatively acellular (3-10% quiescent corneal keratocytes by volume), and comprises aligned arrays of hydrated type I/V heterotypic collagen fibrils (15% wet weight) of uniform diameter (32±0.7nm) (Meek and Leonard, 1993); glucosaminoglycans (GAGs) keratin sulfate and dermatansulfate (1% wet weight (Anseth, 1961)); various proteoglycan (PG) core proteins (Axelsson and Heinegard, 1975) and other protein constituents including fibronectin, laminin and type VI collagen (among other collagens). The collagen fibrils are packed in 300-500 parallel arrays (lamellae) which are generally also parallel to the corneal surface (Hamada et al., 1972) and are principally responsible for the observed tensile mechanical properties of the cornea (reviewed in Either et al., 2004). The PGs and their associated GAGs contribute to the cornea's compressive and swelling material properties (Hedbys, 1961) and to the uniform spacing of the collagen fibrils (Scott, 1991).

The corneal stroma is the current focus of researchers attempting to produce a corneal tissue analog for a number of reasons. First, there have been very few concerted efforts aimed at reproducing the architecture of a natural cornea (Guo et al., 2007; Crabb et al., 2006a,b; Orwin et al., 2003), while there have been multiple and relatively successful attempts to culture the limiting cell layers of the cornea (on a stromal scaffolding) (Li et al., 2005; Germain et al., 2004; Li et al., 2003 Griffith et al., 2002, 1999; Germain et al., 1999; Zieske et al., 1994; Minami et al., 1993) fully reviewed in Ruberti et al.

(2007). Second, the corneal stroma provides the majority of the principal functions of the corneal tissue. No corneal analog will work without a mechanically strong and clear, properly shaped stroma. Third, the stroma is extremely organized on the nanoscale, making it a very difficult and interesting basic materials engineering problem. Finally, because of the highly organized nature of the stromal matrix, successful reproduction of the architecture requires detailed examination of *in vivo/in vitro* matrix assembly and the development of novel engineering methods to control collagen fibrillogenesis. Such methods have broader implications for connective tissue remodelling, homeostasis and pathology (Ruberti and Zieske, 2008).

Corneal function. The native cornea has three fundamental functional attributes to the ocular optical system: protection, transmission and refraction of the incident light to the retina. These attributes are also considered essential design requirements for an artificial corneal construct.

Protection. The cornea provides both transport protection (in the form of a barrier) and mechanical protection.

The *transport protection* is represented by the transport of deleterious chemicals and pathogens that is impeded by the tight junctions of superficial squamous cells of the corneal epithelium (Sugrue and Zieske, 1997). Thus, any natural, stromal analog should be inductive for the migration of epithelial cells from the host peripheral corneal tissue and support the formation of a multilaminar, adherent epithelium with complete tight junctions (as donor corneas do (Boot at el., 1991)).

The *mechanical protection* of the fragile intraocular contents is provided by the tensile properties of the stromal extracellular matrix. The tensile mechanical strength of the tough ocular tunic (of which the cornea is a continuous part) must be high enough to withstand chronic tensile stress induced by the intraocular pressure (IOP) and permit survival of significant traumatic impacts without rupture. The overall biomechanical properties of

the proper cornea are complex because the stromal tissue is highly anisotropic, heterogeneous and viscoelastic (Either et al., 2004). Biomechanical properties are typically derivative of the orientation of collagen fibrils in load-bearing connective tissue. This is also true for the cornea when one is considering the tensile modulus in the direction of tangential loads. As might be expected, in the human corneal stroma, the preferred collagen fibril orientation, as determined by X-ray (Aghamohammadzadeh et al, 2004; Meek and Boote, 2004) and SEM analysis (Radner and Mallinger, 2002; Radner et al., 1998) (Figure 1.7A), is reflected in the measured tensile strength of excised test specimens (Figure 1.7B). It is also reflected clinically by the tendency of astigmatic axes to be aligned with either tangential or sagittal meridians.

It is important to note that the fibril organization model of Meek and Boote (Aghamohammadzadeh et al, 2004) is relatively recent and is the result of full-thickness integrations or averages of X-ray interactions with the collagen fibrils, result that helps the understanding of the complex arrangement of fibrils in the corneal stroma.

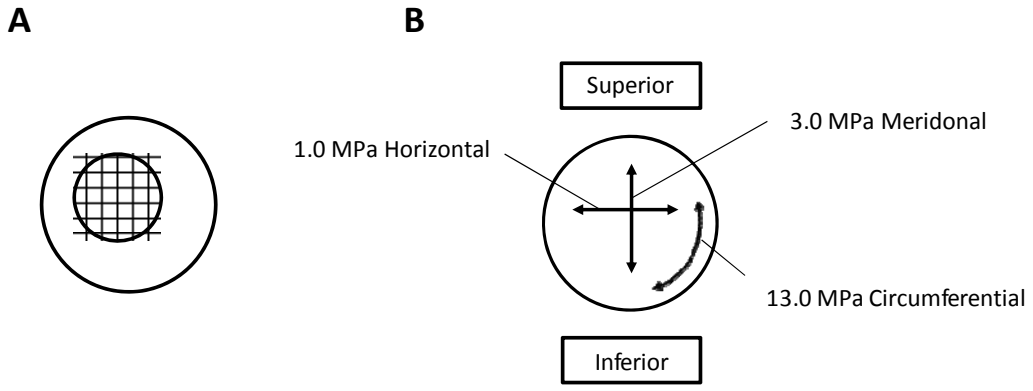

Figure. 1.7. (A) Proposed model of fibril orientation in the cornea based on X-ray synchrotron data. (B) Variation in corneal tensile strength as a function of direction. Though the cornea is typically considered a simple nematic stack of lamellae comprising aligned collagen which alternate in orientation by 90 degrees, recent investigations demonstrate an array of fibrils which run circumferentially around the periphery. Preferred fibril orientation and aligned fibril concentration are reflected in the tensile strength or modulus. The figure shows the tensile modulus found in test strips excised and loaded in the direction of the arrows. ((A) Meek and Boote, 2004 and (B) Ruberti et al., 2007).

It has been known for over 100 years that stromas will swell and become opaque if excised and placed in hypotonic fluid (Leber, 1873). The compressive properties of the cornea are not critical to protect the globe, but are a consequence of the presence of the proteoglycans which are thought to maintain the collagen fibrillar spacing (Scott, 1991). Nonetheless, any accurate reproduction of a natural collagen/GAG based stroma will also require the same sort of hydration control system (due to the fixed charges on the GAGs) to maintain transparency. It is important to note that if a corneal analog can be produced which does not swell and remains clear, a transport system which deturgesces the cornea may not be required. This is the ostensibly valid argument of researchers pursuing synthetic hydrogel-based corneas which promote epithelialization (Sweeney et al., 2003). In the case of these synthetic porous implants, the epithelium would still be required to provide a barrier function and to maintain the tear/air interface. Research has demonstrated however that endothelial cells may still be necessary to aid the formation of healthy epithelium (Orwin and Hubel, 2000; Zieske et al., 1994).

Transmission of light. The native cornea is an extremely efficient transmitter of incident visible light (Cox et al., 1970), with such efficiency dependent on the relative content and distribution of water in the stroma (Goldman et al., 1968). The transmission of light is critical to the function of the tissue. Thus the transparency of the stromal matrix, which constitutes the majority of the tissue thickness (and the light interaction) is also critical to corneal function. In order to understand the optics of the corneal matrix transparency, it is necessary to examine the stromal collagen architecture at the nanoscale and to examine the role of the keratocytes (Ruberti and Zieske, 2008).

Within the last years, it has been demonstrated that *keratocytes* contribute actively to corneal transparency (Jester et al., 1999a,b). Following corneal wounding, such as PRK surgery, the dedifferentiation to keratocytes to fibroblasts and/or myofibroblasts can lead to a clinically relevant corneal

haze (Jester et al., 1999a,b). The haze has been attributed to poor optical properties of the cells which have undergone dedifferentiation. Their ability to "index match" to allow transmission of light appears to be a function of the content of soluble enzyme crystallins expressed in the cytoplasm of cells with a keratocyte phenotype (Karring et al., 2004). Thus, the cell population in corneal constructs should be of the appropriate phenotype to reduce cell-induced optical haze (West-Mays and Dwivendi, 2006).

Another important factor in the corneal transparency is the *stromal fibril organization*. Maurice (1957) concluded in a landmark paper on corneal transparency that a regular crystalline arrangement of the monodisperse diameter collagen fibrils in the cornea was required to maintain transparency to incident light (Maurice, 1957). Later, Hart and Farrell (1969) and then Benedek (1971) showed theoretically that cornea could be transparent even if there was only limited correlation in the spacing of the collagen. Benedek (1971) demonstrated theoretically that for transparency, it was important that the collagen fibrils should not pack together and that areas of collagen depletion (lakes) larger than the wavelength of light must not exist. The fundamental argument against the requirement of extremely ordered fibrils was derived from examination of Bowman's membrane in the shark which is both transparent and disordered (Figure 1.8) (Goldman and Benedek, 1967). Thus, while it is not necessary that the collagen fibrils in an engineered stroma be uniformly spaced, they should be much smaller than the wavelength of light, have a reasonably monodisperse diameter distribution and exhibit uniform center-to-center spacing. Further, there should not be large regions (on the order of the wavelength of light) devoid of fibrils (Ruberti and Zieske, 2008).

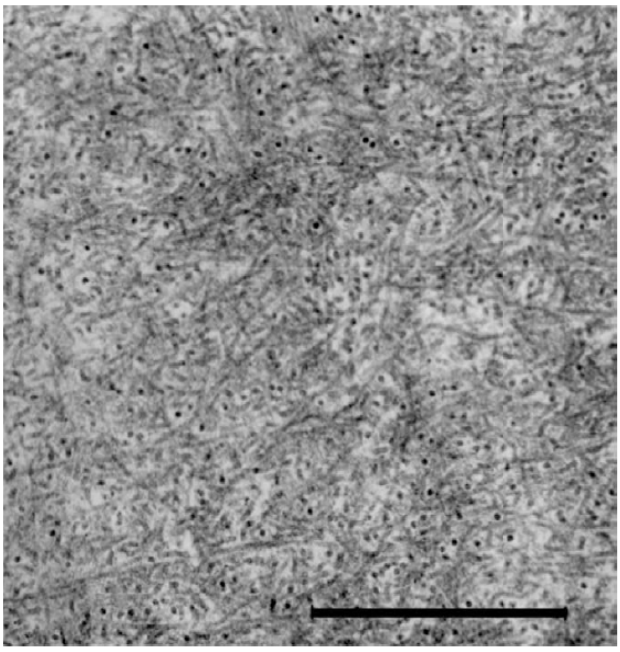

Figure. 1.8. Bowman's layer in the dogfish. There is no discernible "organization" to the fibrils in this layer yet this portion of the cornea is more transparent than the underlying more "organized" stroma proper (Goldman and Benedek, 1967).

Refraction of light. The combination of the nearly perfectly spherical corneal anterior surface and the index of refraction change in the air/tear film interface generate approximately 80% (42 diopters) of the total refractive power of the human ocular system. Precisely how the cornea forms such an effective refractive surface remains a matter of speculation, but it is likely to reside in the details of the stromal collagen nanoscale arrangement coupled with the distribution of the mechanical tensile load (which is a consequence of IOP via Pascal's Principle and Laplace's Law). For instance, the fact that there are (putatively) no covalent crosslinks binding collagen fibrils to one another, fibrils may move relatively freely to distribute the load induced by the IOP. The precise pattern of *in vivo* corneal collagen load-bearing remains difficult to determine (Ruberti and Zieske 2008). After a detailed mechanical analysis of corneal transport, Friedman (1972) concluded that the anterior most lamellae carry the load from the IOP. He cited the clinical

manifestations of sub-epithelial edema as evidence supporting this proposed load distribution. However, evidence has been provided that indicates that in the rabbit (Hennighausen et al, 1998; McPhee et al., 1985) and in the human (Hjortdal, 1996) the IOP load is distributed evenly through the thickness of the corneal stroma. In areas where the stromal lamellae are parallel to corneal surface and given the monodispersity in the fibril diameters, this finding implies that the collagen fibrils should "feel" approximately the same strain (or stretch).some mechanisms must ensure during both development and growth, that the corneal curvature remains reasonably spherical. This requires that the load be distributed with precision among the collagen fibrils. The solution to this question may involve a matrix remodelling control system such as that putatively responsible for ocular globe length control (Troilo, 1992; Triolo and Wallman, 1991).

Linking corneal form and function. As stated before, the stroma comprises 90% of the total corneal thickness, thus it is not surprising that it plays a major role in providing the principal functions of the cornea. Ruberti and Zieske (2008) suggest that the stroma owes its success in simultaneously meeting the three corneal design requirements (protection, transmission and refraction) to its exquisite nanoscale organization. Figure 1.9 shows the organization of the stromal collagen fibrils, which have a virtually monodisperse diameter distribution (transparency), reasonably uniform local interfibrillar spacing (transparency), no interfibrillar covalent crosslinks (refraction) and are arranged in parallel arrays which are generally tangential to the corneal surface (mechanical strength). The authors also assert that this remarkable and persistent nanoscale arrangement of fibrils which persists throughout the cornea (with the exception of Bowman's membrane) is directly responsible for corneal function and thus links corneal form and function at the level of the nanoscale.

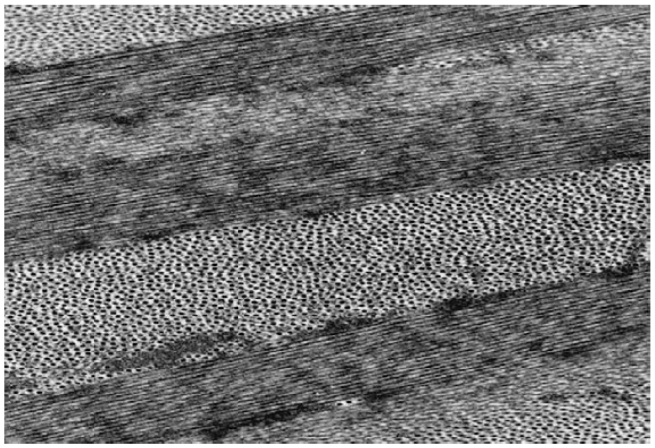

Figure 1.9. Transmission electron micrograph of collagen fibril arrangement in cornea.Corneal collagen fibrils have a highly monodisperse diameter distribution and arearranged in oriented arrays within lamellae which are approximately 1–2 mm thick (Section is normal to tangent plane) (Ruberti and Zieske, 2008).

The stromal organization appears to be the main reason why attempts to engineer a viable cornea have been unsuccessful to date. Any corneal analog comprising a natural collagenous extracellular matrix (ECM) must closely mimic this arrangement or risk being too weak, too opaque or too irregular to form an appropriate refractive surface. It is for this reason that the efforts to produce a natural cornea via tissue engineering should focus on reproducing the stroma and in particular on reproducing the nanoscale stromal architecture.

Artificial corneas. Artificial corneal substitutes are needed to address the shortage of human donor tissues as well as the current disadvantages of some clinical indications, which include immune rejection. The main types of artificial corneas range from keratoprosthese (*KPros*) (Bakri et al., 2006; Myung et al., 2005; Jacob et al., 2005; Sweeney et al., 1998), self-assembled corneal substitutes (Carrier et al., 2008; Guo et al., 2007; Du et al., 2007; Du et al., 2005; Gaudreaultet et al., 2003), acellular tissue-engineered scaffolds (Merrett et al., 2008; Liu et al., 2008; Crabb et al., 2006b; Borene et al., 2004)

to tissue engineered scaffolds (Cardona et al., 2011; Gonzalez-Andrades et al., 2009; Alaminos et al., 2006; Nakamura et al., 2006; Han et al. 2002; Rama et al., 2001), allowing different degrees of regeneration of the host tissues.

Human oral mucosa

Oral mucosa anatomy. The oral cavity is a multi-site organ with several anatomical sites, as shown in Figure 1.10A. In general, the oral cavity is covered by a squamous epithelial tissue called oral mucosa. Figure 1.10B shows that the oral mucosa can be divided into two major layers: the squamous epithelium and the underlying connective tissue.

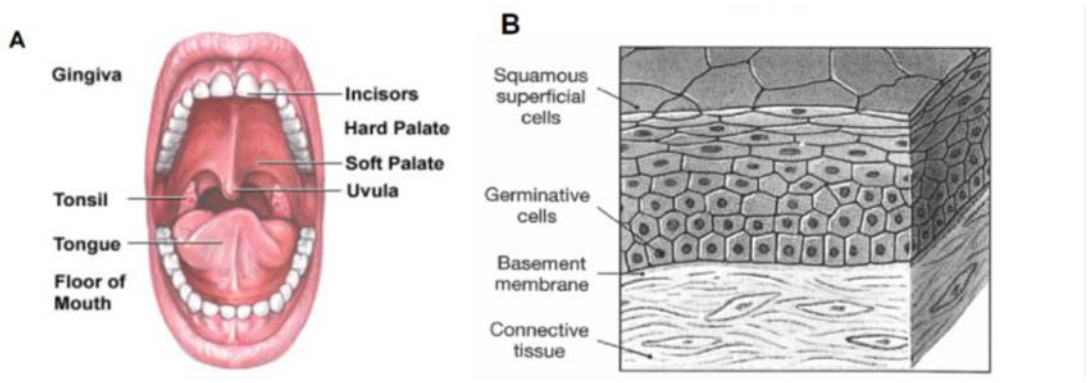

Figure 1.10. Anatomy and architecture of the oral cavity.(A) Major anatomical sites of the oral cavity; (B) Basic architecture of stratified squamous epithelium.

These two major layers, the oral epithelium and the lamina propria are equivalent to the epidermis and dermis of the skin. The lamina propria is a layer of interlocking fibers which gives strength to the epithelium above. It consists mostly of tough collagen fibers, some elastic fibers and reticulin. In between the fibers are the cells which form them, the fibroblasts, and other connective tissue cells.

Beneath the lamina propria of the mucosa, a layer called the submucosa is usually found. It is a loose connective tissue containing fat, blood vessels, nerves and lymphatics. In some places like the hard palate, the submucosa is also called fibrous and binds the overlying mucosa quite firmly.

But there is no submucosa at all beneath the gingival mucosa. The lamina propria of the gingiva is bound directly onto the periosteum. It is therefore often referred to as a mucoperiosteum (Figure 1.11).

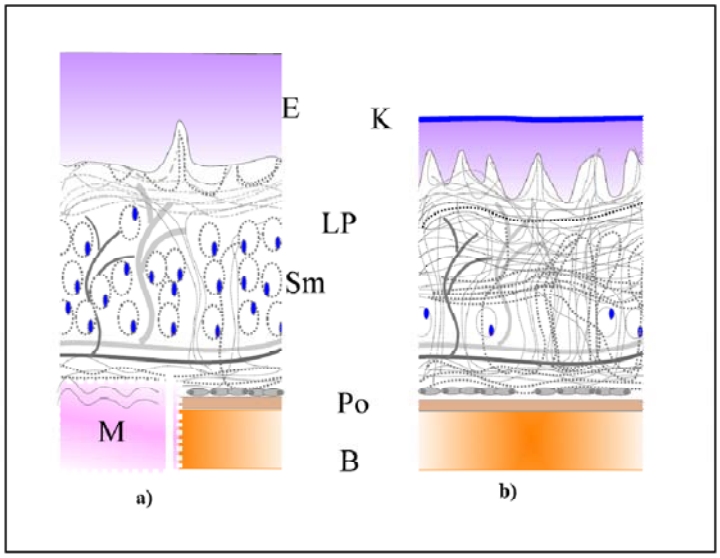

Figure 1.11. Components of oral mucosa. a) The lining mucosa has a relatively thick epithelium (E), supported by thin lamina propria (LP). The submucosa (Sm) contains blood vessels and minor salivary glands, in a loose connective tissue. The submucosa may be attached to muscle (M) or the periosteum (Po) covering bone. b) Masticatory mucosa has keratinized epithelium (K) and a dense lamina propria of collagen fibers which attach the epithelium directly to the periosteum.

Oral epithelium. The oral epithelium is a stratified layer of squamous cells which may either be keratinized or non-keratinized, according to the region of the mouth. The epithelium exhibits four layers of cells: the basal layer, spinous layer, granular layer and the superficial layer, known as the cornified layer in the skin and the keratinized layer in oral mucosa. Keratinization involves the transformation of viable keratinocytes in the granular layer into dead surface cells devoid of organelles and packed with dense masses of cytokeratin filaments. In non-keratinized oral epithelium, the granular layer is replaced by the surface layer, the cells of which lack keratohyaline granules. Basal layer keratinocytes are progenitor cells that

undergo terminal differentiation as they migrate to the surface. In addition to keratinocytes, the oral epithelium contains non-keratinocyte clear cells:

- The melanocytes produce pigment and transfer it to the keratocytes around them. The number of melanocytes is no greater in heavily pigmented epithelium, but their activity is increased.
- The Langherhans cells are active in the immune response of the epithelium. They act as sentries, detecting the presence of foreign antigens on the surface of the oral epithelium. They then migrate from the epithelium to local lymph nodes where they present information about surface antigens to T lymphocytes. Langerhans cells do not have desmosome attachments and so, during histological processing, the cytoplasm shrinks down around the nucleus producing a clear halo. Hence, these cells are referred to as clear cells.
- The Merkel cells are mechanical receptors for tactile sensations.

Adhesion between epithelial cells is achieved by desmosomes. The basal layers are attached to the underlying lamina propria through hemidesmosomes and the basement membrane, which contains collagen type IV, laminin and fibronectin.

In 1975, Rheinwald and Green (1975) proposed a method to grow human keratinocytes in serial culture *in vitro*, using a feeder layer composed of irradiated 3T3 mouse fibroblasts and a specific culture medium called Green's medium. This method is frequently used for the culture of keratinocytes and production of single-layer epithelial sheets. Several investigators have been successful in culturing sheets of oral keratinocytes without an irradiated feeder layer (Lauer, 1994; Arenholt-Bindslev et al., 1987), but, these epithelial sheets are fragile, difficult to handle and apt to contract. Monolayer cultures have been extremely helpful for the study of basic biology and responses to stimuli of both oral and skin keratinocytes and many studies have used them. However, the oral epithelium is a complex multilayer structure, with cells undergoing terminal differentiation and monolayers cultures may not be a good model of what is happening *in vivo*.

Thus, the development of a three-dimensional multilayer culture system was a major breakthrough in epithelial biology and tissue engineering. This new system facilitated the culture of keratinocytes on permeable cell culture membranes at the air/liquid interface.

Lamina propria. The lamina propria consists of an abundant network of type I collagen fibers and the deeper layers contain collagen type III fibers and elastic fibers in various amounts, depending upon the site. Many fibroblasts are present, but only very occasional macrophages, plasma cells, mast cells and lymphocytes are found. Being the most common cells in the connective tissue (lamina propria), fibroblasts can be easily isolated and cultured in monolayers by conventional cell culture technique. Berthod and collaborators (Berthod et al., 1993) showed that fibroblasts cultured on three-dimensional porous scaffolds produce significantly higher levels of extracellular matrix than do fibroblasts grown on monolayers.

Fibroblasts play an important role in epithelial morphogenesis, keratinocyte adhesion and the formation of complex dermal-epithelial junction (Saintigny et al., 1993). The epithelial phenotype and keratin expression are extrinsically influenced by the nature and origin of the underlying fibroblasts (Okazaki et al., 2003) and the mesenchymal substrate (Merne and Syrjanen, 2003). It has been reported that without fibroblasts in the matrix, the epithelium ceases to proliferate (Fusenig, 1994), while differentiation continues (Smola et al., 1998). The significance of fibroblast has also been shown by an experiment in which degenerative vacuolization was seen in co-cultures grown in absence of fibroblasts. The use of oral buccal and vaginal fibroblasts led to a non-keratinized epithelium, in contrast to cultures with skin fibroblasts, which showed slight parakeratinization (Atula et al., 1997). Thus, fibroblasts may influence the differentiation potential of the epithelium toward that found at the site of origin of the fibroblasts.

The lamina propria also contains vascular components, which form extensive capillarity loops in the papillae between the epithelial ridges. Lymphatic vessels, nerves and nerve endings are also present, as well as the

ducts of salivary glands, whose acini are usually found in the deeper submucosa. Varying numbers of sebaceous glands are found in the oral cavity, but are not associated with hair follicles (Atkinson et al., 2000)

Functions of the oral mucosa. The oral mucosa has a *protective,* a *secretory* and a *sensory* function.

The *protective* function is served by its resistance to tearing and compression which is provided by the tough and yet resilient lamina propria. The oral mucosa is also mostly impervious to the penetration of bacterial toxins. Protection from microorganisms is also afforded by the shedding (desquamation) of the surface layer of cells. Bacterial colonies attached to these surface cells are thus regularly carried away when the cell sloughs off and is carried away and swallowed in the saliva.

The mucosa provides a suitable site for sensory nerve endings, such as those associated with pain, touch, temperature and the taste receptors of the tongue and palate. Some of these receptors are important in the initiation of reflexes, like swallowing or jaw opening.

Minor salivary glands in the submucosa secrete via ducts passing through the mucosa. These secretions help to keep the mucosa moist and free of excessive accumulations of bacteria. There are also sebaceous glands sometimes seen on the inside of the cheek, (also called Fordyce´s granules). They have no function but are important to recognise as being normal.

Artificial oral mucosas. Histological section of a normal native and a tissue engineered oral mucosa are presented in Figure 1.12. In order to create an ideal full-thickness engineered oral mucosa that resembles normal oral mucosa and optimize the generation process, many factors have to be taken into account. Among them, the choice of scaffold, the cell source and the culture medium are the most important ones.

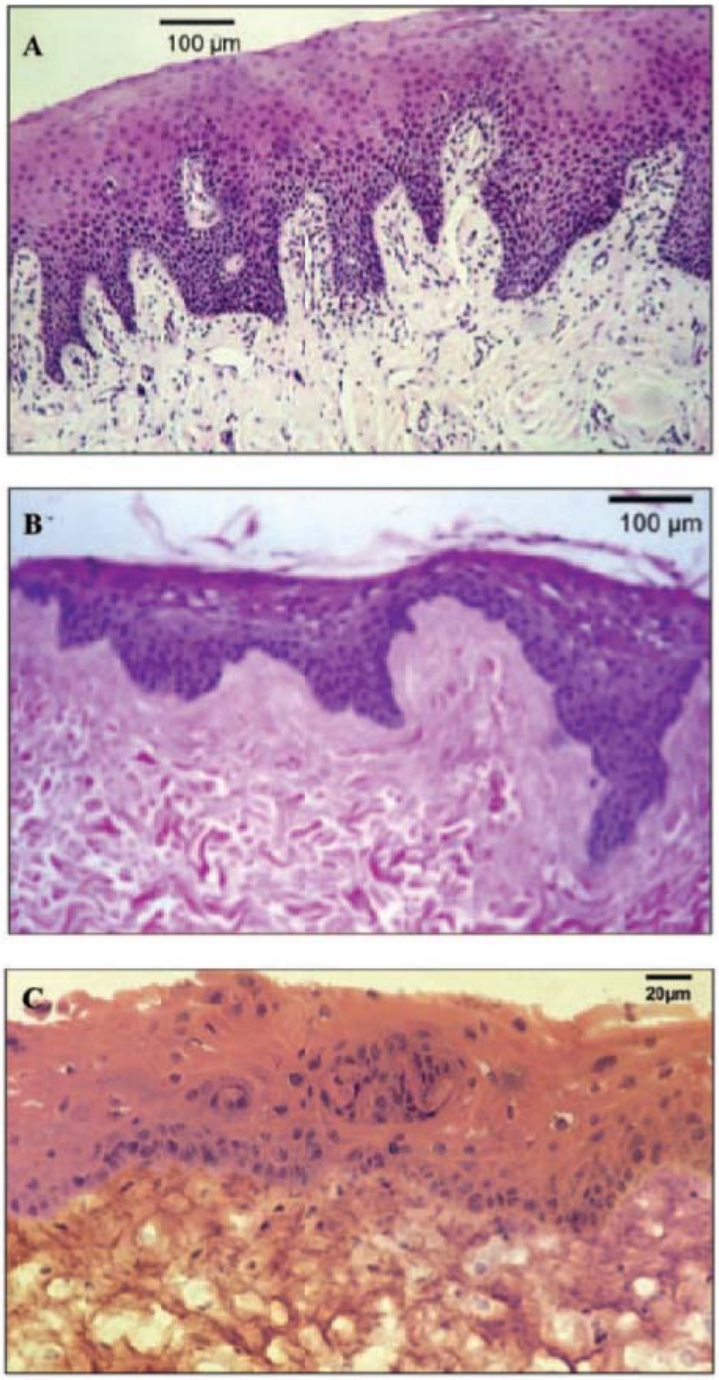

Figure 1.12. Histological sections of (A) normal oral mucosa biopsy, (B) tissue-engineered skin and (C) tissue-engineered oral mucosa (Moharamzadeh et al., 2007)

Different types of scaffolds have been used in oral mucosa and skin reconstruction. These types can be divided in several categories: (1) naturally derived scaffolds, such as amniotic membrane (Nakamura et al., 2003; Moriyama et al., 2001); (2) collagen-based scaffolds (Ma et al., 2003); (3) gelatin-based scaffolds (Lee at el., 2003; Mao et al., 2003; Choi et al., 2011; Hong et al., 2001); (4) fibrin-based materials (Rodriguez et al., 2012; Sanchez-Quevedo et al., 2007); (5) hybrid or synthetic scaffolds (El Ghalbzouri et al., 2004)

Cell source. The type and origin of fibroblasts and keratinocytes are important factors in oral mucosa reconstruction. Fibroblasts are usually isolated from the dermal layer of the skin or by oral mucosa biopsy, and are used at early passages for tissue engineering, because it has been demonstrated that the extracellular matrix production by dermal fibroblasts decreases as the passage number increases (Takeda et al., 1992; Khorramizadeh et al., 1999). Keratinocytes can be obtained from different sites of the oral cavity, such as the hard palate (Cho et al., 2000), gingiva (Yoshizawa et al., 2004), or buccal mucosa (Bhargava et al., 2004). Normal human keratinocytes should also be used at very early passages.

Culture medium. The commonly used culture medium for oral mucosa reconstruction is Dulbecco's modified Eagle medium (DMEM)-Ham's F-12 medium (3:1), supplemented with fetal calf serum(FCS), glutamine, epidermal growth factor (EGF),hydrocortisone, adenine, insulin, transferrin, tri-iodothyronine, fungizone, penicillin, and streptomycin.

Applications of tissue engineered tissues. There are generally two major applications for bioengineered tissues: (1) clinical applications, and (2) as *in vitro* test systems and models. It is important to realize that tissue engineering approaches may be different for each purpose. As an example, for clinical applications such as grafting, transplantation, and guided tissue regeneration, a biodegradable scaffold with optimal mechanical properties is desirable, because it will be replaced by the host tissue, and it must resist natural forces in the oral cavity, while a non biodegradable scaffold may

result in a foreign body reaction. Also, transmission of infection and tissue rejection are major issues. The scaffold should have maximum biostability to maintain its structure throughout the testing procedure.

Until now, the morphological and functional characteristics of the two tissues of interest in the present study, cornea and oral mucosa, have been described. Not only these characteristics are important when generating a tissue-like replacement by means of tissue engineering, but also the physical properties, such as optical and mechanical properties, of the tissue substitute are of interest. A major step in improving medicine is the step of identifying different, effective and efficient methods for diagnosis and treatment of abnormal or diseased tissues. One of the problems often associated with conventional medical therapies and diagnostic tools is that they often cause pain and discomfort to the patient. However, the current trends in healthcare have seen a shift towards improved medical therapies and diagnostics with emphasis on patient comfort. This has led to the development of many non-invasive medical techniques and devices. Non-invasive methods often utilise some form of light either a laser, LED etc. and therefore knowledge about the interaction between the tissue and these light sources is important. Determination of the optical properties of tissue, such as the absorption and scattering coefficients (μ_a and μ_s, respectively) is thus a fundamental property in refining the available as well as optimising new optically based methods and technologies in health care and life sciences.

2. MOTIVATION AND OBJECTIVES
MOTIVACIÓN Y OBJETIVOS

La medicina regenerativa es un área emergente que busca la reparación o sustitución de tejidos y órganos mediante la aplicación de métodos procedentes, entre otros, de la ingeniería tisular. Es importante señalar que la evaluación de los tejidos generados en laboratorio mediante ingeniería tisular constituye un aspecto fundamental de la terapia celular y tisular en el ámbito de la medicina regenerativa y de la sanidad pública. A este respecto, el Real Decreto 1301/2006 (BOE 270 de 11 de noviembre de 2006) establece disponer de sistema de control de calidad de los procesos que se suceden desde la obtención de las células y los tejidos hasta su implantación, así como la necesidad de investigar nuevos sistemas de valoración que aseguren la idoneidad de los tejidos, lo cual obligan a que la investigación en este campo tenga carácter multidisciplinar.

Nuestro grupo de investigación ha generado en laboratorio sustitutos tisulares de cornea y mucosa oral humanas basados en biomateriales de fibrina y fibrina-agarosa con una posible utilidad, en última instancia, en la investigación básica y la práctica clínica. Específicamente, el estudio de las propiedades ópticas de dichos biomateriales es fundamental tanto para el control de calidad, como para aplicaciones médicas de diagnóstico y tratamiento. En concreto, en el caso de los tejidos generados en laboratorio para remplazar corneas afectados por distintas enfermedades y patologías, el estudio de sus características ópticas es fundamental para su viabilidad. Dentro de un marco general, la distribución cuantitativa de la intensidad de la luz en medios no homogéneos, tal como tejidos biológicos, puede obtenerse mediante la solución de la ecuación de transporte radiativo. No obstante, en estos medios debido a las inhomogeneidades e irregularidades inherentes a sus configuraciones físicas, no existe una solución analítica de la ecuación de transporte. A pesar de ello, resolviendo dicha ecuación es posible obtener una estimación de la distribución de la intensidad de la luz en este tipo medios. La solución aproximada de la ecuación de transporte requiere conocer los valores de los coeficientes de absorción y esparcimiento del medio y por tanto, son necesarios métodos experimentales apropiados para medir estas propiedades ópticas.

Por todo ello, en la presente Tesis Doctoral nos planteamos los siguientes objetivos:

Objetivo general:

Evaluar tejidos humanos generados mediante ingeniería tisular basados en fibrina-agarosa utilizando métodos ópticos.

Objetivos específicos:

1. Estudiar las propiedades reológicas de sustitutos de estroma corneal nanoestructurados y no nanoestructurados de fibrina y fibrina-agarosa.

2. Desarrollar un método óptico para la evaluación de la calidad óptica y evaluar sustitutos de estroma corneal basados en fibrina, fibrina-agarosa y colágeno.

3. Determinar las propiedades ópticas de un modelo de córnea lamelar anterior humana generado mediante ingeniería tisular basado en fibrina-agarosa.

4. Determinar las propiedades ópticas de un modelo biomimético de mucosa oral humana generado mediante ingeniería tisular basado en fibrina y fibrina-agarosa.

De acuerdo con el planteamiento de estos objetivos, la presente Tesis Doctoral se estructura a continuación en 4 capítulos, cada uno describiendo los materiales y la metodología utilizados, los resultados obtenidos y su correspondiente discusión, con el fin de cumplir con los objetivos propuestos (capítulos 3-6). El capítulo 7 presenta las conclusiones finales de nuestro estudio. Todas las referencias que se proporcionan en el capítulo 8, mientras que el capítulo 9 enumera las publicaciones científicas relacionadas con el trabajo presentado en esta Tesis

Regenerative medicine is an emerging field that seeks to repair or replace tissues and organs by applying different methods including, among others, tissue engineering techniques. Importantly, the assessment of the tissues generated in laboratory by tissue engineering is a fundamental aspect of cell and tissue therapy in the field of regenerative medicine and public health. In this regard, the Spanish Real Decreto 1301/2006 (BOE 270 of November 11th, 2006) has established that the research developed in this field has to be provided with quality control systems for the processes that occur from the procurement of cells and tissues to its implementation, and to investigate new evaluation systems to ensure the suitability of the tissues. This requires that research in the biomedical field has to be multidisciplinary.

Our research group has generated in laboratory cornea and human oral mucosa tissue substitutes based on fibrin and fibrin-agarose biomaterials, with potential value in basic research and clinical practice. Specifically, the study of the optical properties of such biomaterials is critical for quality control, as for medical diagnosis and treatment. In the case of bioengineered tissues generated in the laboratory in order to replace corneas affected by various diseases and disorders, the study of their optical characteristics is essential for their suitability for possible clinical applications. In a general context, the quantitative distribution of the light intensity in inhomogeneous media, such as biological tissues, can be obtained using the solution of the radiative transport equation. However, there is no analytic solution of the transport equation for these media, due to inhomogeneities or irregularities inherent to their physical configurations. Nonetheless, solving this equation it is possible to obtain an estimation of the distribution of light intensity in such media. The approximate solution of the transport equation requires the knowledge of the absorption and scattering coefficients of the medium and therefore appropriate experimental methods are needed to measure these optical properties.

Therefore, in this PhD thesis we set the following objectives:

Main objective:

To evaluate human tissues generated by tissue engineering based on fibrin-agarose using optical methods.

Specific objectives:

1. To study the rheological properties of fibrin and fibrin-agarose nanostructured and no nanostructured corneal stroma substitutes.

2. To develop an optical method for optical quality evaluation and to evaluate corneal stroma substitutes based on fibrin, fibrin-agarose and collagen.

3. To determine the optical properties of a model of human anterior lamellar cornea generated by tissue engineering based on fibrin-agarose.

4. To determine the optical properties of a biomimetic model of human oral mucosa generated by tissue engineering based on fibrin and fibrin-agarose.

According to these objectives, this PhD thesis is then structured in 4 Chapters, each one describing the materials and methodology used, the results and corresponding discussion obtained in order to accomplish the proposed objectives (Chapters 3-6). Chapter 7 shows the final conclusions of our study. All the references are provided in Chapter 8, whereas Chapter 9 enumerates the published papers related with the work presented in this Thesis.

3. RHEOLOGICAL PROPERTIES OF BIOENGINEERED CORNEAS BASED ON FIBRIN AND FIBRIN-AGAROSE

BACKGROUND

Fibrin hydrogels are an attractive material for use in tissue engineering since their principal component, the fibrin, is a polymeric protein that together with platelets acts to form a thrombus or blood clot and as such constitutes a intrinsic scaffold for repair and regeneration (Orlando et al., 2012). Fibrin hydrogels are biocompatible, biodegradable and possess a suitable interaction with cells and other macromolecules (Breen et al., 2009; Ahmed et al, 2008; Bensaid et al., 2003; Sierra, 1993;). Therefore, fibrin has been used as a scaffold to deliver cells, drugs and therapeutic molecules in a wide range of tissue engineering applications (Steward, 2012; Ahearne et al., 2011; Pelaez et al, 2009; Bhang et al., 2007; Eyrich et al., 2007; Willerth et al., 2007; Albes et al, 1994;). Being a naturally occurring physiological scaffold, it supports angiogenesis and tissue repair (Amrani et al., 2001). In addition, fibrin naturally contains sites for cellular binding, and has been shown to have excellent cell seeding effects and good tissue development (Ye et al., 2000). Moreover, modification and functionalization of fibrin matrices has been used to provide controlled release of genes (Trentin et al., 2006) and growth factors (Schmoekel et al., 2005). Furthermore, fibrin gels can be produced from the patients' own blood and used as an autologous scaffold for the seeded cell without the potential risk of a foreign body reaction (Ye at al., 2000).

Agarose is a typical naturally-occurring polysaccharide that is known to form thermoreversible gels when a homogeneous solution is cooled from 99°C to a temperature below the ordering temperature, which is around 35°C for normal agarose (Normand et al., 2000). Agarose gels are widely used in

various fields of biomedical research, particularly in tissue culture systems, because it permits growing cells and tissues in a three-dimensional suspension (Sakay et al., 2007). In addition, they have been investigated as delivery vehicles for drugs (Jain et al., 2006; Liu and Li, 2005) and living cells (Sakai et al., 2005; Yang et al., 1994). Moreover, due to their soft tissue-like mechanical properties and biocompatibility, agarose gels have been investigated as potential scaffolds for neural (Jain et al., 2006) and cartilage (Gruber et al., 2006; Gruber et al., 1997) tissue engineering.

Using tissue engineering techniques, biological substitutes that restore, maintain, or improve tissue function or even a whole organ have been developed (Langer and Vacanti, 1993). In the past years several researchers have focused their efforts on the development of an autologous artificial substitute of the human cornea by tissue engineering (González-Andrades et al., 2009; Alaminos et al., 2006; Nishida, 2003; Reichl and Muller-Goymann, 2003; Schneider et al., 1999), reducing this way the risk of rejection. In this context, our research group generated a novel biomaterial based on a mixture of human fibrin and agarose that allowed the successful development *in vitro* of substitutes for rabbit (Alaminos et al., 2006) and human cornea (González-Andrades et al., 2009).

The rheological properties of biomaterials used in tissue engineering are important for establishing appropriate mechanical support to cells within load bearing defects and facilitating manipulation of these constructs prior to implantation (Rosso et al, 2005). Additionally, several studies have shown that the stiffness of a substrate can direct cellular activity, such as attachment, migration and differentiation (Murphy et al., 2012; Haugh et al., 2011; Engler et al., 2006; Yeung et al., 2005; Engler et al., 2004;). Thus rheological properties take on further importance, since they can affect the clinical performance of the substitute. Thus, in the development of a bioengineered construct that could replace a diseased cornea, it is necessary to accurately evaluate these properties. Since the cornea provides protection

to the intraocular contents, it is required that the biomaterial used as tissue substitute possess adequate viscoelastic properties.

The aim of this study is to determine the rheological properties of bioengineered human corneas based on fibrin and fibrin-agarose scaffolds and generated by tissue engineering using a new method based on plastic compression that allows the partial dehydration of the biomaterials.

MATERIALS AND METHODS

Human corneas. To isolate corneal stromal cells, human corneal–scleral limbal rims of cca. 14mm diameter were obtained at the University Hospital of San Cecilio, Granada, Spain, after the removal of ±7mm central corneal buttons for corneal transplantation (Figure 3.1).

All experimental protocols, including the use of human tissues, were approved by the Institutional Review Board Committee of Granada University Hospital San Cecilio. For the use of human corneal rims after trephination of the donor buttons for research purposes, a written approval was obtained from the legal representatives of the donors according to the protocols established by the Spanish National Organization for Human Transplantation.

Figure 3.1. Human corneal-scleral limbal rims.

Isolation and culture of human cells. Primary cultures of human keratocytes were generated as previously described (Alaminos et al., 2006; González- Andrades et al., 2009). Stromal keratocytes were isolated from corneas stripped of both endothelium and epithelium using sterile forceps. After the corneal epithelial and endothelial layers had been dissected, the remaining stroma was cut into small pieces and digested at 37ºC using collagenase I (Invitrogen-Gibco, Carlsbad, CA) for 6 hours. Isolated keratocytes were harvested by centrifugation and cultured in Dulbecco modified Eagle medium (DMEM) supplemented with 10% fetal bovine serum (Sigma- Aldrich), 4mM L-glutamine, and 1% antibiotic–antimycotic solution (Invitrogen-Gibco). Cells were incubated at 37ºC in 5% carbon dioxide under standard culture conditions until cells reached subconfluence (Figure 3.2). The culture medium was changed every 3 days.

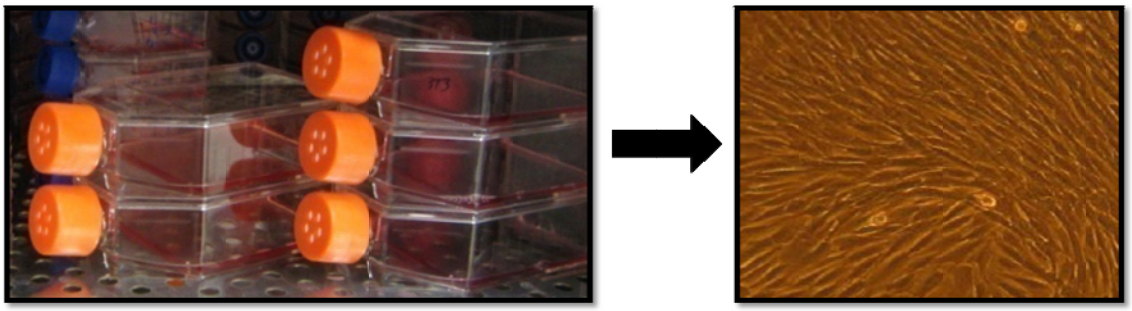

Figure 3.2. Primary cultures of human keratocytes.

Construction of artificial human cornea stroma substitutes. Two types of bioengineered corneal stroma substitute were generated in the laboratory: human fibrin stromas and human fibrin with 0.1% concentration of agarose non-nanostructured constructs (N-NCCs), and nanostructured constructs (NCCs). In all cases, 21ml of human plasma were added to 1.8ml of DMEM in which 250,000 cultured keratocytes had been previously suspended, and 200µL of tranexamic acid (Amchafibrin, Fides-Ecofarma, Valencia, Spain) were added to avoid spontaneous fibrinolysis. Then, 2ml of 1% of $CaCl_2$ were added to the solution to precipitate the polymerization reaction of the

hydrogel. In the case of the fibrin–agarose gels, previously melted type VII agarose dissolved in PBS (phosphate-buffered saline) was supplemented in the last step. After polymerization, 15ml of culture medium were added to the surface of the bioengineered corneal stromas (as shown in Figure 3.3), which were incubated at 37ºC in 5% carbon dioxide. Samples of the different stromal substitutes were studied weekly until eight weeks of development in culture. Once generated, half of them were nanostructured (NCCs) and the other half were studied directly (N-NCCs).

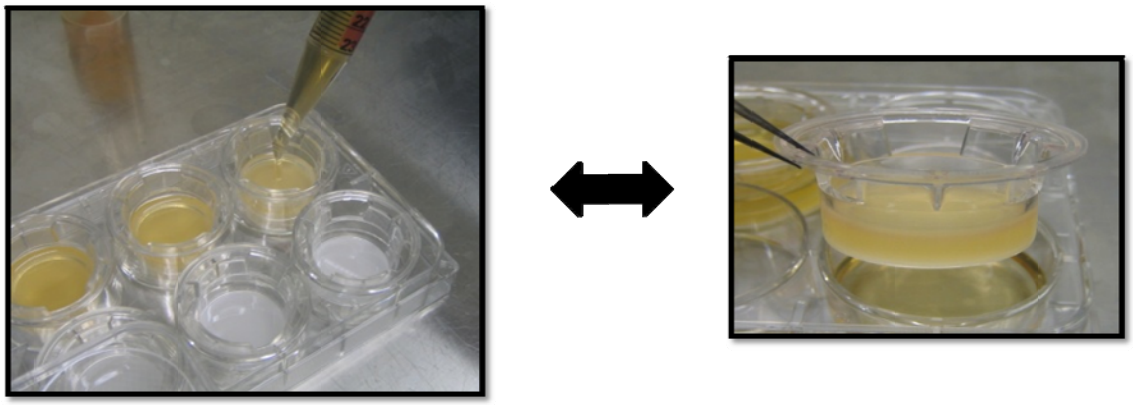

Figure 3.3. Generation of the fibrin and fibrin-agarose corneal substitutes.

The nanostructuring technique is based on previously described methods by Hadjipanayi and collaborators (Hadjipanayi et al., 2011), who described a technique that is able to allow fluid ultrafiltration retaining the fibril structure and to modify the biomechanical properties of the biomaterials. The nanostructuring method used here would induce a series of complex interfibrillar changes at the nanometrical scale (nanostructuring) that could in turn modify the properties of this biomaterial. The dehydration of the fibrin–agarose biomaterials was carried out since it has been reported that small amounts of water can contribute to slippage during the rheological measurements (Shin et al., 2002).

For nanostructuring, samples were transferred to a specific polycarbonate chamber in which 4–6 layers of sterile Whatman 3MM

absorbent paper were put above and below the sample to facilitate dehydration of the artificial tissue. To prevent the stromal construct sticking to the paper layers, a filter nylon membrane (0.4µm pore size) was settled between both faces of the sample and the paper layers. Then, a flat crystal surface was set on top of the system and a total of 1000Pa of pressure was applied to compress the bioengineered tissues. Figure 3.4 shows a schematic representation of the nanostructuring bioreactor. The process was carried out for 3–5min, and then the nanostructured tissues were removed from the chamber and maintained in PBS until the moment of the analysis.

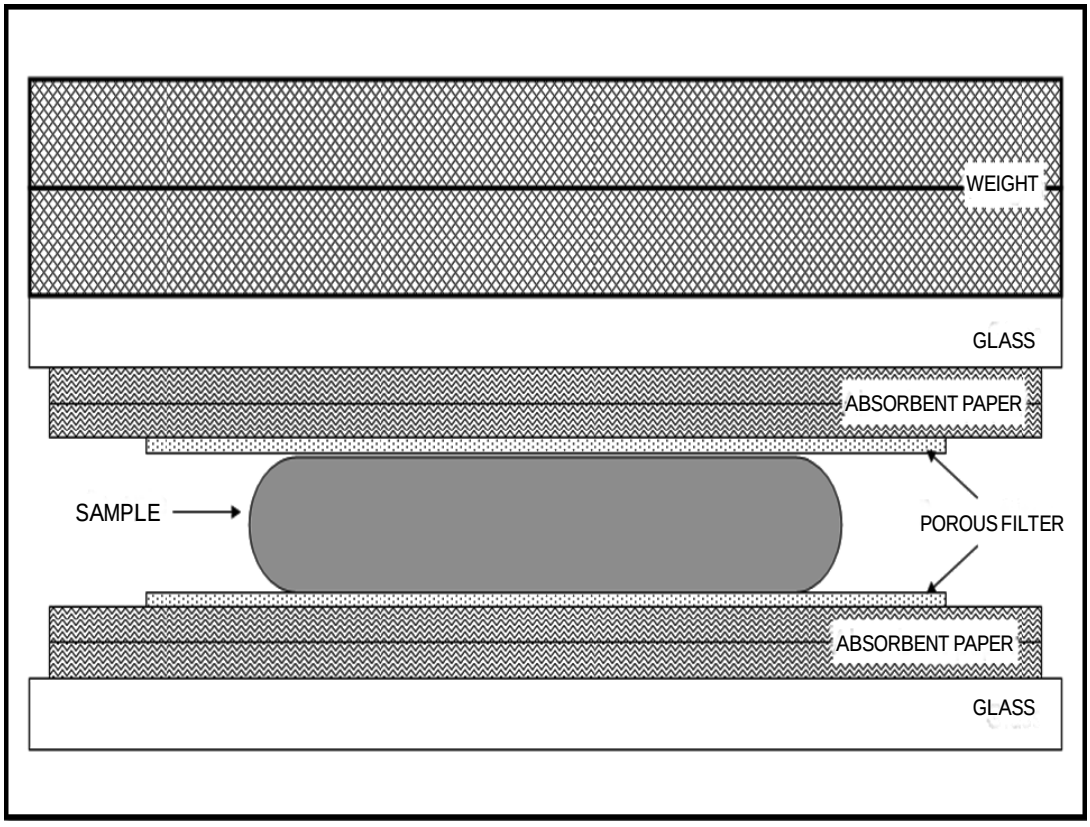

Figure 3.4. Squematic representation of the nanostructuring method.

All corneal construct samples (approximately 0.5 mm thick) were generated and analyzed in triplicate.

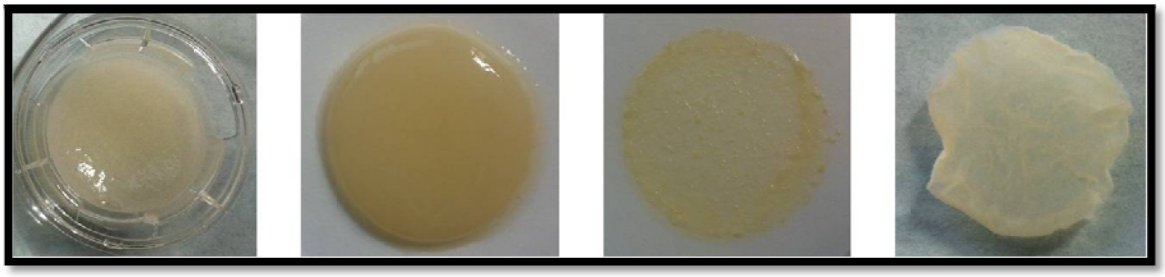

Figure 3.5. Steps of the nanostructuring method

As controls, ten fresh porcine corneas were obtained from adult pigs immediately after their death at a local slaughterhouse. The eyes selected for the study had integral corneal surface with a horizontal corneal diameter of 12–14mm. The native porcine cornea was removed using a 16mm corneal trephine. The corneas were washed thoroughly in PBS. All ten control corneas were subjected to the same mechanical tests as the bioengineered artificial corneal constructs.

Histological analysis of the extracellular matrix. For light-microscopy analysis, samples corresponding to N-NCCs and NCCs were fixed in 4% formaldehyde, dehydrated in ethanol series, and embedded in paraffin. Then, 4μm thick sections were cut. For the analysis of collagen synthesis and deposition by the cells immersed in the hydrogels, deparaffinized tissue sections were stained by using picrosirius histochemical methods. In short, sections were stained for 30min in 0.2% picrosirius solution (Sirius Red F3BA, BDH Laboratory Supplies, UK, in saturated picric acid) and counterstained with Harris's hematoxylin for 5 min at room temperature. After being washed in water, the sections were dehydrated through an ethanol and xylene series and covered using mounting medium.

To identify the synthesis of proteoglycans in the bioengineered corneal stroma, safranin O histochemistry was used. In this case, deparaffinized tissue sections were stained in Weigert's hematoxylin for 10min and washed in water for 10min. Then, the samples were counterstained in aqueous fast

green for 5min, rinsed in 1% acetic acid and stained in 0.1% safranin O for 5min. Finally, slides were dehydrated in alcohol series and xylene and covered using mounting medium.

Rheological measurements. Measurements of the rheological quantities of interest were performed for all NCCs and N-NCCs and, also, for the porcine control cornea. A controlled shear stress rheometer (Bohlin CS-10, UK) was used. The measuring cell (Bohlin PP4-40) had a plate–plate geometry (the diameter of the rotor plate was 40 mm) with a gap thickness of 1 mm. All measurements were performed at 37.0 ± 0.1 ◦C. During the measurements, the samples were maintained in a water-vapor-saturated atmosphere to avoid drying. In addition, undesired wall-slip phenomena were prevented by using roughened plates, as recommended by Barnes (1995).

Figure 3.6. Bohlin CS-10 rheometer during measurements

First, steady-state shear stress versus shear rate (σ versus $\frac{d\gamma}{dt}$) experiments were conducted. A shear stress ramp was applied to record the corresponding shear rate at time intervals of 3s. The rheograms showed a plastic behavior, characterized by the yield stress required to provoke the viscous deformation of the materials studied. Hence the yield stress σ_y was determined by fitting the $\sigma - \frac{d\gamma}{dt}$ data in the post-yield regime to the Bingham equation

$$\sigma = \sigma_y + \eta \frac{d\gamma}{dt} \qquad (3.1)$$

Oscillatory tests were also performed by applying a sinusoidal shear stress ($\sigma = \sigma_0 sin\omega t$) and recording the subsequent sinusoidal strain ($\gamma = \gamma_0 \sin(\omega t + \delta)$). The constitutive equation for linear viscoelasticity can be expressed as (Macosko, 1994)

$$\sigma^*(\omega, t) = G^*(\omega)\gamma^*(\omega, t) \qquad (3.2)$$

where $G^*(\omega)$ is the complex rigidity modulus, σ^* is the oscillatory shear stress, and γ^* is the oscillatory shear strain in complex notation. The real part of the rigidity modulus, G' is the elastic or storage modulus, and its imaginary part, G'', is the viscous or loss modulus. Equation (3.2) assumes a linear dependence between $\sigma^*$and γ^*, which is usually accomplished for low stress amplitude values into the so-called viscoelastic linear region (VLR).

Two kinds of oscillatory measurement were performed:

(i) *VLR determination*. A stress of increasing amplitude (σ_0) and constant frequency (ω= 1 Hz) was applied to the sample: G' and G'' were constant (amplitude independent) until a critical σ_0 was reached. This stress corresponds to the upper limit of the VLR.

(ii) *Oscillograms*. A stress of amplitude 2Pa (within the VLR) was applied, with frequencies ranging between 0.1 and 10Hz, and both G' and G'' were recorded as a function of ω.

Statistical analysis. As normality (and homogeneity of variance) assumptions were not satisfied, non-parametric tests were used. To test the significance of observed differences between the study groups, the Kruskal–Wallis one-way analysis of variance by ranks (K–W) and the Mann–Whitney *U* test (M–W) were applied. A value of $p<0.05$ was considered to be statistically significant. The statistical analysis was performed using the SPSS 20.0 software package (Chicago, USA).

The Rho-de-Spearman correlation coefficient (ρ) was also determined between all the parameters measured in this study.

RESULTS AND DISCUSSION

Sequential analysis of extracellular matrix deposition

Histochemical analysis of the bioengineered cornea stromas using picrosirius staining revealed the presence of neoformed collagen fibrils after seven weeks of development in culture for fibrin scaffolds, for both the N-NCCs and the NCCs. Stromas with 0.1% agarose concentrations showed no collagen deposition for the entire study period (eight weeks of development in culture). Illustrative images of the sample analysis using picrosirius staining are shown in Figure 3.7. However, proteoglycans staining of the corneal substitutes analyzed in this work using safranin O histochemistry proved completely negative for all samples, suggesting that these components were absent from the different tissue constructs.

Rheological properties

Steady-state measurements. The existence of yield stress or minimum stress needed for the corneal constructs to start to flow was observed. The data in the post-yield regime were fitted to equation (3.1). From the intercept

of this fitting, the yield stress of each material was determined. Figure 3.8 shows the yield stress values corresponding to the different bioengineered corneal-stroma substitutes (N-NCCs and NCCs) and to the control native cornea.

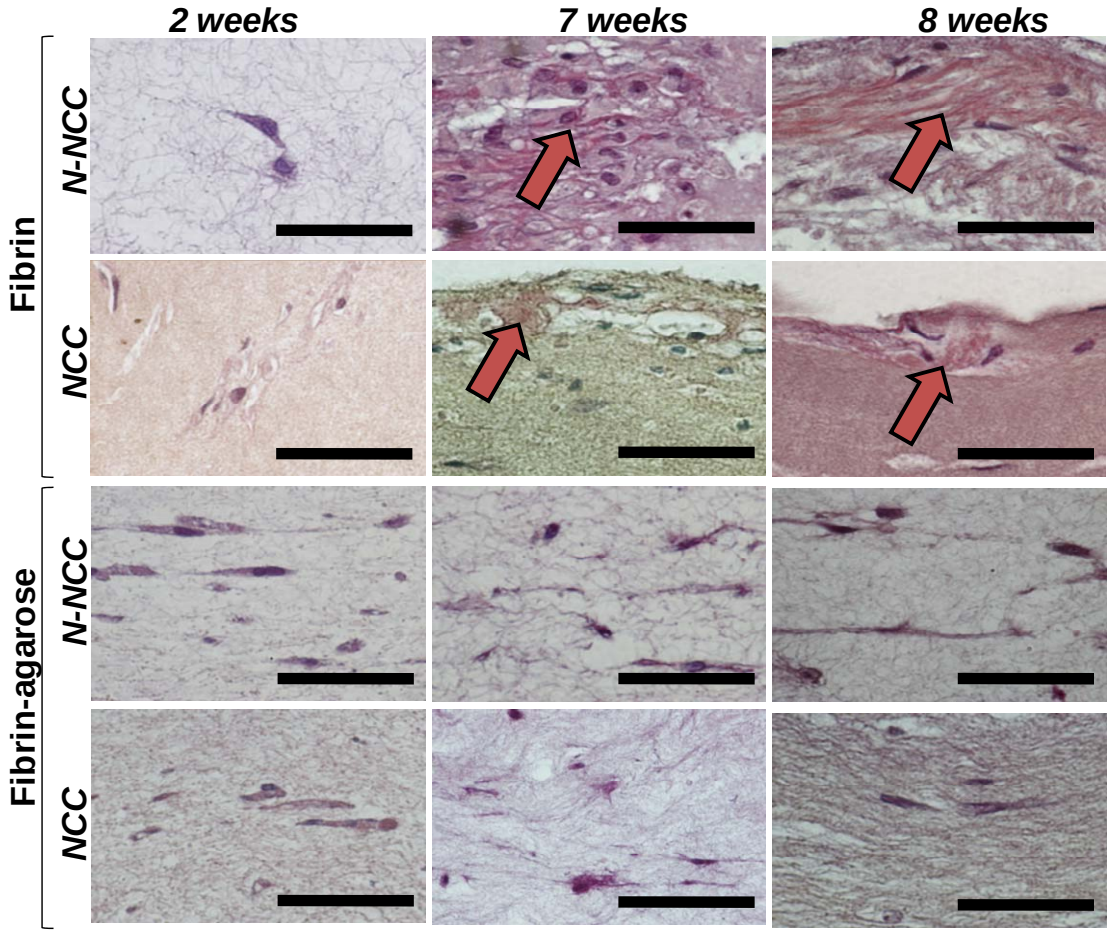

Figure 3.7. Histochemical analysis of collagen synthesis as determined by picrosirius staining in the different samples analyzed in the present work after two, seven and eight weeks of development in culture. Percentages correspond to the agarose concentration in the fibrin-agarose scaffolds. NCC: nanostructured cornea constructs; N-NCC: non-nanostructured cornea constructs. Arrows indicate collagen deposition. Bars size: 50µm.

This evaluation was made as a function of the culture time. No degradation was detected in the bioengineered corneal samples for culture times of over three weeks.

As shown in the Figure 3.9, the yield stress of the N-NCCs decreased with increasing time in culture (ρ<0). This result is confirmed by the Rho-de-Spearman correlation coefficient, that, for the fibrin constructs was ρ=-0.520 whereas for the fibrin-agarose was ρ=-0.756, in both cases statistically significant differences (p<0.001) being found. For the fibrin NCCs, no significant correlation was found between the yield stress and the time in culture (ρ=0.071, p=0.328). Contrary to what happens for the fibrin-agarose N-NCCs, for the nanostructured samples a positive correlation was found between the yield stress and the time in culture (ρ=567, p<0.001), i.e. the yield stress increases with increasing time in culture (e.g., it varies from 4.67± 0.23Pa for the first week until 28.91 ±1.44Pa for seventh week in culture). Table 3.1 shows the correlation coefficients found for the time in culture and the rheological parameters studied in this work.

Rho-de-Spearman correlation coefficient		***Yield stress*** (σ_y)	***Elastic modulus*** (G')	***Viscous modulus*** (G'')
Fibrin	**N-NCC**	-0.520 *p<0.001*	-0.727 *p<0.001*	-0.470 *p<0.001*
	NCC	0.071 *p=0.328*	-0.378 *p<0.001*	-0.4998 *p<0.001*
Fibrin-agarose	**N-NCC**	-0.756 *p<0.001*	0.456 *p<0.001*	0.614 *p<0.001*
	NCC	0.567 *p<0.001*	0.511 *p<0.001*	0.066 *p=0.360*

Table 3.1. Rho-de-Spearman coefficient found for the correlation between time in culture and rheological parameters.

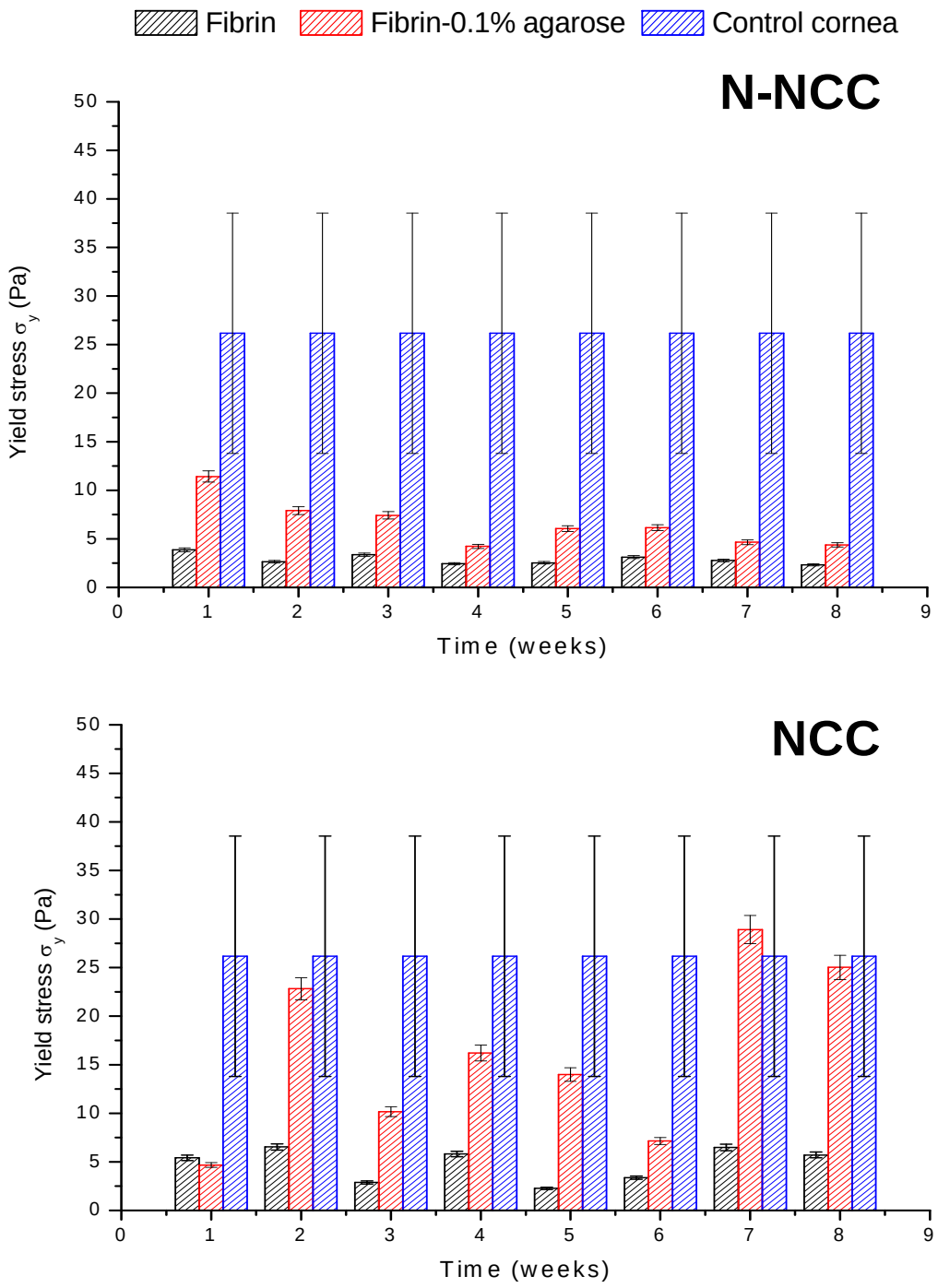

Figure 3.8. Yield stress values corresponding to the different bioengineered corneal-stroma substitutes.

When comparing these values of the corneal constructs, non-nanostructured and nanostructured, with the yield stress values of the porcine control cornea, it was found that the NCCs with 0.1% agarose concentration were the ones that most exactly resembled the native tissue yield stress, especially after four weeks of development in culture. Specifically, the fibrin with 0.1% agarose concentration NCCs after four to eight weeks in culture had yield stress values very close to that of the porcine control cornea, except for the sixth week. This observation might be explained by interaction between the agarose and the fibrin gel that influences the properties of the biomaterial (Ionescu et al., 2010), since the nanostructuring technique dehydrated the fibrin–agarose constructs, making them more resistant. In this case, nanostructured bioengineered corneas could be more stiff than N-NCCs due to the lack of water within the fibril mesh and due to the existence of complex three dimensional interactions among the fibrils as a consequence of the nanostructuring process. The nanostructuring process is therefore able to irreversibly modify the biomaterial used for the generation of an artificial tissue and to increase the elasticity and resistance of this tissue. These properties are essential for the proper function of the artificial tissue once implanted in the human cornea.

Oscillatory measurements. Studies of the elastic (G') and viscous (G'') moduli were also performed on the corneal stroma equivalents and native porcine cornea. In Figure 3.9, the oscillogram for the fibrin NCC after five weeks in culture is displayed as an example of the oscillograms determined for all the samples (but not all are shown for brevity). The elastic and viscous moduli of each sample were determined at the frequency of 1Hz (with shear amplitudes into the VLR).

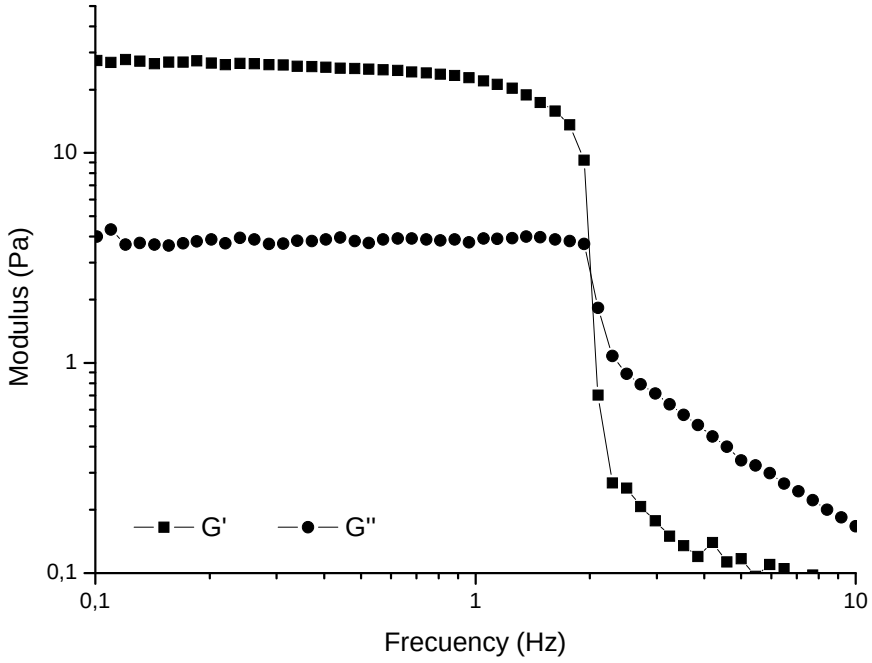

Figure 3.9. Oscillogram example for the fibrin NCC after five weeks in culture. The elastic (G') and the viscous (G'') moduli of each sample were determined at the frecuency of 1 Hz (with shear amplitudes into the VLR)

Previous works have determined the rheological behavior of strips of cornea by performing normal (or compressive) stress–strain tests for determining the values of the Young modulus (Hoeltzel et al., 1992; Nash et al., 1982; Andreassen et al., 1980; Nyquist, 1968), whereas others have measured the Young modulus of the cornea in intact eyes (Hjortdal and Koch-Jensen, 1992; Jue and Maurice, 1986). Due to the viscoelastic behavior of the cornea (Kobayashi et al., 1973), its mechanical properties cannot be fully described by a single elastic parameter such as the Young modulus. Until now, only in a recent work of Grobe and Reichl (2011) have the shear viscoelastic moduli of human cornea been determined. In their work, the elastic (storage) modulus of a human corneal equivalent based on collagen was 1500Pa and the viscous (loss) modulus 125Pa, but this large variation in

values is due to the method of testing (the measurement parameters differ from the ones used in the present study).

The variation of the elastic and viscous moduli values with time in culture, both for the N-NCCs (top) and NCCs (bottom), as for the native porcine cornea is shown in Figures 3.10 and 3.11, respectively.

In the present study, for all cases analyzed, G' was higher than G'' (M–W $p < 0.001$), at a frequency of 1Hz, suggesting that these biomaterials are more elastic than viscous. It can be seen that, for both types of biomaterial (NCCs and N-NCCs), in the first stages of development in culture, the corneal stroma substitutes show almost constant G' values, contrary to what happens for times longer than five weeks in culture, for which these values decrease for the fibrin substitute (N-NCC: ρ=-0.727, p<0.001; NCC: ρ=-0.378, p<0.001) and increase for the fibrin-agarose one (N-NCC:ρ=0.456, p<0.001; NCC: ρ=0.511, p<0.001). The elastic modulus values of the NCCs were three to six times higher than those of the N-NCCs (M–W p <0.001). Regarding the viscous behavior of the samples studied in this work, G'' had almost constant values in the case of the N-NCCs (with a mean value of 3.09±0.84 Pa), while, for the NCCs, the G'' values were two to six times higher (M–W $p < 0.001$), varying from 6.44±0.32Pa to 19.30±1.05Pa. From table 3.1 it can be seen that for the fibrin samples, the correlations with the elastic and viscous moduli were negative for both N-NCCs and NCCs, while for the fibrin-agarose the same correlations were found to be positive. The differences found were statistical significant.

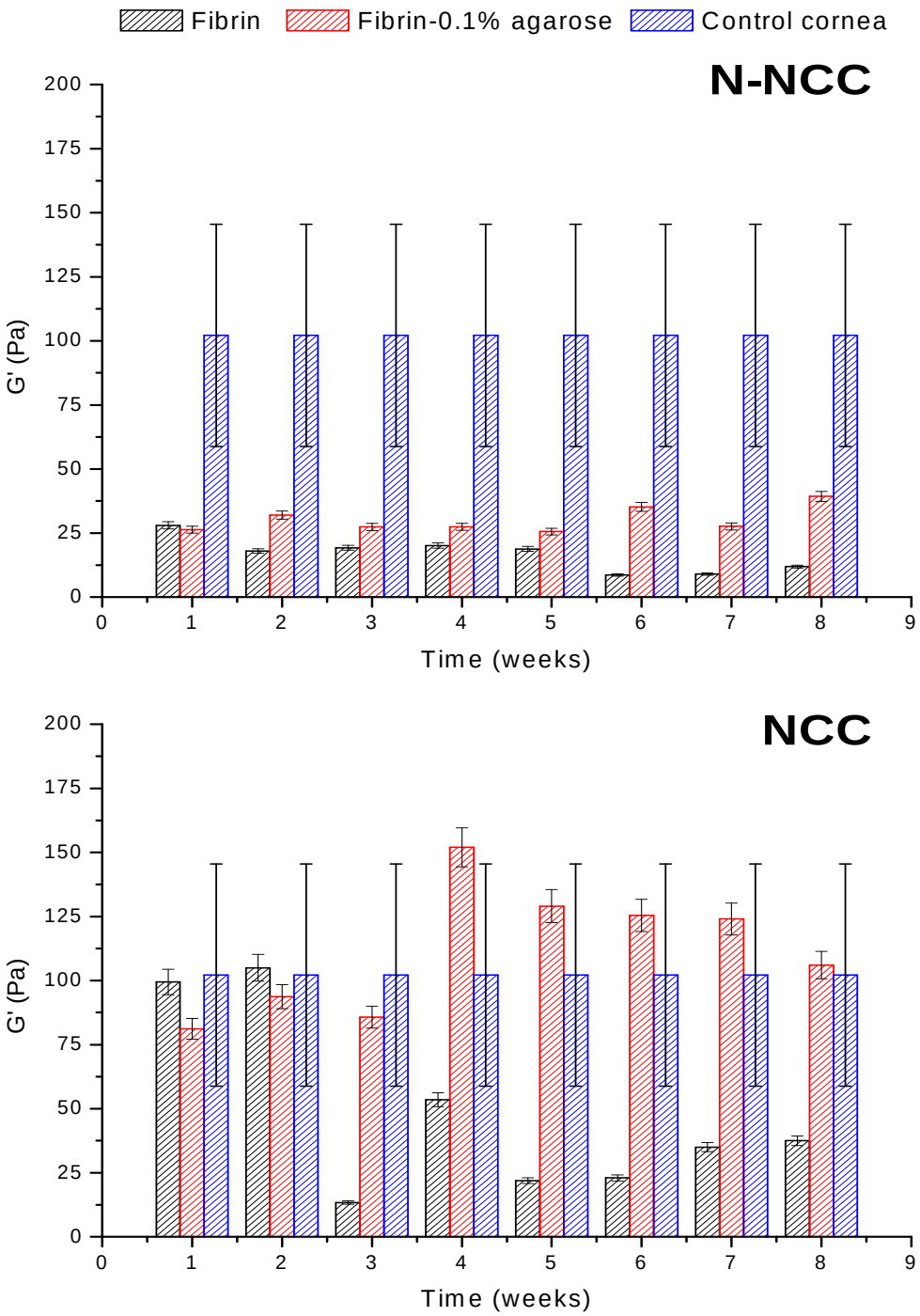

Figure 3.10. Temporal variation of elastic modulus values of the N-NCCs (top) and NCCs (bottom), and of the control porcine cornea.

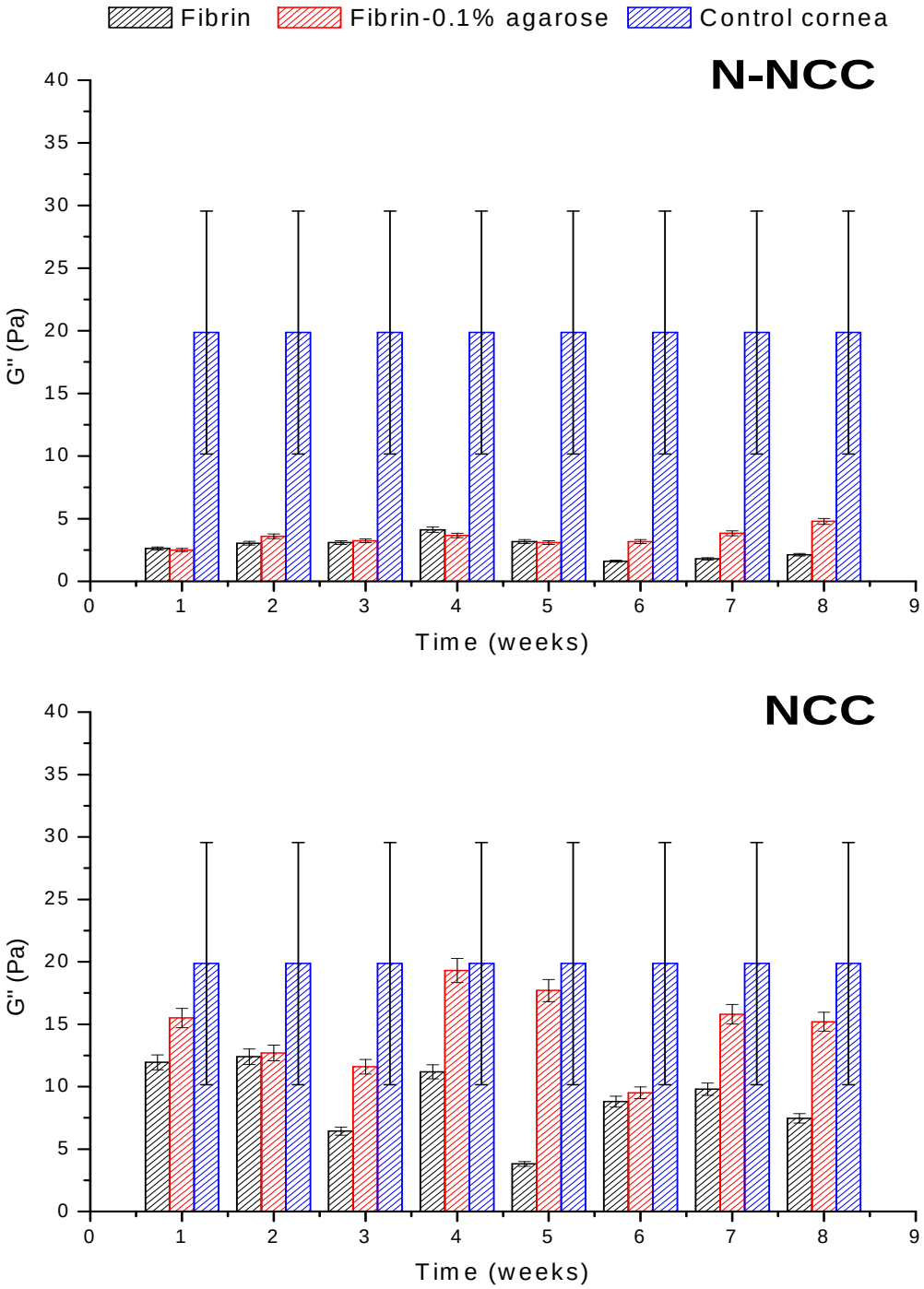

Figure 3.11. Temporal variation of viscous modulus values of the N-NCCs (top) and NCCs (bottom), and of the control porcine cornea.

In addition, Figures 3.10 and 3.11 show that the N-NCCs did not accomplish the elasticity and viscosity displayed by the ex vivo native porcine cornea. Moreover, the fibrin NCCs had elasticity values in the range of the control cornea for the first two weeks in culture. For longer periods of time, these values rapidly decreased, reaching only 25% of the elastic modulus values of the porcine cornea. The fibrin-agarose NCCs displayed elasticity values similar to those of the control corneal and even higher than the native tissue itself in the fourth week in culture. Whereas the viscosity values are concerned, a similar behavior was observed. In this case, the viscous modulus values for the fibrin NCCs reached 50% of the viscosity values of the control cornea after 2 weeks in culture, while for the fibrin-agarose NCCs the viscosity values were in the values range of the native tissue during the entire time period analyzed in the present work.

The large variation in the moduli values determined in these studies may be due to the three-dimensional structure of the tissue after the nanostructuring process. Note that the nanostructuring method refers to a structural change involving the generation of links less than one micron in size between the fibrin fibers and the molecules of agarose. This process includes dehydration via mechanical compression that changes the elasticity of the construct (Enrione et al., 2010), and thus allows the generation of a novel biomaterial with improved/optimal levels of consistency and flexibility that cannot be attained naturally.

As stated above, the highest values of G' and G'' were found for the NCCs with a small concentration of agarose (0.1%) supporting the idea that the agarose content and nanostructuring technique had an important role in the changes that occurred in the viscoelasticity of the artificial corneal constructs. These values were determined for an oscillatory shear stress of 1 Hz, well within the order of the natural oscillations of the human cornea. By contrast, the elastic and viscous modulus values of the human cornea reported by Wang and collaborators (Wang et al., 1996) were $(1.8\pm0.4)\ 10^6$ Pa and $(1.5\pm0.4)\cdot10^6$ Pa, respectively. However, it should be noted that in this

latter work the exciting frequency applied by ultrasound was as high as 2.25MHz, a value far from the natural mechanical frequencies of the human eye.

The statistical analysis determined significant differences when comparing the N-NCCs and the NCCs for both types of bioengineered human corneas (fibrin and fibrin-agarose) ($p<0.001$), suggesting that the agarose concentration and nanostructuring technique can notably influence the biomechanical properties of the biomaterials. These results agree with the findings of Orwin and collaborators (Orwin et al., 2003), who stated that changes in the viscoelastic behavior of the corneal stroma can be influenced by the matrix composition and culture time. Also, Haugh and collaborators (Haugh et al., 2012) showed that the nanostructuring technique (plastic compression) significantly increased the compressive properties of fibrin gels without impairing cellular viability and subsequent extracellular matrix synthesis. The authors concluded that this method of generation of bioengineered tissues may provide a useful tool in tissue engineering applications that require an increase in gel density and mechanical properties prior to implantation or at the inset *in vitro* culture.

In previous studies, non-nanostructured fibrin with 0.1% agarose biomaterials were used for the development of a bioengineered animal (Alaminos et al., 2006) and human cornea (González-Andrades et al. 2009; Ionescu et al., 2010; Cardona et al., 2011). In addition, this biomaterial has been efficiently used for the development of other tissue types in the laboratory, including oral mucosa (Sanchez-Quevedo et al., 2007; Garzón et al., 2009), periodontal tissues (Garzón et al., 2009) and even bone, cartilage, adipose, and neural tissues (Nieto-Aguilar et al., 2011). Data obtained in our study showed that the nanostructured construct of fibrin with 0.1% agarose had an intriguing time-dependent rheological behavior. In this regard, the properties of this type of corneal substitute were similar to those of the fibrin substitutes in the first two weeks of culture (lower elastic modulus), whilst, for larger periods of time in culture, this rheological behavior resembled that

of the native tissue (higher elastic modulus) (Figure 3.11). Besides, fibrin with 0.1% agarose concentration displayed elastic and viscous modulus values in the values range of the native porcine tissue for all times of culture studied, except for the sixth week in culture in the case of the viscous modulus. This result suggests that the nanostructured fibrin with 0.1% agarose biomaterial is a proper substitute for corneal application and regeneration. In addition, the nanostructuring technique represents a step forward in the generation of corneal substitutes for clinical application by means of tissue engineering, since the NCCs have more appropriate rheological characteristics, due to their similarity with those of the native porcine cornea chosen as control, than the N-NCCs.

However, note that the principal functions of the human cornea are the refraction and transmission of light. Therefore, for these bioengineered corneas to be potentially useful from a clinical standpoint, their optical quality and levels of transparency need to be additionally determined.

4. NEW METHOD FOR OPTICAL QUALITY CONTROL OF BIOENGINEERED CORNEAS

BACKGROUND

Sight has been a primary factor of advantage in natural selection and evolution, thereby conferring great importance to proper operation of the visual system and, above all, the maintenance of corneal transparency (Fernald, 2000). The cornea's primary physiologic functions are transmission and refraction of incident light as well as protection of the intraocular structures from trauma and pathogens (Bennett and Weissman, 2004). Also, the cornea is responsible for more than 60% of the total refractive power of the eye, playing a vital part in the process of focusing incoming light onto the retina for posterior visual processing (Land and Fernald, 1992).

To fulfill an optimal vision situation, the cornea must efficiently transmit incident light by maintaining its transparency. If the transparency of a native cornea cannot be maintained at a minimum functional level for the patient, the corneal transplantation is usually the next step toward improvement of the optical quality of patient's visual system. Once transplanted, it has been reported that the major cause of corneal graft failure is allograft rejection (Barandan-Rafii et al., 2007; Sangwan et al., 2005, Alldredge et al., 1981).

Using tissue engineering development techniques, several biomaterials have been used as substitutes of the corneal stroma, including collagen (Torbet et al., 2007; Orwin and Hubel, 2000; Minami et al., 1993;), chitosan (Chen et al., 2005), polyglycolic acid (Hu et al., 2005), and fibrin (Han et al., 2002).

Fibrin is an important biomaterial used for many tissue engineering applications (Eyrich et al., 2007; Farhat et al., 2006; Willerth et al., 2006;

Birla et al., 2005; Cox et al., 2004; Yamada et al, 2003;). As shown in Chapter 3, it has been used together with a small amount of agarose to succesfully develop a human cornea substitute with rheological properties similar to the ones of a native cornea.

Another important biomaterial with a vast range of applications both in vivo and in vitro is collagen, one of the major components of the human extracellular matrix and subsequently one of the most abundant structural proteins within connective tissue. In the specific case of the cornea, the collagen is found within the stroma, which lies below the corneal epithelium, and comprises predominantly type I and V collagens (Newsome et al., 1982). In the stroma, collagen fibrils are highly aligned and packed in tight sheets. This high level of organization of the collagen fibrils it is directly correlated with the transparency of the cornea (Maurice, 1957). If used as a substrate, it has been shown that the collagen is highly compatible with low levels of immunogenicity (Bell et al., 1979), making it an excellent structure for tissue engineering applications. In a recent study, Mi and collaborators (Mi et al., 2010a), showed that compressed collagen scaffold embedded with keratocytes produced a novel, thin, mechanically strong, transparent, and potentially transplantable membrane. Such a scaffold was found to facilitate the survival, proliferation, stratification, and differentiation of limbal epithelial cells into corneal epithelial cells, thereby demonstrating the suitability of this new substrate for tissue engineering ocular surface models.

The optical characterization of these biomaterials is essential to ensure their proper functionality since they are intended to replace the principal refractive component of the eye and, to a great extent, the main responsible of image-forming. One of the most common problems found when assessing optical quality of biomaterials is that specific equipment, such as light detectors, spectrophotometers, a laser or a homogeneous light source, are not available in the biological sciences departments where artificial tissues are generated. In this case, proper measurements of the transmitted/reflected/absorbed/scattered incident light throughout the

samples are impossible to perform. In some cases, the assessment of tissue transparency is made by simply placing the sample on top of a reference image and visually estimating the similarities with a control sample. All observations are subjective and observer-dependent and no quantitative data are provided (Fu et al., 2010; Proulx et al., 2010; Xu et al., 2008). In this sense, it becomes of high interest the development of a simple, yet precise method, which can be easily implemented in the biological laboratories and which will allow the researchers to report quantitative and physically relevant data on the optical quality of their bioengineered tissues.

As a first intent to overcome (address) this issue, we developed, using a digital single lens reflex (DSLR) camera, a backlight Liquid Cristal Display, digital bar patterns and a subsequent image analysis, a non-invasive method, based on the determination of the Contrast Transfer Function (CTF), for evaluating the optical quality of artificial human corneal tissues.

The Contrast Transfer Function (CTF) is defined as a measure of contrast between adjacent objects, and provides information on how faithfully an optical system reproduces (or transfers) details from the object to the image of the same object produced by the optical system. Thus, it represents an important measurement tool of the optical quality of an imaging system. In our study, the optical system is represented by the bioengineered corneal constructs generated by tissue engineering.

Therefore, the aim of this study was to develop an optical method for the evaluation of the optical quality and to evaluate corneal stroma substitutes based on fibrin, fibrin-agarose and collagen in order to determine their suitability for potential clinical use.

MATERIALS AND METHODS

Construction of corneal equivalents with a fibrin-agarose stromal substitutes.

Corneal stroma substitutes consisted of cultured human keratocytes entrapped in (1) a gel of human fibrin, and (2) gel of human fibrin with 0.1% type VII agarose. They were generated following the method described on Chapter 3.

Samples of the fibrin-agarose corneal constructs were studied after 2 and 4 weeks of development in culture.

Construction of the collagen gels.

Stromal keratocytes were isolated from human corneas stripped of both epithelium and endothelium. After the corneal epithelial and endothelial cells had been dissected, the remaining stroma was cut into small fragments and washed in a solution prepared with 10ml of Dulbecco's minimal essential medium and Ham's F12 medium (DMEM/F12, 1:1) and 20mg of collagenase (Sigma Aldrich/Gibco) during 3 hours at 37°C in 5% CO_2. The culture of the corneal cells was performed using a trypsin (Sigma Aldrich/Gibco) solution at 37°C for 10 minutes. Once the cells had been harvested by centrifugation, stromal keratocytes were cultured in DMEM/F12 medium and incubated at 37C in 5% CO_2 under standard culture conditions. The culture medium was changed every 3 days.

Acellular and cellular collagen gels were generated as previously described by Brown and collaborators (Brown et al., 2005) with some modifications. The acellular gels were prepared by neutralising 2 ml sterile rat-tail type I collagen (2.2 mg/ml in 0.6% acetic acid, First Link Ltd) in 0.5

ml modified Eagle's minimum essential medium (Fisher Scientific), 0 and 0.25 ml 1 M sodium hydroxide (Fisher Scientific). In the case of the cellular gels, 0.077mL keratocytes suspended in basal medium ($2.6 \cdot 10^6$ cells/mL) were added to the previous mixture. The solutions were gently mixed and cast into circular moulds (aprox. 2.2cm diameter) prior to gelling at 37°C, 5% CO_2 for 30 min.

Following the initial setting of the gels, they were then subsequently compacted by a combination of compression and dehydration. Specifically, collagen gel compaction was achieved by placing a metallic grid on a double layer of absorbent paper and on top of it a layer of nylon mesh (50-µm mesh size). The collagen gel was then placed on the nylon mesh, covered with a second nylon mesh, and loaded with a 134g weight for different time periods (1 and 3 min) at room temperature, leading to the formation of a flat collagen sheet protected between two nylon meshes (Figure 4.1) (Feng et al., 2012).

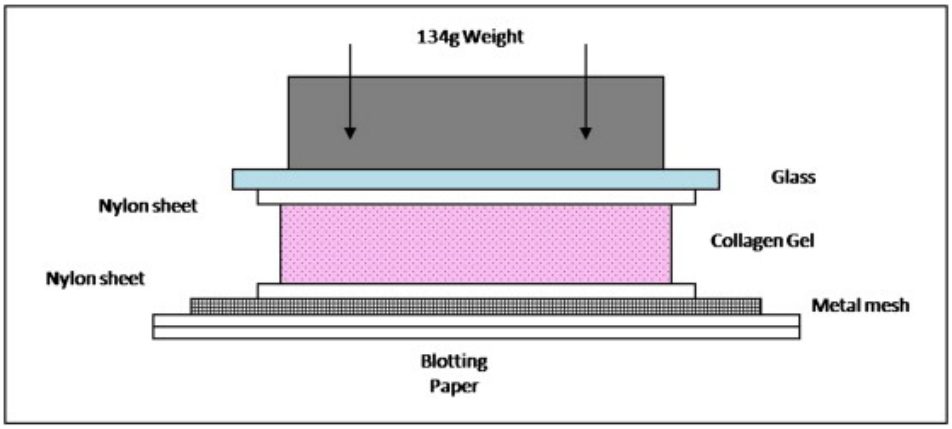

Figure 4.1. Manufacture of compressed collagen gels (Feng et al., 2012).

After compression, gels were kept in serum free media (DMEM supplemented with antibiotics (1%), ascorbic acid (0.25mg/ml), Insulin Transferin Selenium supplement (1%), glutamine (1%) and glucose (1mg/ml) at 37C, 5% CO_2. The compressed collagen gels were left to develop in culture during 10 days before optical measurements were performed.

All the manufacturing processes, including the generation and the development of the collagen gels, as well as all optical analysis were performed at the Laboratory of Stem Cells and Nanomaterials at the University of Reading, UK.

It should be mentioned that, for the fibrin and fibrin-agarose corneal constructs the use of the CTF method was aimed to determine differences in the optical quality due to matrix composition and time of development in culture (two and four weeks), whereas for the collagen gel, these differences should be accounted for different compression time (one and three minutes) and the presence or absence of corneal cells in the gel.

Experimental setup.

For the optical evaluation of the bioengineered corneal constructs, five digital bar patterns with increasing frequencies (0.20, 0.40, 0.65, 1.00 and 2.00 cycles/mm) were designed and displayed on a LCD screen (Figure 4.2)

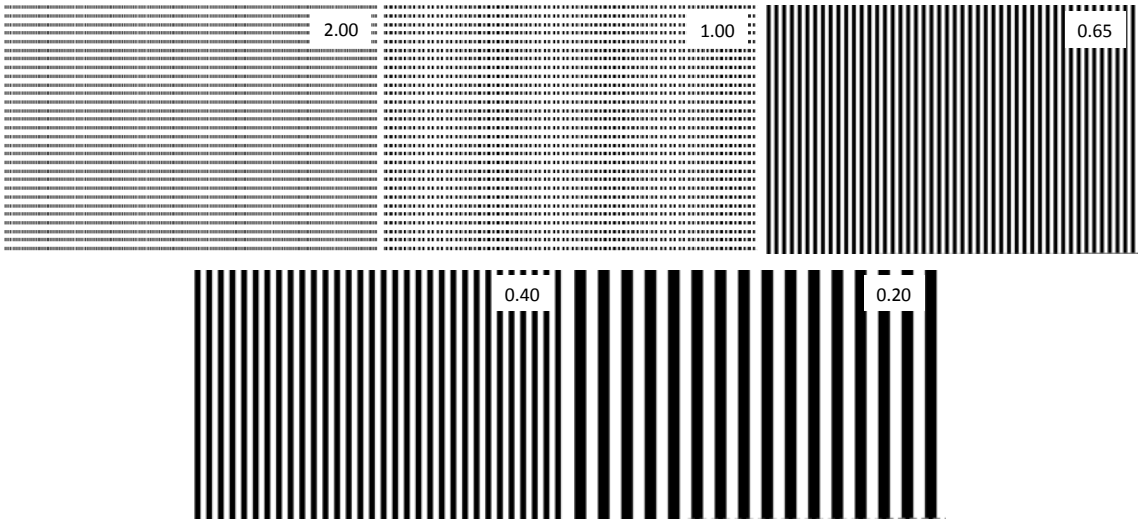

Figure 4.2. Digital bar patterns with increasing frequencies used to determine the CTF.

Digital images of all three types of human corneal substitutes were obtained using a Digital Single Lens Reflex (DSLR) Camera. Prior to digital image acquisition, the photographic camera was white balance calibrated using a white/gray card (QP101 Calibration Card, QPCard, Sweden). For digital imaging, all samples were placed on transparent holders and positioned in a central position on top of the LCD screen. The digital camera was placed at approximately 30cm from the samples, in a completely dark room. The experimental set-up is schematically shown in Figure 4.3. The camera mode was set to manual, and all shooting parameters (ISO 200, exposure time 1/125, F_{stop} 5.6) were maintained constant throughout the whole process, in order to ensure proper comparison between the samples. All measurements were performed by the same user in order to avoid experimenter-related differences. Ten consecutive pictures for each bar pattern, both with and without the samples placed on top, were captured and stored as an uncompressed file system.

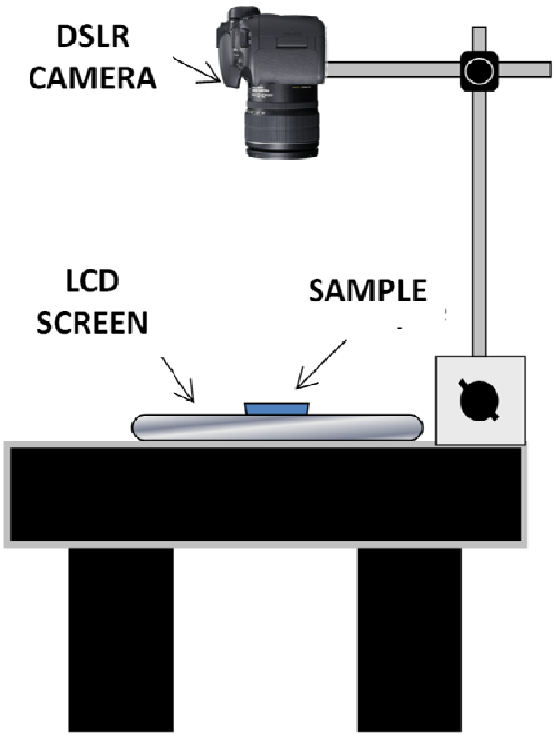

Figure 4.3. Schematic representation of the experimental setup for the CTF data acquisition.

For each photograph, a central area of 450x200 pixels was manually selected, a plot profile was carried out and the minimum (I_{min}) and maximum (I_{max}) gray values were determined (Figure 4.4). The results obtained for the 10 images were averaged.

Using the maximum and minimum gray values obtained, the input (i) and output (o) modulations were calculated as

$$Modulation_i = \frac{I_{i,max} - I_{i,min}}{I_{i,max} + I_{i,min}}$$

$$Modulation_o = \frac{I_{o,max} - I_{o,min}}{I_{o,max} + I_{o,min}}$$

Consequently, the CTF is given by

$$CTF = \frac{Modulation_o}{Modulation_i}$$

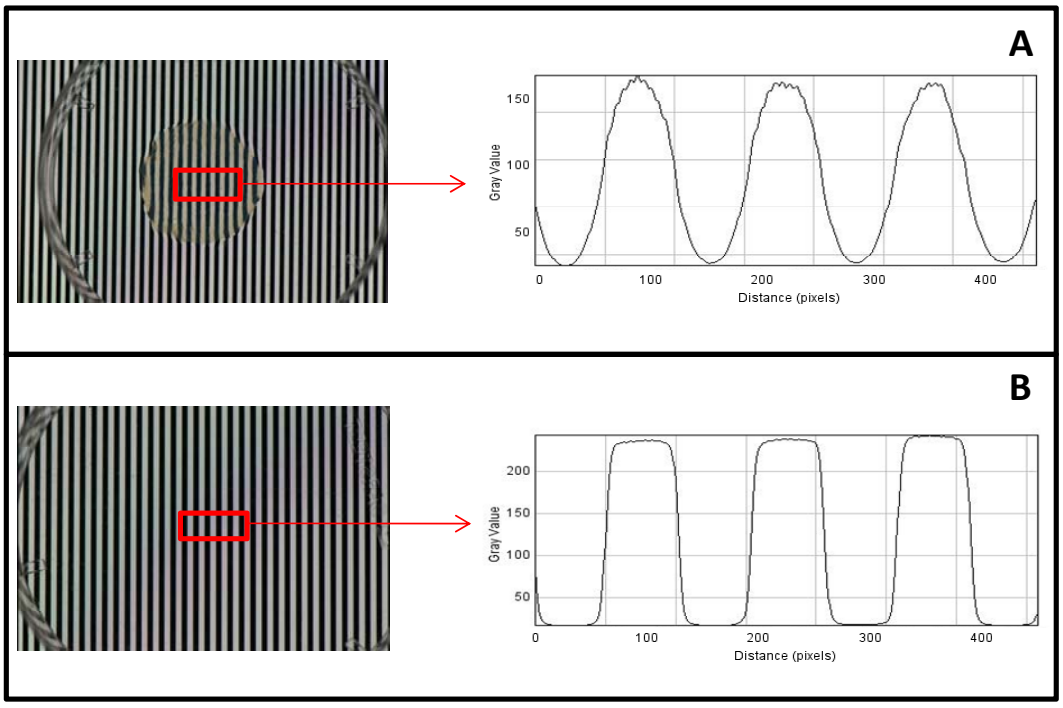

Figure 4.4. Example of the images obtained and the area considered for the CTF values calculation: A. Output modulation; B. Input modulation.

All image analysis steps were performed using the public domain software ImageJ (NIH, Bethesda USA).

Statistical analysis

To study the variations in the CTF values, we used the Mann-Whitney U statistical test, a non-parametric test that enables the pair-wise comparison of two distributions. This statistical test was used because the samples do not fulfill the test of homogeneity of variance. A significance value below 5% was considered as statistically significant

To determine the level of similarity between two different distributions, the VAF (variance accounting for) coefficient with Cauchy-Schwarz's inequality was used as follows:

$$VAF = \frac{(\sum_k a_k b_k)^2}{(\sum_k a_k^2)(\sum_k b_k^2)}$$

where a_k is the value of each absorption or scattering (for each wavelength) and b_k is the equivalent for another measurement. The closer this coefficient gets to unity (100%), the more similar the curves are.

RESULTS AND DISCUSSION

The non-invasive method and experimental set-up proposed allow evaluating the optical quality of bioengineered corneal constructs without modifying the conditions of culture. The newly proposed CTF-based method provides indirect control of tissue development, by addressing the optical quality of the bioengineered corneal constructs depending on their time of development in culture and matrix composition. Also, it is suitable to evaluate different compression times for collagen gels, differentiating, from an optical point of view, between cellular and acellular collagen constructs.

Study of the fibrin and fibrin-agarose human corneal substitutes.

Figure 4.5 shows the CTF values as a function of the frequency (cycles/mm) for the a) fibrin and b) fibrin–0.1% agarose corneal substitutes after 2 and 4 weeks of development in culture. Table 4.1 presents the results of the VAF comparisons between fibrin and fibrin–0.1% agarose constructs, both after the two periods of time culture considered.

The values of the contrast transfer function decrease with increasing frequency in all cases. It is important to highlight that, from 0.65 cycles/mm on, the CTF values are reduced by approximately 70% with respect to the values recorded for 0.2 cycles/mm. This severe drop is expected to critically affect the optical quality of the system. The area under the graph is an indirect measure of the magnitude of the CTF values for all frequencies, and is an accurate tool for comparison between different types of constructs and/or development periods. For both the fibrin and the fibrin–0.1% agarose constructs, although the behavior of the CTF graph is almost identical (VAF≥99.47% in all cases) (Table 4.1), for the second week of development the area under the graph is higher than for the fourth week, although the values are very similar (0.4846 compared to 0.4320 for the fibrin substitute and 0.4991 compared to 0.4662 for the fibrin-agarose substitute). The small differences found between the second and fourth week of development in culture for each type of constructs, suggest that, in what concerns the CTF, no major changes occur between these two time periods. However, the statistical analysis revealed significant differences between the second and fourth week fibrin samples (p=0.012), contrary to what happened for the fibrin-agarose samples (p=0.396). These results are in good agreement with existing literature. In a recent study, Cardona and collaborators (Cardona et al., 2011), studying the transparency of the same type of constructs as the ones used in our study, found that the number of cells tended to remain constant in the fibrin-agarose corneal substitutes during the second and fourth week of development in culture, whereas in the case of the fibrin constructs a 50% increase was observed. These findings could explain the

statistical differences obtained in our study for the fibrin-based bioengineered corneas.

When comparing the two different types of fibrin-based bioengineered corneal substitutes, both for 2 weeks (0.4991 compared to 0.4846) and 4 weeks (0.4662 compared to 0.4320), the fibrin–0.1% agarose construct registered higher values of CTF. These results suggest that the fibrin–0.1% agarose construct performs better, in terms of CTF, than the fibrin construct, overtaking this latter one in terms of optical quality. Besides, no statistically significant differences were found between the two types of corneal constructs for the second week in culture (p=0.237), whereas for the fourth week in culture these differences became significant (p=0.025) Our results are confirmed by Cardona and collaborators (Cardona et al., 2011) who studied the transparency of these two types of corneal substitutes and concluded that the fibrin–0.1% agarose construct was the corneal model that most resembled the ex vivo native cornea and, considering its transparency values, it is a suitable candidate for the generation of bioengineered tissues for corneal applications. In addition, taking into account the rheological properties found in Chapter 3, the fibrin – 0.1% agarose nanostructured construct is the model that most resembled the physical behaviour of the native cornea and it might serve as an adequate candidate for the generation of an artificial complete cornea, not only for transplanting use but also for conducting pharmaceutical testing and biomedical research.

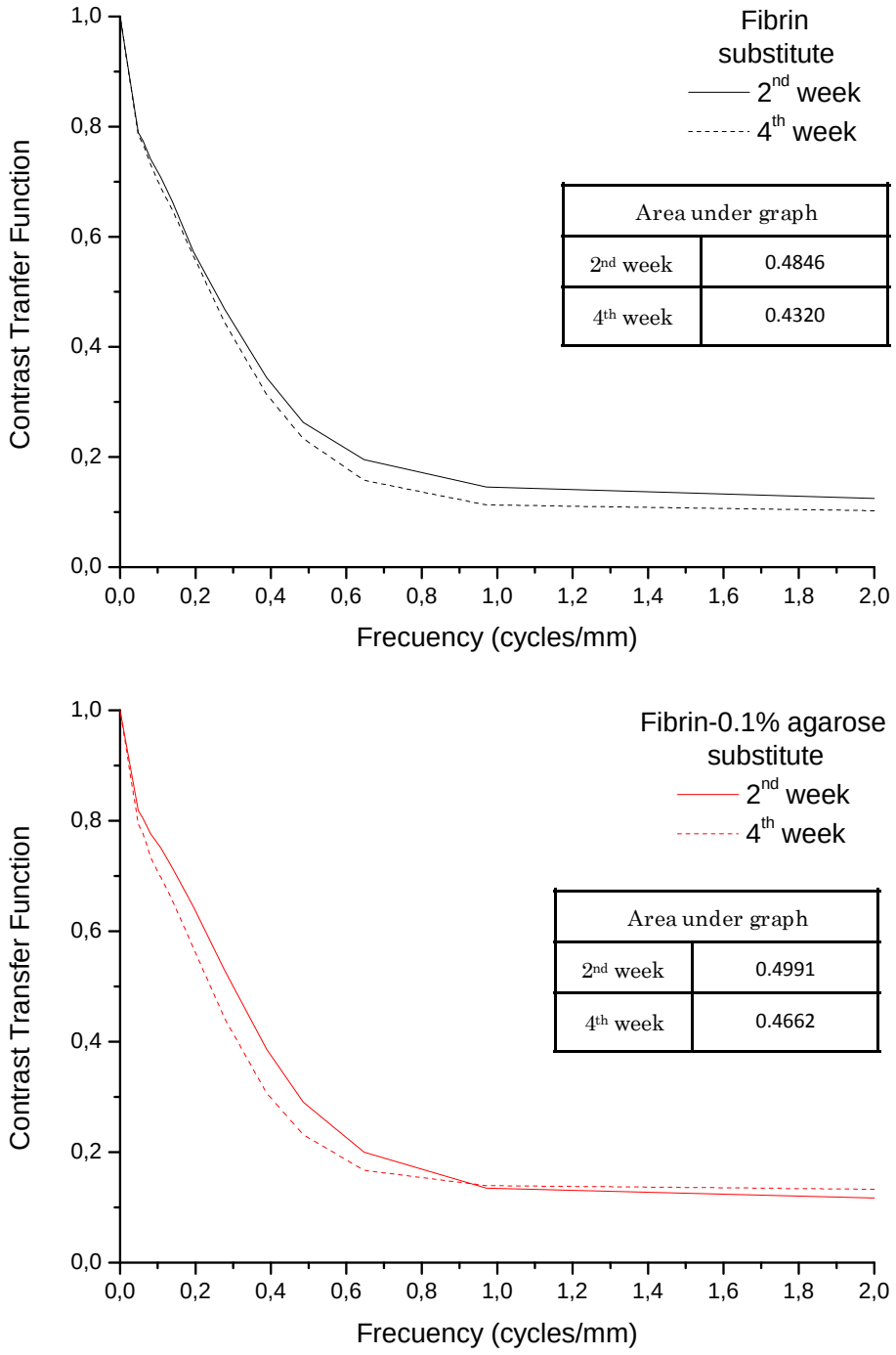

Figure 4.5. CTF values for the fibrin and fibrin-agarose human corneal substitutes after two and four weeks of development in culture

VAF		**FIBRIN**		**FIBRIN-AGAROSE**	
		Development in culture			
		2 weeks	***4 weeks***	***2 weeks***	***4 weeks***
FIBRIN	***2 weeks***	*100%*			
	4 weeks	*99.47%*	*100%*		
FIBRIN-AGAROSE	***2 weeks***	*99.57%*	*99.40%*	*100%*	
	4 weeks	*99.89%*	*99.69%*	*99.28%*	*100%*

Table 4.1. Statistical VAF values for comparison between the the fibrin and fibrin-agarose human corneal substitutes

Study of the compressed collagen gels.

In Figure 4.6 are plotted the CTF values as a function of frequency for both the cellular and acellular collagen gels for a) 1min and b) 3min of compression times. Table 4.2 shows the results of the VAF comparisons for the cellular and acellular gels and for the two compression times studied. As it can be observed in Table 4.2, the behavior of the CTF is very similar for both types of collagen gels and for the two different compression times (VAF ≥ 98.20 in all cases).

As the case of fibrin-based corneal constructs, the values of the CTF registered for 0.65 cycles/mm decreased with respect to the values registered for 0.2cycles/mm, but the relative drop in values is significantly lower, around 40% (compared to 70% in the fibrin constructs case). Still, this loss of sensitivity is expected to affect the final optical quality of the system. From our results, independently of the compression time, the cellular collagen gels presented higher CTF values than the acellular ones (area under graph 0.9888 compared to 0.7631 for 1min and 1.010 compared to 0.9389 for 3min), statistically significant differences being found when comparing cellular and

acellular gels for each time of compression (p<0.001). The corneal transparency is mainly dependent on the arrangement of the collagen fibers within stroma and on the variation of the refractive index between the different cellular components (Mourant et al., 2000). Jester and collaborators (Jester et al., 1999) pointed out the critical importance of minimizing the refractive index fluctuations between cytoplasm and environment for corneal transparency. Therefore, the presence of cells in the compressed collagen gels analyzed in this study could contribute to the changes in corneal clarity, remodeling the gels structure and reducing the variations in refractive index between the collagen gel components. On the other hand, several reports (Meek et al., 2003; Mourant et al., 1995; Benedek, 1971) revealed that microstructural alterations, irregular organizations of the extracellular matrix or the cells of the tissue could also lead to fluctuations of the transparency of a tissue. In our case, although for the shortest time of compression (1min) the differences between the two types of collagen gel corneal substitutes are considerably high (p<0.001), for a longer compression time (3min) these differences narrow (p<0.001), mainly due to the notable increase in acellular CTF values.

Plastic compressed collagen gel is a superior biomaterial in terms of its speed and ease of production and its ability to be manipulated in a clinically relevant manner without breakage. The plastic compression of collagen gels was validated as an appropriate method for ocular surface tissue engineering since it was reported that leads to the generation of a potentially excellent biomaterial for use in therapeutic tissue engineering (Mi et al., 2010b). Compressed collagen gels can produce corneal constructs with a more similar cell morphology, cell density and level of cell stratification to the normal cornea and also support better cell–matrix and cell–cell attachments, suggesting a more robust construct. When we compare the two different times of plastic compression, the CTF values increase with longer compression time (area under graph 1.010 compared to 0.9888 for cellular gels and 0.9389 compared to 0.7631 for acellular gels). These results are in good agreement with previous studies, which related higher compression times with

successful biomaterials. Levis and collaborators (Levis et al., 2010) demonstrated that 5 minutes compressed collagen constructs can form the basis of a biomimetic tissue model for in vitro testing and could potentially provide a suitable alternative to amniotic membrane as a substrate for limbal epithelial cell transplantation. In a more recent work, longer compression times, as long as 15 minutes, but with a considerably lower load (only 35g), were used to successfully generate a novel carrier for expanded human corneal endothelial cells for transplantation (Levis et al. 2012)

However, our statistical analysis found no statistically significant differences for the comparisons between the two cellular gels (p=0.756), contrary to the comparisons between the two acellular gels (p<0.001).

In view of our results, although no significant differences were obtained, the cellular compressed collagen corneal constructs with 3 minutes of compression time presented the highest CTF values, positioning itself as the biomaterial with the best optical quality among the corneal substitutes studied. However, future studies, involving different (and longer) compression times as well as different loads should be performed in order to possess a broader picture of the optical quality of these collagen corneal substitutes.

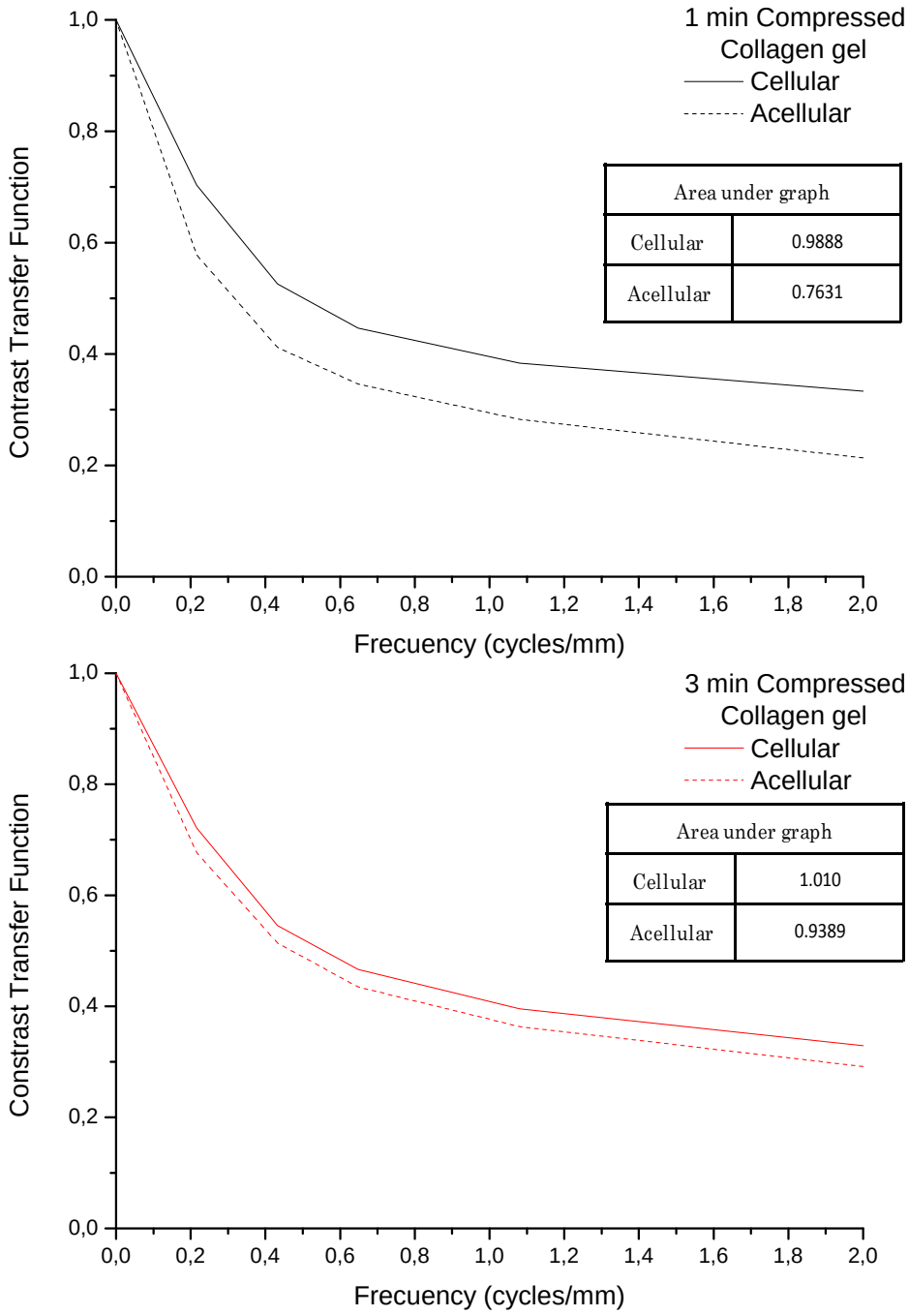

Figure 4.6. CTF values for the compressed collagen gels (cellular and acellular).

VAF		Compression Time 1min		Compression Time 3min	
		Cellular	***Acellular***	***Cellular***	***Acellular***
Compression Time 1min	***Cellular***	*100%*			
	Acellular	*99.98%*	*100%*		
Compression Time 1min	***Cellular***	*98.36%*	*98.20%*	*100%*	
	Acellular	*99.89%*	*99.88%*	*98.98%*	*100%*

Table 4.2. Statistical VAF values for comparison between the acellular and cellular compressed collagen gels (1 min: CC1; 3 min: CC3)

Comparison between the fibrin. fibrin-agarose and cellular collagen gel.

The newly proposed CTF-based method was also used to compare the fibrin, fibrin–0.1% agarose and cellular collagen gels (with 1 and 3 minutes compression times), in order to assess their optical quality. Since the collagen gels were developed in culture for only 10 days, only the fibrin and fibrin – 0.1% agarose substitutes after 14 days (2 weeks) of development in culture were used for comparison. In spite of the different methods used to generate, on one side the fibrin and fibrin-agarose substitutes, and secondly the collagen gels, we consider that their comparison could be of interest in order to establish which type of cornea replacement has better optical quality.

Figure 4.7 show the CTF values as a function of frequency (cycles/mm) for the studied corneal substitutes. Table 4.3 present the results of the VAF analysis for the fibrin and fibrin–0.1% agarose and cellular collagen gels with 1 and 3 minutes of compression time.

The compressed cellular collagen gels presented significantly higher CTF values than the fibrin or fibrin – 0.1% agarose constructs after 2 weeks of development (p<0.001) (area under graph 0.9888 and 1.010 compared to

0.4846 and 0.4991). As previously described, the fibrin based constructs experience a severe drop of the CTF values for frequencies higher than 0.65 cycles/mm, thus resulting in different behaviour of the CTF graph, as reflected by the low VAF values (VAF ≤ 88.16% in all cases). In general, the cellular collagen gels present relative values of the contrast transfer function two times greater than the values registered for the fibrin-based corneal substitutes, especially for higher frequencies.

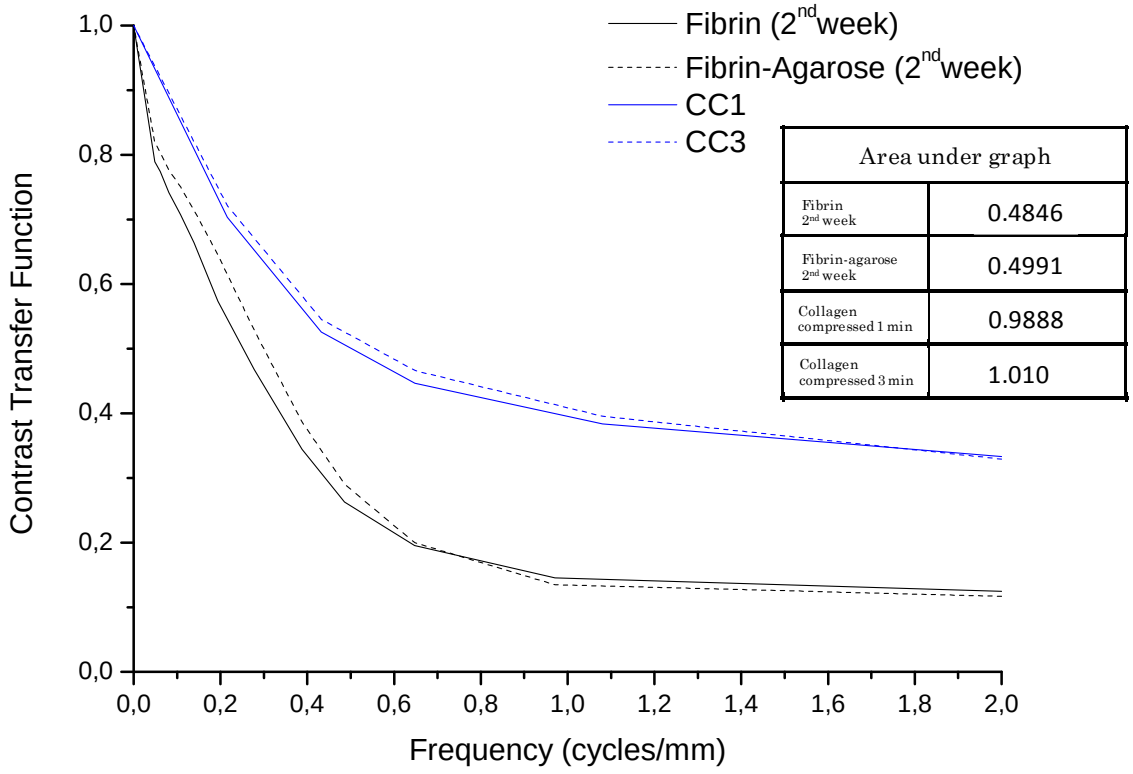

Area under graph	
Fibrin 2nd week	0.4846
Fibrin-agarose 2nd week	0.4991
Collagen compressed 1 min	0.9888
Collagen compressed 3 min	1.010

Figure 4.7. Comparison between the CTF values of the fibrin and fibrin-agarose constructs after 2 weeks of culture, and the cellular compressed collagen gels

VAF	FIBRIN	FIBRIN-0.1% AGAROSE	Cellular Collagen	
			Compression Time 1min	Compression Time 3min
FIBRIN	*100%*			
FIBRIN-0.1% AGAROSE	*99.57%*	*100%*		
Compression Time 1min	*88.16%*	*86.08%*	*100%*	
Compression Time 3min	*87.95%*	*86.02%*	*99.98%*	*100%*

Table 4.3. Statistical VAF values for comparison between the 2 week fibrin and fibrin-agarose and compressed collagen gels (1 min: CC1; 3 min: CC3)

As an overview, although the generation methods used in each case are different, from all types of potentially corneal substitutes analyzed with this method, the cellular collagen gels after a 3 minutes compression time showed the best optical quality, in terms of transfer of details from the object to the image, with considerably higher CTF values for all studied frequencies. Unfortunately, collagen is very expensive to purify, and there is variability in the crosslink density, fiber size, and trace impurities in the isolated collagen (Crabb, 2007). Moreover, the collagen used in the present study has animal origin and therefore has the potential to transmit disease, and can cause an immunogenic response (Crabb, 2007). In contrast, the fibrin-agarose constructs can be produced from the patient's own blood and used as an autologous scaffold for the seeded keratocytes without the potential risk of a foreign body reaction. In addition, the experience acquired by our group developing fibrin-agarose corneal substitutes (Cardona et al., 2011; Ionescu et al., 2011; Ionescu et al., 2010; Gonzalez-Andrades et al., 2009; Alaminos et al., 2006) encourage us to continue investigating their properties. Therefore, Chapter 5 of the present Thesis describes the optical properties of a partial bioengineered human cornea based on fibrin-0.1% agarose, in order to establish, taking into account the previous results on rheological properties and CTF values, its suitability for clinical use.

5. OPTICAL PROPERTIES OF AN ANTERIOR LAMELLAR HUMAN CORNEA MODEL BASED ON FIBRIN-AGAROSE

BACKGROUND

Corneal transparency has been the subject of numerous studies over the last few years (Qazi et al., 2010; Sardar et al., 2009; Meek et al., 2003; Jester et al., 1999). It is now generally accepted that corneal transparency depends on the destructive interference of the incoming light that is scattered away and on the absorption of light by the corneal tissue itself.

Several researchers have demonstrated that the scattering of light in the human cornea depends mostly on the stromal extracellular matrix, and scattering will increase if the fibril diameter increases or if the spatial arrangement or the hydration level of the fibrils is altered (Meek et al., 2003; Freund et al., 1995; Freund et al., 1986). In contrast, other studies suggest that corneal cells might play a relevant role and that stromal keratocytes significantly contribute to corneal light scattering (Maurice et al., 1957). In fact, Jester and collaborators (Jester et al., 1999) suggested that stromal cells contain different corneal 'cristallins', which affect the refractive index of the cell cytoplasm, allowing most of the light to reach the cornea with very low scattering levels. However, situations in which corneal keratocytes change their morphology or spill their contents could result in a significant increase of the scattering capacities of the stromal keratocytes (Moller-Perdersen et al., 2000). For all these reasons, the evaluation of the optical behavior of native cornea and the different bioengineered models of the human cornea, developed as an alternative solution to corneal transplantation due to the shortage of donor organs and to complications resulting from this procedure, is an essential part of the quality-control process of these bioengineered

tissues where cells are maintained under specific cell-culture conditions in which cell proliferation rate is unusually high.

Regarding the previously developed fibrin-agarose human cornea model, biological features such as cells survival rate and proliferation, protein expression, and morphological characteristics (intercellular junctions) were determined using immunocytochemistry and microscopy techniques. Only recently, Cardona and collaborators (Cardona et al., 2011) evaluated the transparency of fibrin and fibrin-agarose corneal stroma substitutes generated by tissue engineering. The authors used the Kubelka-Munk equations to determine the scattering and absorption coefficients of these cornea models and compared them to the ones of a control porcine cornea and a theoretical cornea model proposed by Van der Berg and Tan (1994). The simplicity of the Kubelka-Munk model has made it a popular method for measuring the optical properties of tissues. Unfortunately, the assumptions that this model implies on isotropic scattering, matched boundaries and diffuse irradiance are atypical of the interaction of laser light with tissue. Despite attempts to extend the Kubelka-Munk model to collimated irradiance (van Gemert et al., 1987; Atkins, 1969; Kottler, 1960) and anisotropic scattering (Jacques and Prahl, 1987; Atkins, 1969; Meador and Weaver, 1979), this method remains a weak approximation for laser light propagation in tissue (Niemz, 2007).

In this work, we have evaluated the optical properties of a model of human artificial cornea based on fibrin-agarose scaffolds using the inverse adding-doubling (IAD) method that involves direct measurements of reflectance and transmittance of the samples and a Monte Carlo simulation to determine the scattering and absorption coefficients. Part of the novelty of the current investigation is the use of the IAD method to quantify the optical properties of a novel artificial cornea model generated by tissue engineering using human components (human corneal keratocytes and human plasma–derived fibrin) and a small concentration of agarose. In addition, the nanostructuring technique used in this Thesis proved to be adequate for

generating bioengineered human corneas with improved rheological properties (Chapter 3).

Inverse adding-doubling is a method for generating the optical properties of scattering and absorbing materials. Reflection and transmission measurements, usually made with an integrating sphere, are converted to the optical properties of the sample (scattering and absorption coefficients) using the computer program ***iad***, developed by Professor Scott Prahl (Prahl, 2012). This program has been extensively tested and validated for accuracy and precision (Sardar et al., 2007; Yust et al., 2012) and it has been widely used to determined the optical characteristics of different biological tissues (Sardar et al., 2009; Bashkatov et al., 2005; Ishii et al., 2008; Honda et al., 2009). The general idea is that measurements of reflection and transmission are fed into the program to extract the intrinsic optical properties of the sample to be studied. The program does this by repeatedly guessing the optical properties and comparing the expected observables with those that have been made. Upon matching, those optical properties used to generate the expected observables are the ones that characterize the sample.

THEORETICAL BACKGROUND

Few numerical or analytical options exist that accurately simulate the light propagation in samples with arbitrary scattering and absorption ratios, anisotropic scattering and boundaries (Prahl, 1995). The diffusion equation, random walk models, Kubelka-Munk or Chandrasekhar's X and Y functions are the common approximations used in this situation, but they place restrictions on one or more of the basic tissue properties. The adding-doubling (van de Hulst, 1980) allows accurate solution of the radiative transfer equation for anisotropic scattering and mismatched boundaries. We have selected this method because it works naturally with layered samples, yields reflection and transmission readily and it has important light using

diagnostic applications (Prahl, 1995). Furthermore, the only parameters needed when measuring the optical properties of biological samples are the total reflection and transmission of the sample (Ishii et al., 2008; Sardar et al., 2007; Bashkatov et al., 2005; Prahl et al., 1993).

General description of the adding-doubling method. The doubling method requires the knowledge of the reflection and transmission properties of a single thin homogeneous layer. If the slab doubles its thickness, the reflection and transmission of this slab are found by juxtaposing two identical slabs and summing the contributions from each slab (van de Hulst, 1980; Plass et al., 1973). The reflection and transmission of an arbitrarily thick slab are obtained by repeatedly doubling until the desired thickness is reached. The adding method allows the simulation of a media with different layers and/or reflection at boundaries, extending in this way the doubling method to dissimilar slabs (Prahl, 1995).

The adding-doubling method has the advantage that it requires only integrations over angle, the physical interpretation of the results can be made at each step, the method is equivalent for isotropic and anisotropic scattering, and results are obtained for all angles of incidence used in the integration (Irvine, 1975). The disadvantages are that it is (1) difficult to calculate internal fluences, (2) restricted to layered geometries with uniform irradiation and (3) necessary for each layer to have homogeneous optical properties. In practice, the first issue is not a problem since internal fluences are often not needed. Still, if fluences are needed at a certain depth, they can be calculated by finding the reflection and transmission matrices for light propagation through the material above that depth as well as the matrices for everything below. These matrices are then used to obtain the upward and downward radiance at the interface between these layers. The fluence follows directly once the radiance as a function of angle is known. Issues (2) and (3) represent restrictions on the sample geometry: the samples must have homogeneous layers and be uniformly illuminated. Prahl (Prahl et al., 1993)

used the adding-doubling method to solve the radiative transport equation and implemented it into the development of the inverse adding-doubling (***iad***) program, inverse implying a reversal of the usual process of calculating reflection and transmission from optical properties.

As stated before, the IAD method involves direct measurements of reflection and transmission of the samples (usually performed using integrating spheres) and a Monte Carlo simulation to determine the scattering and absorption coefficients. Figure 5.1 shows the steps followed in this method (Prahl et al., 1993).

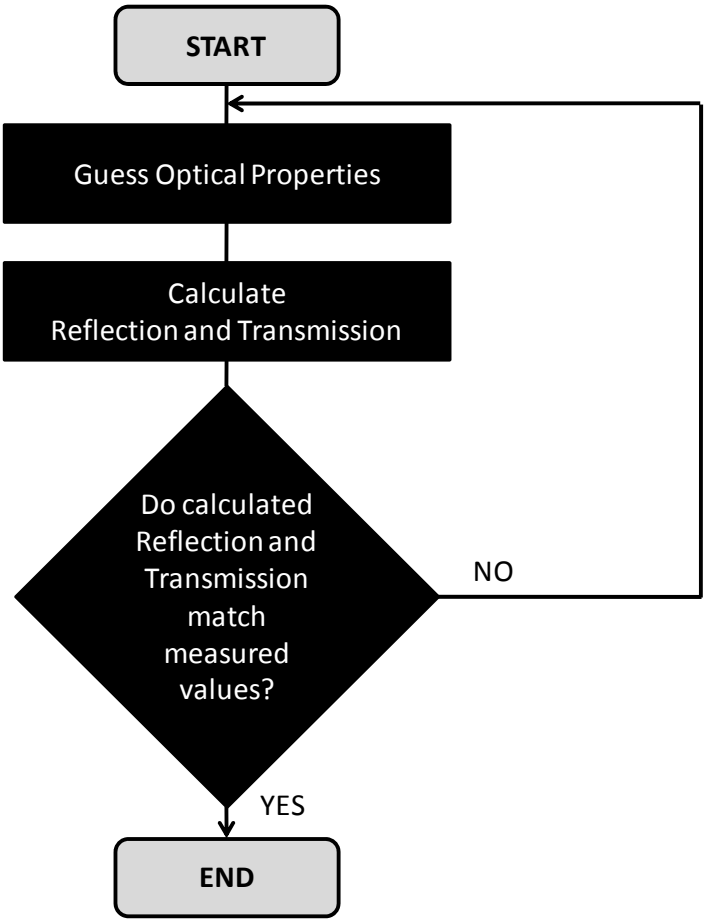

Figure 5.1. Schematic representation of the IAD method steps (Prahl, 1988). The method involves guessing the optical properties of a tissue, calculating the reflection and transmission for these properties, comparing the calculated with the measured reflection and transmission, and repeating this process until the calculated and measured transmission match. (courtesy of Prof. Scott Prahl)

The set of optical properties that generates reflection and transmission values matching the measured values is taken as the optical properties of the sample. The results obtained with the IAD method are accurate for all optical properties and have been validated for a variety of biological tissues (Sardar et al., 2009; Bashkatov et al., 2005; Sardar and Levy, 1998; Cheong et al., 1990).

However, the following assumptions are made when using the IAD method:

- no time dependence;
- a geometry consisting of uniform layers of finite thickness and infinite extent in directions parallel to the surface;
- tissue layers with uniform scattering and absorbing properties;
- uniform illumination by collimated or diffuse light.

Integrating sphere theory. An integrating sphere is an optical component consisting of a hollow spherical cavity with its interior covered with a diffuse white reflective coating, with small holes for entrance and exit ports (Figure 5.2).

Figure 5.2. Integrating sphere

Different variables are needed when describing the light propagation within an integrating sphere. There are variables describing areas within the sphere, reflection and transmission of the sphere wall, detector and sample, and illumination power. Table 5.1 and 5.2 show the notations used to describe the areas within the sphere, and the reflection, transmission and light power respectively.

Description	Area	Normalized area
Inside area of the sphere	A	$\frac{A}{A} = 1$
Area of the sample port	A_s	$\frac{A_s}{A} = a_s$
Area of the detector port	A_d	$\frac{A_d}{A} = a_d$
Area of the entrance port	A_e	$\frac{A_e}{A} = a_e$
Area of the sphere wall	A_w	$\frac{A_w}{A} = a_w$ $a_w = 1 - a_s - a_e - a_d$

Table 5.1. Notations of the areas within the integrating sphere

Description	Reflection	Transmission	Light Power
Sphere wall	r_w		P_w
Detector	r_d		P_d
Reference standard	r_{std}		
Sample			P_s
Diffuse illumination	r_s	t_s	
Collimated illumination	r_s^{direct}	t_s^{direct}	
Incident illumination			P

Table 5.2. Notations of the reflection, transmission and light power when using an integrating sphere

Single integrating sphere. The integrating spheres have the advantage that they collect almost all the light reflected by or transmitted through a sample. The fraction of light that is redirected to the detector after having interacted with the sample depends on the sphere geometry and the reflectivity of the sphere walls and sample. The *sphere gain* is a concept that describes the increase in the irradiance on the detector due to the reflective sphere walls. It is not a constant of the sphere, varying with the reflectance of the sphere.

If the sphere is illuminated with a diffuse light of power P that reaches all of the parts of the sphere (the light is not blocked by a baffle), then the multiple reflections that light suffers within the sphere will increase the power falling on non-white areas of the sphere. Note that the subsequent reflections are restricted by the baffle situated between the sample and the detector. The total light power falling on the different regions of the sphere after first incidence, for the diffuse light is:

$$P_w^{(1)} = a_w P, \qquad P_s^{(1)} = a_s P, \qquad P_d^{(1)} = a_d P. \qquad (5.1)$$

The second incidence on the wall is

$$P_w^{(2)} = a_w r_w P_w^{(1)} + (1 - a_e) r_d P_d^{(1)} + (1 - a_e) r_s P_s^{(1)} \qquad (5.2)$$

The light from the detector and sample are multiplied by $(1 - a_e)$ and not by a_w because the light from the detector (or sample) is not allowed to hit either the detector or sample. On the kth incidence, the light that hits the walls has the same form as above

$$P_w^{(k)} = a_w r_w P_w^{(k-1)} + (1 - a_e) r_d P_d^{(k-1)} + (1 - a_e) r_s P_s^{(k-1)} \qquad (5.3)$$

Since the light falling on the sample or detector can only come from the wall due to the baffle, then

$$P_s^{(k)} = a_s r_w P_w^{(k-1)}, \qquad P_d^{(k)} = a_d r_w P_w^{(k-1)} \qquad (5.4)$$

Therefore, the incident light on the wall for the kth incidence becomes

$$P_w^{(k)} = a_w r_w P_w^{(k-1)} + (1 - a_e) r_w (a_d r_d + a_s r_s) P_w^{(k-2)} \qquad (5.5)$$

The total power that will hit the detector is

$$P_d = a_d P + \sum_{k=2}^{\infty} a_d r_w P_w^{(k-1)} = a_d P + a_d r_w \frac{a_w + (1-a_e)(a_d r_d + a_s r_s)}{1 - a_w r_w - (1-a_e) r_w (a_d r_d + a_s r_s)} P \qquad (5.6)$$

The gain $G(r_s)$ in the irradiance on the detector relative to a black sphere is defined as

$$G(r_s) = \frac{P_d / A_d}{P / A} = 1 + \frac{r_w}{a_w} \frac{a_w + (1-a_e)(a_d r_d + a_s r_s)}{1 - a_w r_w - (1-a_e) r_w (a_d r_d + a_s r_s)} \qquad (5.7)$$

The gain for a detector in a transmission sphere is similar (Pickering et al., 1992). For a black sphere ($r_w = 0$, $r_s = 0$, and $r_d = 0$) the gain is $G(0) = 1$.

In summary, the gain gives the number of times light bounces within the sphere compared to a black sphere. Ideally, a constant gain is required when doing the experimental measurements.

Single sphere measurements. The power falling on the detector in a single reflectance sphere is

$$P_d = a_d \cdot (initial\ uniform\ diffuse\ light) \cdot G(r_s) \qquad (5.8)$$

In a typical measurement, the initial diffuse light arises from (a) the incident light that hits the sphere wall before the sample and (2) the incident light that first hits the sample. If we define as f the fraction of light that first hits the sphere wall, then the first reflection is $r_w f P$. However, this is not uniformly diffuse. Therefore, the light must hit the walls one more time before becoming uniform. The first portion is given by $f r_w^2 (1 - a_e) P$.

The light reflected by the sample is $(1 - f) r_s^{direct} P$. Since the baffle doesn't allow the reflected light to directly hit the detector, the light must bounce of the sphere walls to become a uniform diffuse source. Thus, the contribution is $(1 - f) r_s^{direct} (1 - a_e) r_w P$.

The measured reflection is

$$R\left(r_s^{direct}, r_s\right) = a_d(1-a_e)r_w\left[(1-f)r_s^{direct} + fr_w\right]P \cdot G(r_s) \qquad (5.9)$$

For the measured transmission we obtain a similar relation

$$T\left(r_s^{direct}, r_s\right) = a'_d t_s^{direct} r'_w (1-a'_e)P \cdot G'(r_s) \qquad (5.10)$$

In order to not have a power dependence, the sample reflectance is defined as

$$M_R = r_{std}\frac{R\left(r_s^{direct}, r_s\right) - R(0,0)}{R(r_{std}, r_{std}) - R(0,0)} \qquad (5.11)$$

M_R is the ratio of the difference in power measured between a sample and an open sample port to the difference in power measured between a reflection standard and an open sample port. The experimental setup for each measurement is showed in Figure 5.3.

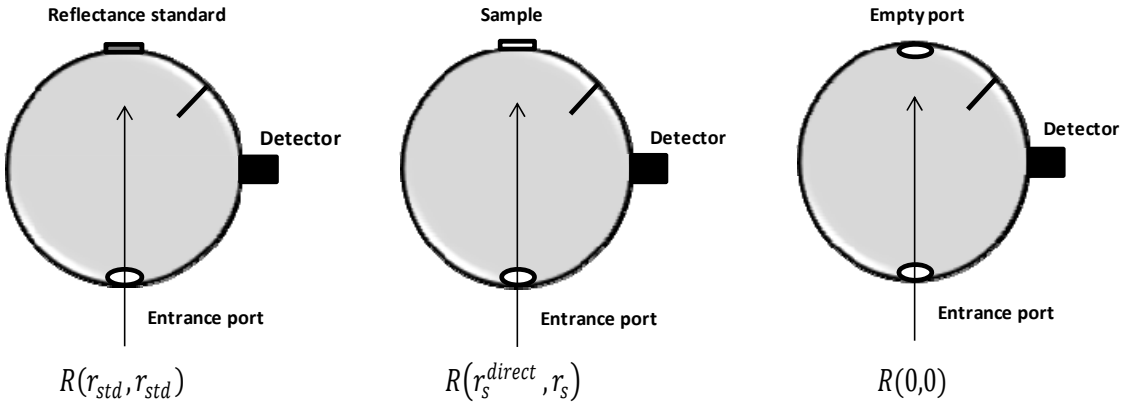

Figure 5.3. Integrating sphere reflection measurements needed to make a reflectance measurement using a single integrating sphere.

By subtracting the dark signal measurement, error is reduced especially for low reflection sample. In addition, $R(0,0)$ is largely a measure of the fraction of light that initially is incident on the sphere wall f. Subtraction of $R(0,0)$ implies that the effect of f is accounted for without a direct method for measuring its value.

Similarly, the measured transmittance is defined as

$$M_T = \frac{T(r_s^{direct}, r_s) - T_{dark}}{T(0,0) - T_{dark}} \qquad (5.12)$$

Figure 5.4 specifies the experimental setup for the three measurements needed.

Note that the reflectance and transmittance values determined using the method described before, have a range between 0 and 1. Also, another important aspect is understanding the difference between reflection (or transmission) and reflectance (or transmittance). Reflection is light reflected by the sample, whereas reflectance is light reflected by the sample normalized by the incoming light (as shown in equation 5.11). The same idea applies to transmission and transmittance.

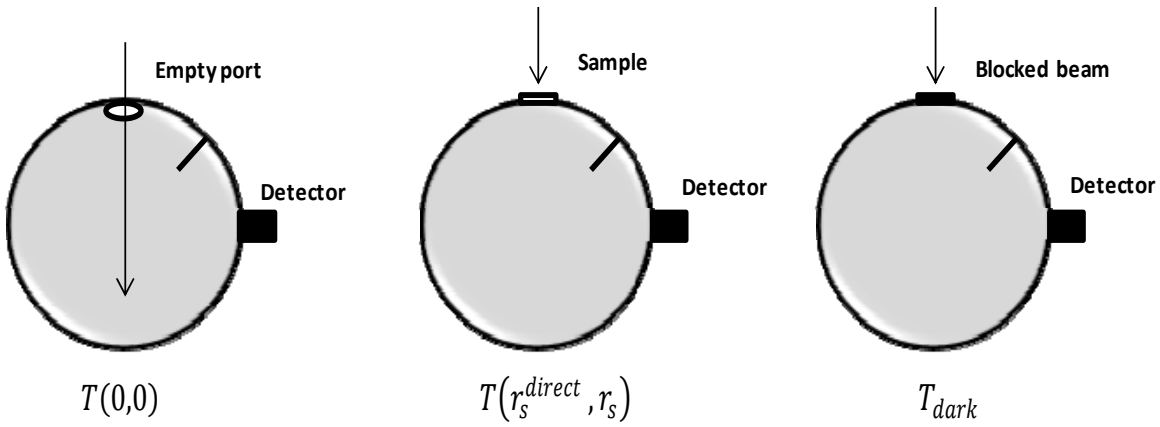

Figure 5.4. Integrating sphere transmission measurements needed to make a transmittance measurement using a single integrating sphere.

Sphere parameters. To fully evaluate the reflectance and transmittance of the sample, a sphere calibration is needed. The reflectance of the sphere wall r_w is critical. It can be determined with two measurements that use diffuse illumination. One measurement has an open sample port ($R_0^{diffuse}$) and the other a reflectance standard in the sample port ($R_{std}^{diffuse}$). To obtain

the light diffuse, the incident light is directed on the sphere wall, between the baffle and the sample port (Figure 5.5)

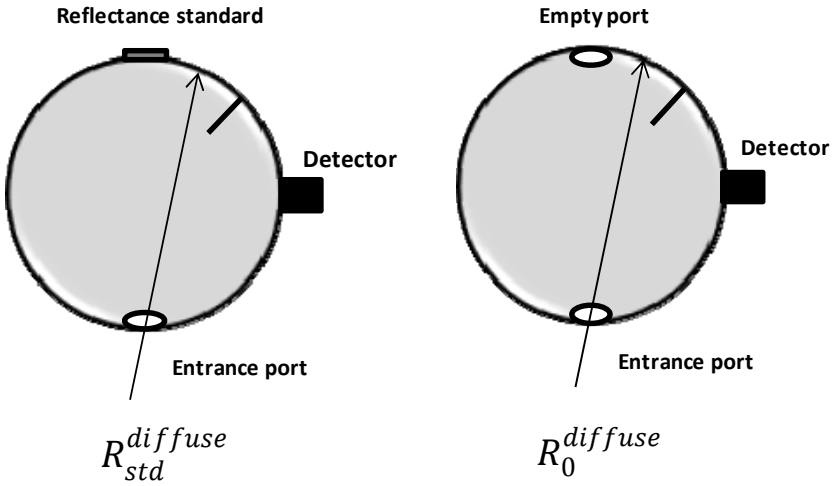

Figure 5.5. Experimental setups needed to determine the sphere wall reflectance r_w.

A solution for the sphere wall reflectance is then

$$r_w = \frac{1-\frac{R_0^{diffuse}}{R_{std}^{diffuse}}}{\left(1-\frac{R_0^{diffuse}}{R_{std}^{diffuse}}\right)(a_w+(1-a_e)(a_d r_d+a_s r_{std})} \qquad (5.13)$$

Ultimately, only two calibration measurements (per integrating sphere), $R_0^{diffuse}$ and $R_{std}^{diffuse}$ are necessary to perform sphere correction. There are six other constants to be calculated: the normalized area of the sphere wall a_w, the normalized area of the sample port a_s, the normalized area of the detector a_d, the normalized area of the entrance port a_e, the reflectance of the detector r_d, the reflectance of the reference standard r_{std}. These parameters in combination with six additional measurements form a complete set of data necessary to implement in the IAD Monte Carlo simulation in order to determine optical properties, three reflection

measurements $R(r_s^{direct}, r_s)$, $R(r_{std}, r_{std})$ and $R(0,0)$, and three transmission measurements $T(r_s^{direct}, r_s)$, $T(0,0)$ and T_{dark}.

Monte Carlo Simulation. The Monte Carte simulation used by the IAD method was specially designed to study the light propagation in biological tissues (Prahl, 1988). The accuracy of the Monte Carlo technique is proportional to $1/\sqrt{N}$, where N is the photons number considered in the simulation. Therefore, in order to have an acceptable relative error, the number of photons must be between 10^6 and 10^9 and computation time must be elevated.

The method begins by launching a photon downwards into the tissue. The photon is then moved a distance Δs where it may be absorbed, scattered, propagated undisturbed, internally reflected or transmitted out of the tissue. If it escapes from the tissue, the reflection or transmission of the photon is recorded, and if it is absorbed, the position of the absorption is recorded. Once this process has ended, a new photon is launched. The process of launching new photon is repeated until the desired number of photons has been propagated. The recorded reflection, transmission absorption or scattering profiles will approach true values (for a tissue with specified optical properties) as the number of photons propagated is getting close to infinity.

The distance Δs the photon is moved each propagation step within the tissue is variable. The stepsize Δs is chose in such a way that it is the distance at which the photon is either scattered or absorbed. It can be generated as a function of random number ξ uniformly distributed between zero and one

$$\Delta s = -\ln \xi \qquad (5.14)$$

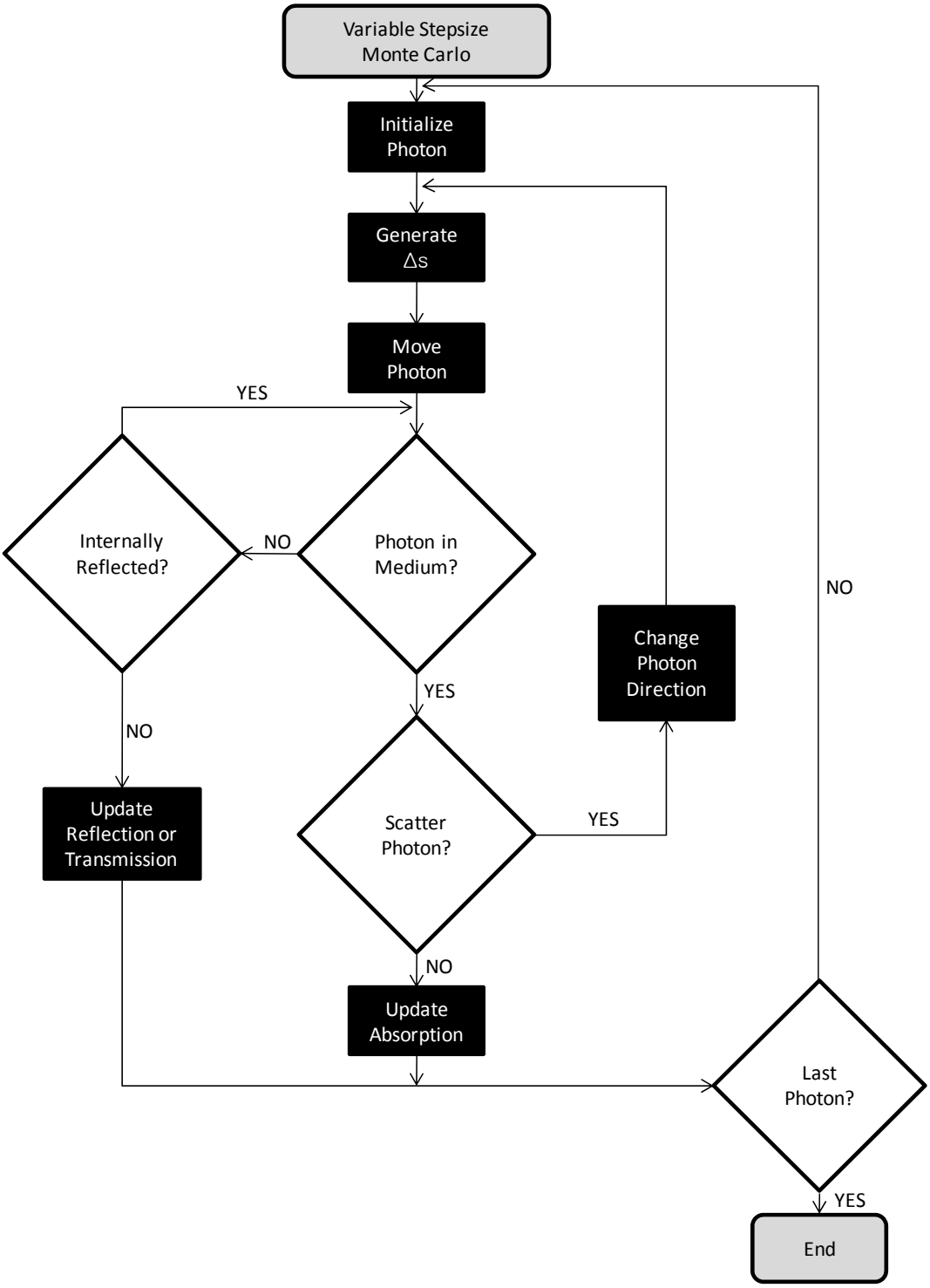

Figure 5.6. Schematic representation of the variable stepsize Monte Carlo technique (courtesy of Prof. Scott Prahl)

This way, the photon is forced either to scatter or to be absorbed after each propagation step. Thus, the probability that it is scattered is equal to the ratio of the scattering coefficient to the sum of the absorption and scattering coefficients (albedo). Therefore, the photon is scattered if

$$\xi < \frac{\mu_a}{\mu_a+\mu_s} = a \qquad (5.15)$$

Otherwise, the photon is absorbed. If the photon is scattered then a new photon direction is chosen based on the phase function, otherwise the photon is absorbed. The process is repeated until the photon is absorbed. Figure 5.6. resumes this variable stepsize Monte Carlo technique.

In order to reduce the number of photons used in the Monte Carlo simulation, a weight is assigned to each photon as it enters the tissue (implicit capture technique). Since the weight of the photon is reduced by the probability of absorption after each propagation step, this technique provides absorption information at each photon step rather than just at times when the photon is completely absorbed (Wang et al., 2009). In the case of the variable stepsize Monte Carlo, when propagating many photons (a packet) along each path through the tissue, the packet's weight is reduced by a factor of $(1 - a)$, this factor representing the fraction of photons absorbed at each propagation step. Thus, the weight coefficient is reduced accordingly and the photon packet keeps propagating until this coefficient drops below a specified tolerance. However, the weight coefficient never reaches zero value and continuing to propagate a photon with a very small weight adds little relevant information to the propagation in tissue. Furthermore, if all the remaining weight is absorbed or discarded, the energy conservation is violated. This is the reason why, a technique called the Russian roulette is applied to terminate the photon once its weight has reached a value below a specified minimum. This technique gives a photon with w weight one chance in m to 'survive' with a mw weight or else its weight is reduced to zero. Thereby, the energy conservation is not compromised. Figure 5.7 shows the

schematic representation of the Monte Carlo variable step size with the implicit capture technique.

Another technique that can be used to improve statistics is splitting. When a photon with w weight passes into a more 'interesting' region, it can be split into m different photons, each one with a w/m weight. This way, energy is conserved and statistics improves. If the region is less 'interesting', then roulette is the technique used to reduce the number of photons in that region.

The Monte Carlo simulation uses reflection and transmission measurements made with integrating spheres. It was included in the ***iad*** program to obtain an accurate evaluation of the optical properties of the samples studied.

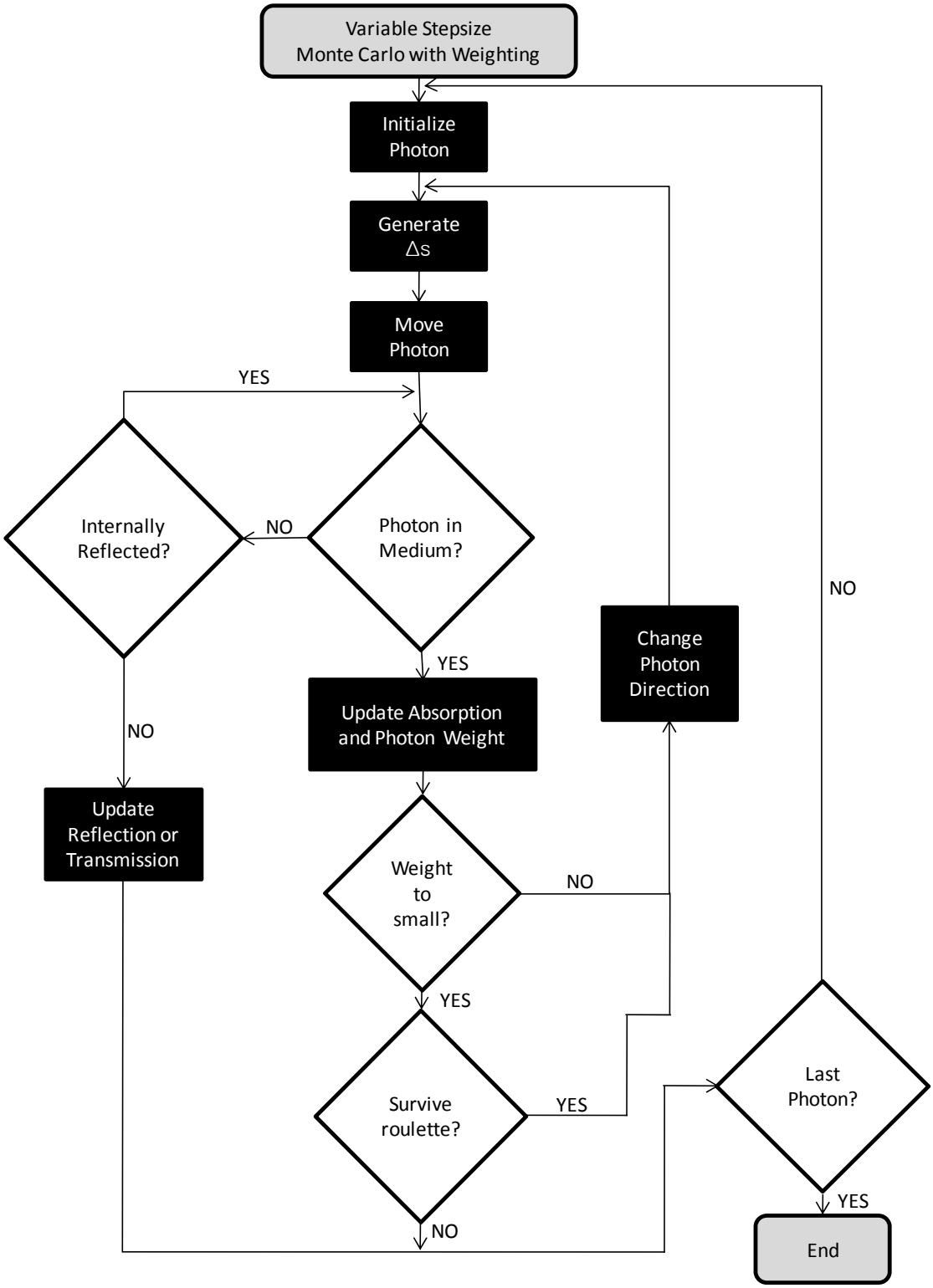

Figure 5.7. Schematic representation of the Monte Carlo variable stepsize with the implicit capture technique (courtesy of Prof. Scott Prahl).

MATERIALS AND METHODS

The materials used in this work were generated using the same method described in Chapter 3 seeding epithelial cells on top of the human corneal stroma substitutes. Taking into account the results obtained in the previous Chapters, in this study only fibrin with 0.1% agarose concentration constructs were used.

Isolation and culture of human cells.

To obtain epithelial cells, the corneal scleral rings of the human corneas were dissected by cutting circumferentially, approximately 1mm on either side of the cornea and conjunctival junction, according to published methods (Chen at el., 2005.). Split thickness limbal rings were cut into $2mm^2$, 100μm thickness explants that were placed, epithelial side up, directly on a culture plate containing a small amount of culture medium, to allow the explants to attach to the culture surface. Six hours later, the tissue was submerged in DMEM medium supplemented with 10% FCS (Sigma-Aldrich), 4 mM L-glutamine and 1% antibiotic solution (Invitrogen-Gibco). To prevent fibroblast overgrowth and favor epithelial growth (Talbot et al., 2006), in some cases, the corneal scleral rings were cocultivated in the absence of a feeder cells layers. Stromal keratocytes were isolated as described in Chapter 3.

Construction of corneal equivalents with a fibrin-agarose stromal substitutes.

Anterior lamellar corneal substitutes consisted of cultured human keratocytes entrapped in a gel of human fibrin with 0.1% type VII agarose.

They were generated following the method described on Chapter 3. Twenty-four hours after the stromal substitute had solidified, human epithelial cells were seeded on top of the constructed stroma (500,000 epithelial cells per construct), and cultured for 2 weeks submerged in culture medium (Figure 5.8). When epithelial cells reached confluence, the air–liquid culture technique was used for two more weeks.

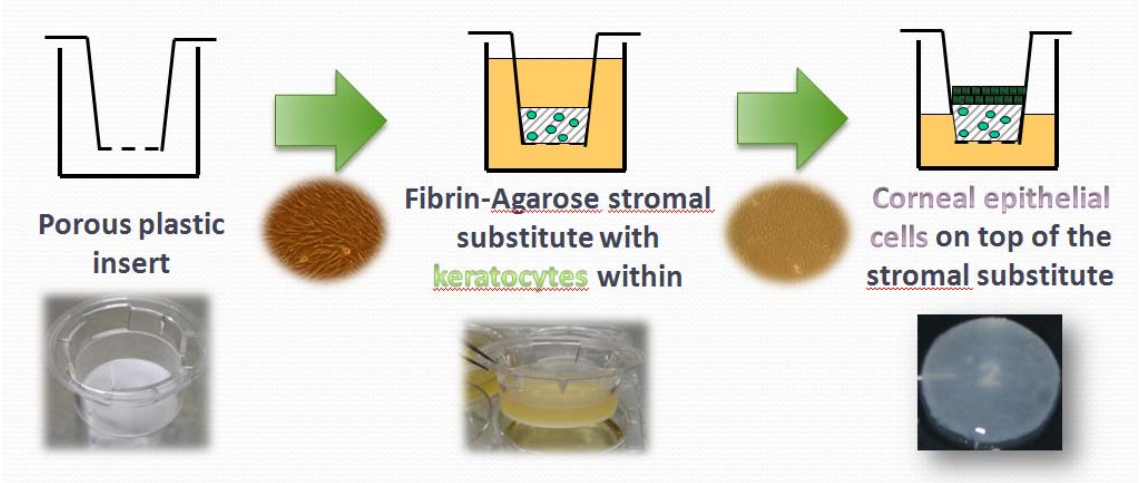

Figure 5.8. Serial construction of human corneal substitutes using porous culture inserts. First, a fibrin-agarose stromal substitute with keratocytes embedded is constructed in direct contact with the porous membrane of the plastic insert. Then, epithelial cells are seeded on top. The air–liquid culture technique is used to promote epithelial stratification and full formation of the corneal equivalent.

Samples of the bioengineered partial human corneas were studied weekly until four weeks of development in culture. Before proceeding to the optical measurements, the samples were nanostructured, using the same technique described in Chapter 3, and kept in phosphate buffered saline (PBS) until the moment of analysis (Figure 5.9).

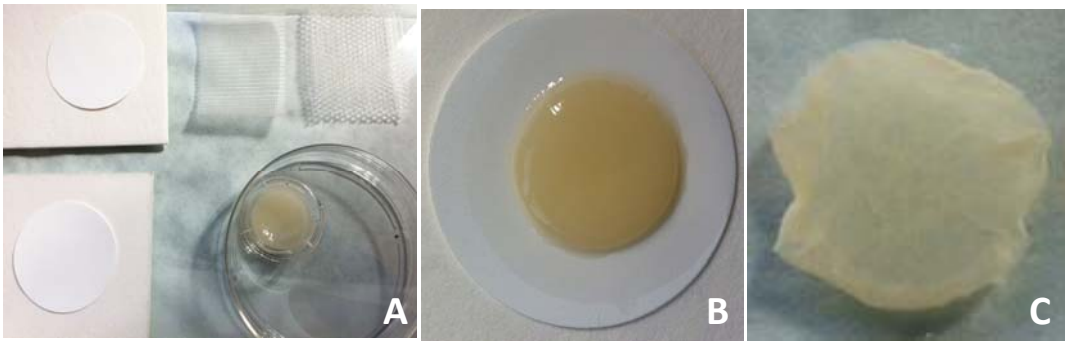

Figure 5.9. Before and after nanostructuring of the anterior lamellar human cornea substitute: A. Material used for nanostructuring technique; B. Non-nanostructured corneal construct and C. Nanostructured corneal construct

As controls, 3 fresh porcine corneas (Figure 5.10) were obtained from adult pigs immediately after death and analyzed under the same conditions as the artificial corneal constructs.

Figure 5.10. Porcine cornea used as control sample.

Microscopic evaluation of the artificial corneal construct.

Samples for scanning electron microscopy (SEM) were fixed in cacodylate-buffered 2.5% glutaraldehyde and postfixed in 1% osmium tetroxide for 90 minutes. After fixation, the samples were dehydrated in increasing concentrations of acetone (30%, 50%, 70%, 95% and 100%), critical point dried, mounted on aluminum stubs, sputter coated with gold according to routine procedures (Sanchez-Quevedo et al., 1994), and examined in a scanning electron microscope (Quanta 200; FEI, Eindhoven, The Netherlands) using a high vacuum mode. The corneal construct evaluated by SEM corresponds to the second week of development in culture.

Phantoms.

To mimic light distribution in living tissues, phantoms that simulate the optical characteristics of tissues are often used. Tissue phantoms are designed and utilized to calibrate optical devices. In 2006, Prof. Scott Prahl and collaborators (Moffit et al., 2006) proposed a method for the preparation of a polyurethane phantom to simulate the optical properties of biologic tissues. The phantom consisted of three components: polyurethane, absorbing chromophores and a scattering agent. The authors repeatedly determined the optical properties of the phantom using the inverse adding-doubling method and established that they were stable over a period of 14 months, making the optical phantom suitable for use as reference standard.

To ensure the accuracy of the experimental setup used in our study, a polyurethane optical phantom with known optical properties was measured. It was obtained by courtesy of Prof. Dr. Scott Prahl from the University of Oregon. Figure 5.11 illustrates the phantom used in our study.

Figure 5.11. Polyurethane optical phamtom used for the calibration of the experimental setup.

Reflectance and transmittance measurements.

Inverse adding doubling was used to find the scattering and absorption of the artificial human corneas and native porcine corneas using total reflection and total transmission measurements made with a single integrating sphere. Three measurements on each sample were made. Figure 5.12 shows the experimental setup used for the reflection and transmission measurements.

Total diffuse reflection measurements were made using a 158.2mm-diameter integrating sphere (Oriel, model 70674. Newport. USA) (Figure 5.13) with an 11mm-diameter detector port and a 15mm-diameter sample port with a baffle between ports. The entrance port had 15mm diameter. The measurements were performed for the bioengineered human corneas and native porcine corneas at 457.9nm, 488nm and 514.5nm from an argon ion laser (Stellar-Pro-L Model, Modu-Laser, USA) and 632.8nm from a He-Ne laser (30564 Model, Research Electro-Optics, USA). The maximum output power of the lasers was 1000mW±5% for the argon laser and 12 mW for the He-Ne laser. The diameter of both argon and He-Ne lasers beams was 2mm.

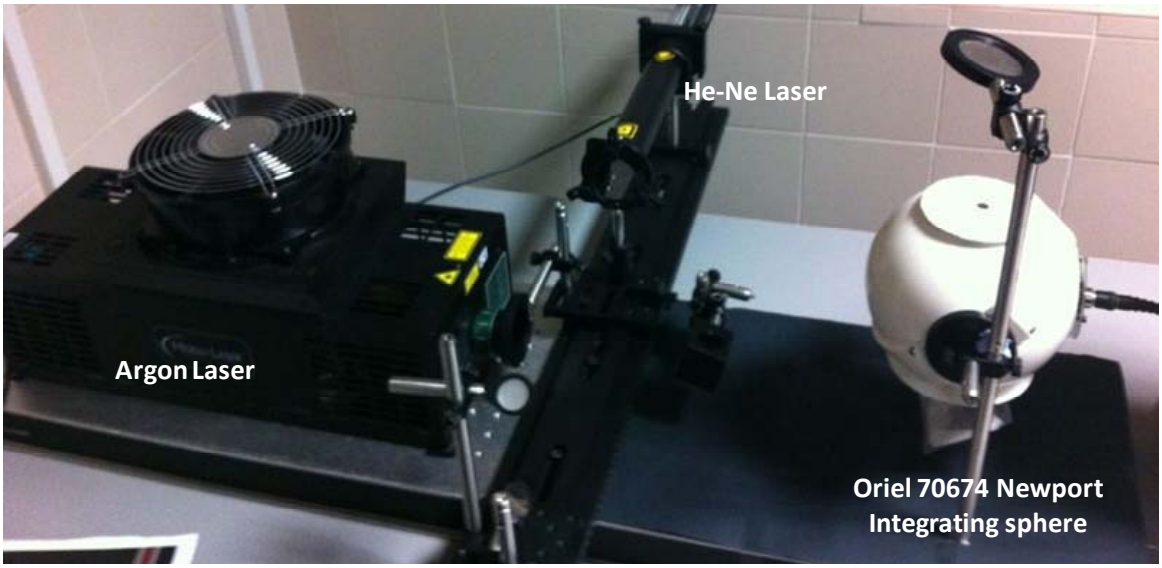

Figure 5.12. Experimental setup used to perform the reflection and transmission measurements.

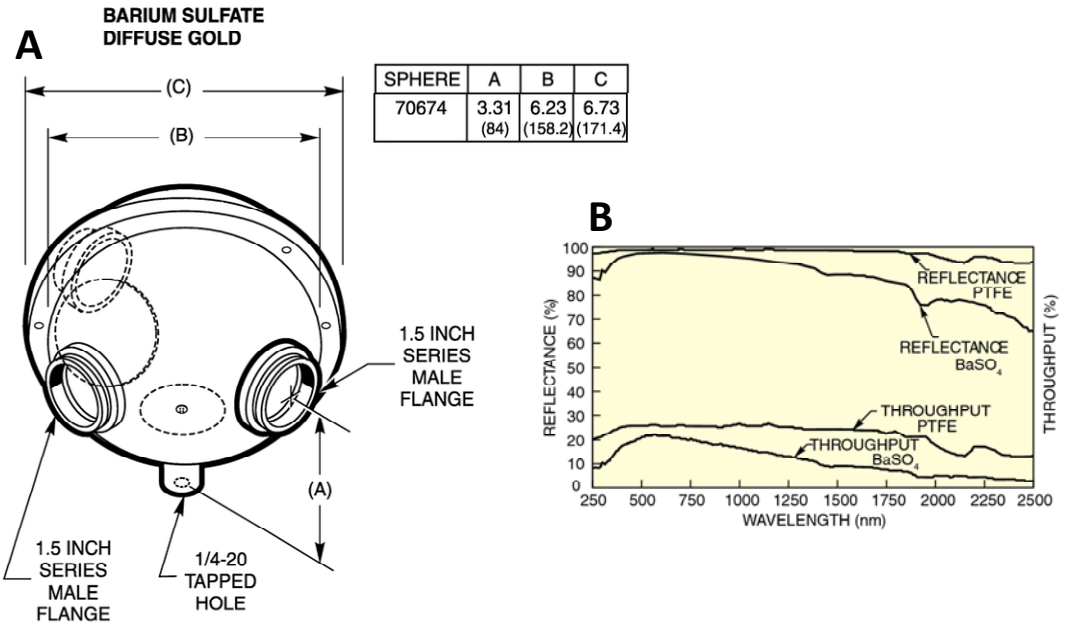

Figure 5.13. Integrating sphere used in the present work: A. Geometry parameters; B. Reflectance spectrum.

A schematic of the experimental setup for measuring the total diffuse reflectance and total diffuse transmittance is shown in Figure 5.14. Neutral density filters were used to reduce the intensity of the incident lasers beams

in order to prevent oversaturation of the detector. The detector (53-2754 Model, Coherent, USA) was attached to the integrating sphere and powered by a rresearch power supply (C2719, Hamamatsu, Japan). The signal from the detector was measured by a digital multimeter (34401A Model, Agilent Technologies, USA). Three reflection measurements were made on each sample. Measurements were referenced to a 98% Optopolymer reflectance standard (OPST3-C, Optopolymer, Germany) and a dark measurement (with the sample port open) (see Figure 5.3 and 5.4). The measured reflectance (M_R) was calculated using equation 5.11.

Although values of the sphere wall reflectivity are given by the manufacturer, the reflectivity may change if port reducers are used. Measurements of $R_0^{diffuse}$ and $R_{std}^{diffuse}$ were performed as shown in Figure 5.15 (following the setup in Figure 5.5) in order to calculate the reflectance of the sphere wall r_w. The integrating sphere was rotated with respect to the collimated beam so that the light was directed upon the sphere wall between the sample port and the baffle. The normalized area of the sphere wall a_w, sample port a_s, detector a_d, entrance port a_e were also measured. Finally, when calculating the sphere wall reflectance r_w (equation 5.13), we assumed that the reflectance of the detector was null.

The same integration sphere used for the reflection measurements was also used for the total diffuse transmission measurements. A mirror system diverted the laser beam as shown in Figure 5.14B. Therefore, the sample was not moved after the reflection measurements, and the reflection and transmission measurement were performed in the same spot of the sample. In this setup, only two ports were open, the 15mm-diameter sample port and the 11mm-diameter detector port with a baffle between ports. Again, three transmission measurements were made on each tissue sample. Measurements were referenced to 100% with the lasers illuminating the open port hole, and a dark measurement with an open port but with no illumination from the lasers. The measured transmittance (M_T) was calculated using equation 5.12.

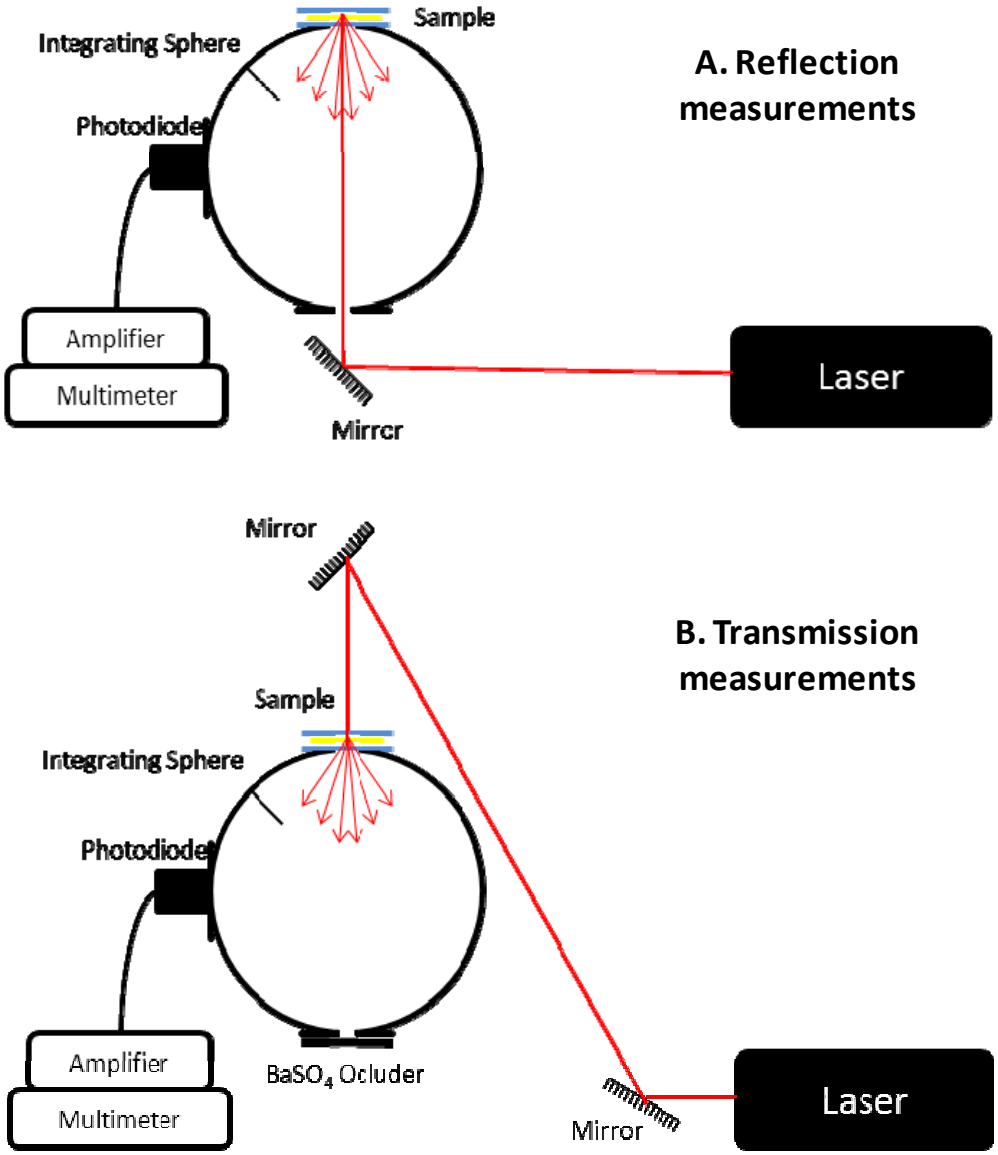

Figure 5.14. Schematic representation of the experimental setup, A) Configuration for Reflection measurements; and B) Configuration for Transmission measurements.

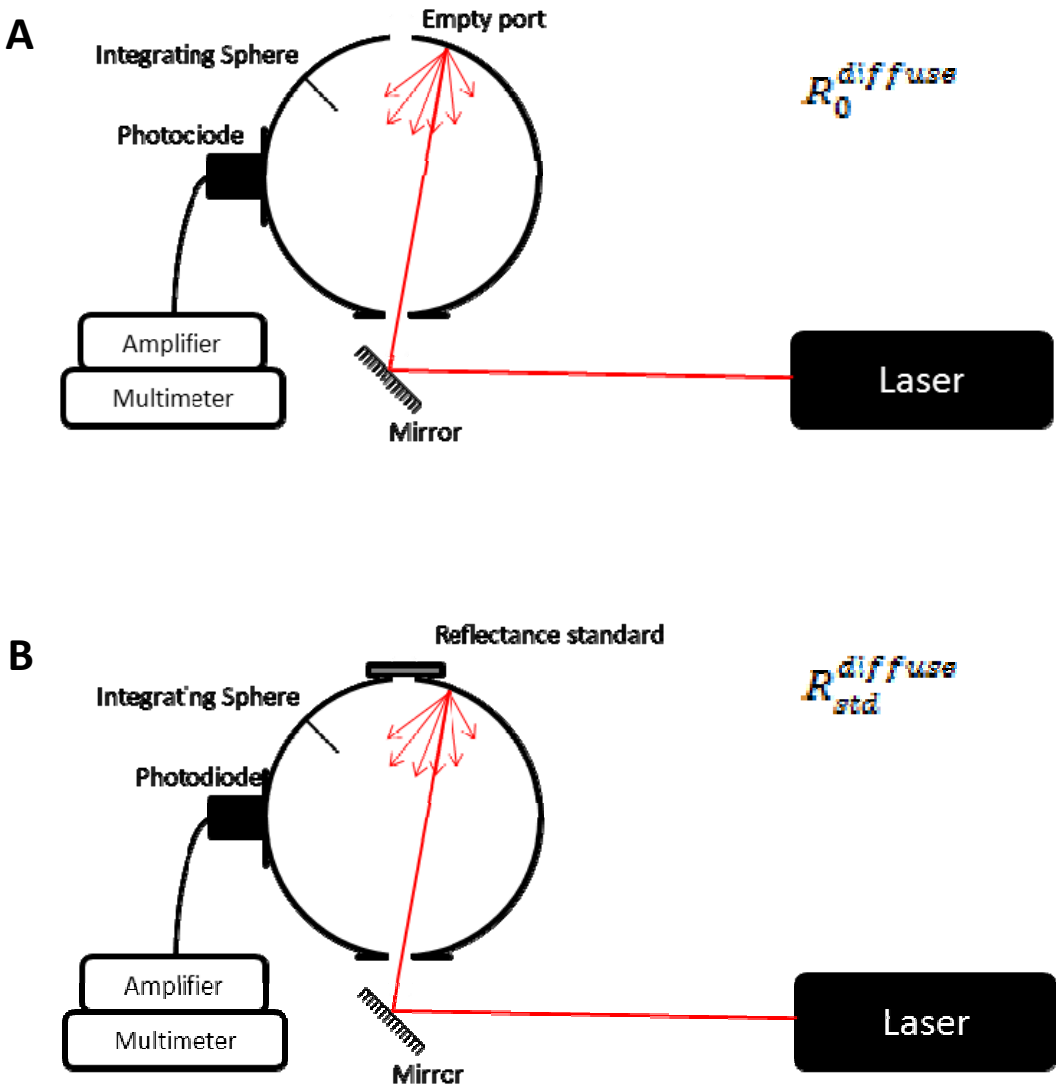

Figure 5.15. Schematic representation of the experimental setup used for the reference sphere calibration measurements.

Two other values are needed in the ***iad*** program to determine optical properties. The thickness of each tissue sample was measured using a Nikon Eclipse 90i light microscope (Nikon Instruments Inc., USA). The refractive index of the artificial human corneas samples was measured using an Abbe refractometer at 589nm (PCE Iberica, Spain). Changes in the refractive index over the wavelengths used in the present study were assumed negligible and, therefore, we considered the refractive index measured with the Abbe refractometer as constant for all the wavelengths studied in the present work.

Sample handling.

Biological tissue samples provide a unique challenge to evaluate optically. Tissue dehydration affects the refractive index of the tissue (Meek et al., 2003; Goodfellow et al., 1978), its scattering characteristics (Huang and Meek, 1999) and even absorption (Farrell et al., 1973). Therefore, the artificial human cornea and the porcine cornea were sandwiched between glass slides to limit the rate at which they dehydrated and provide support, and also to define the boundary conditions. PBS was used to ensure a good refractive index matching between the sample and the slide and to secure the hydration level of the samples.

Compression of tissue can lead to an increase in scattering and absorption due to a reduction in tissue volume that increases chromophore and scatterer concentrations (Tuchin, 2007). This is not a problem when using the IAD method since the program calculates the Fresnel reflections of incident light from the sample. The flat surface that sandwiching the samples produces, simplifies the accounting for Fresnel reflections.

*Inverse adding-doubling (**iad**) program*.

The ***iad*** program was developed by Prof. Scott Prahl from the University of Oregon and it is available at http://omlc.ogi.edu/software/. The measured

reflectance (M_R) and transmittance (M_T) are input data to the program along with experiment specific values. The values included the thickness and refractive index of the sample and any cover slides, the number of sphere used, the port diameters for each sphere, the reflectance of the wall of each sphere, and the reflectance of the calibration standard.

The basic structure of the data file the ***iad*** program uses consists of a header section followed by the effective measurements of reflectance and transmittance. The header describes details of the experiment and was designed to be:

(1) easily annotated,

(2) sufficiently flexible to accommodate all common experiments,

(3) readily analyzed by computer,

(4) filled with entries that have a simple physical meaning,

(5) a complete description of the experimental geometry, and

(6) devoid of rarely-used parameters.

An example of header of the data files used in the present work consists of

```
IAD1       # Must be first four characters

# The order of the entries is important
# Anything after # is ignored

1.3365     # Index of refraction of the sample
1.5        # Index of refraction of the top and bottom slide
0.322           # (mm) Thickness of the sample
1          # (mm) Thickness of the slides
2          # (mm) Diameter of the laser beam
0.9554     # Reflectance of the calibration standard
1          # Number of spheres used during each measurement

# Properties of the integrating sphere used for reflection measurement

158.2           # (mm) Sphere diameter
15         # (mm) Sample port diameter
15         # (mm) Entrance port diameter
11         # (mm) Detector port diameter
0.9246     # Reflectance of the sphere wall

# Properties of the integrating sphere used for reflection measurement

158.2           # (mm) Sphere diameter
15         # (mm) Sample port diameter
15         # (mm) Entrance port diameter
11         # (mm) Detector port diameter
0.9246     # Reflectance of the sphere wall
5          # Number of measurements
```

#Lambda	M_R	M_T	M_U	r_w	r_std
457	0.21487	0.62431	0	0.9246	0.9554
488	0.18942	0.61791	0	0.9324	0.9548
514	0.12245	0.67958	0	0.9127	0.9544
633	0.16221	0.73173	0	0.9327	0.9519

Note: M_U represents the measured unscattered transmission and was not studied in the present work. The program allows the assignation of zero value to the parameter that is unknown.

The ***iad*** program is run from the command line. It is used with data files that contain header like the one shown before. Also, the program consists of command line switches that assign different values to variables that have not been measured. Figure 5.16 lists some of the command line options.

Figure 5.16. Command line options of the ***iad*** program.

For each sample and time in culture studied, an .rxt file was created containing the header and measurements values experimentally obtained.

The program logic is schematized by the flow chart in Figure 5.17. The program initializes by calculating a course grid for measured reflectance and transmittance values with preset absorption (μ_a) and scattering coefficients (μ_s) and anisotropy (g) (when unscattered transmission is input) with the adding-doubling algorithm. The lost light through the sample edges is initialized to zero. The adding-doubling algorithm then loops to calculate the diffuse and direct reflectance and transmittance for a set of optical coefficients (μ_a, μ_s and g), subtracts the lost light proportionally for the diffuse and direct fractions, and calculates the total reflectance and transmittance. The process is repeated by changing the optical coefficients until the calculated values equal the measured values. When they match, the Monte Carlo simulation is performed to calculate the fraction of lost light. The adding-doubling loop is repeated to find new optical coefficients with the lost light correction. The Monte Carlo simulations are repeated until both the change in the predicted absorption and scattering coefficients is less than 0.1%.

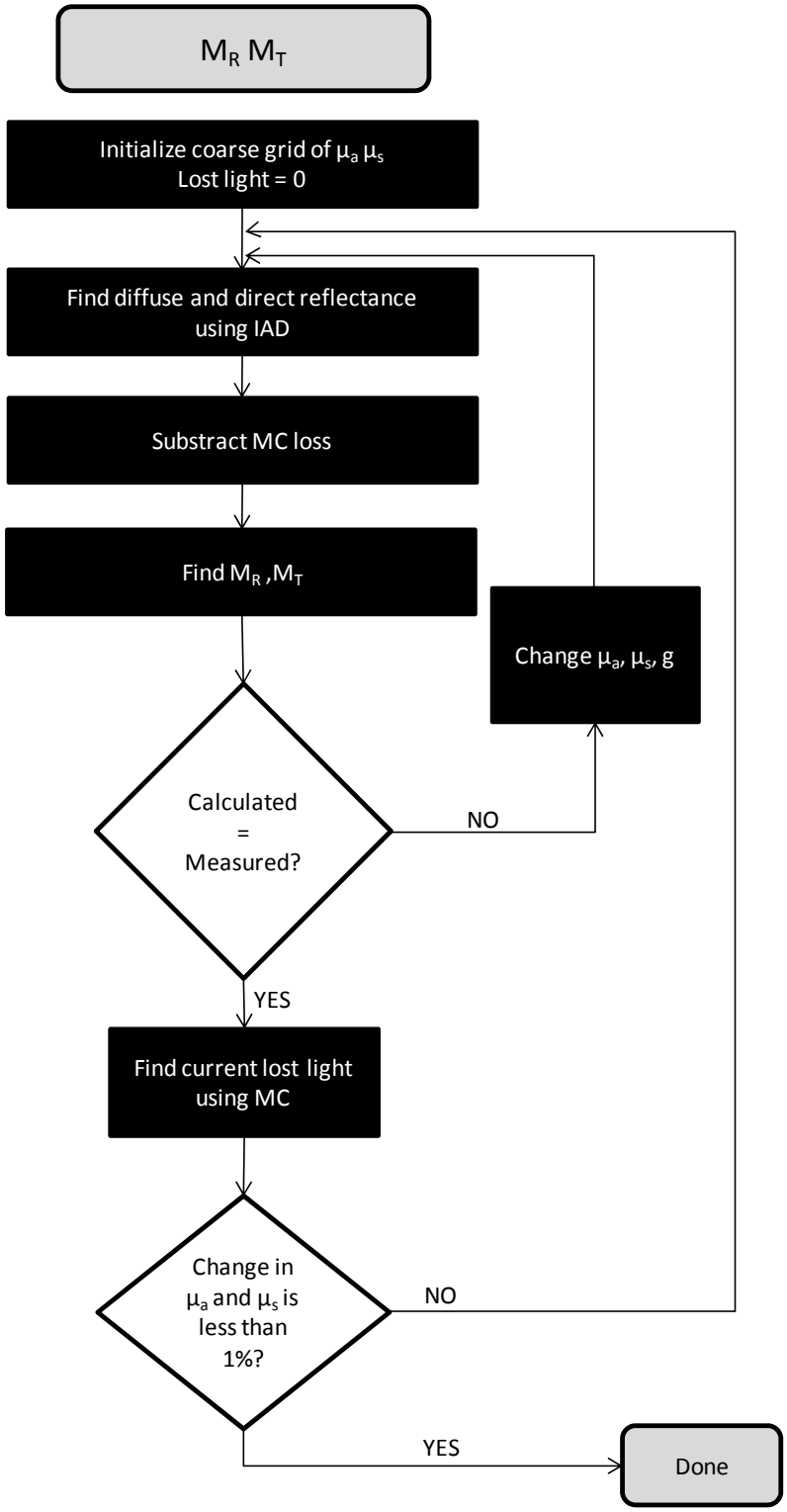

Figure 5.17. The logic flow of the inverse adding-doubling program (courtesy of Prof. Scott Prahl).

Statistical analysis.

To study the variations in reflectance, transmittance, scattering and absorption levels, we used two statistical tests: the Kruskal-Wallis one-way analysis of variance by ranks, which is a nonparametric method for testing average equality of measures among groups, and the Mann-Whitney U test. This latter test is a non-parametric test that enables the pair-wise comparison of two distributions. These two non parametric tests were used because the samples do not fulfill the test of homogeneity of variance. A significance value below 5% was considered as statistically significant.

To determine the level of similarity of two different distributions, the VAF (variance accounting for) coefficient with Cauchy-Schwarz's inequality was used as follows:

$$VAF = \frac{(\sum_k a_k b_k)^2}{(\sum_k a_k^2)(\sum_k b_k^2)}$$

where a_k is the value of each absorption or scattering (for each wavelength) and b_k is the equivalent for another measurement. The closer this coefficient gets to unity (100%), the more similar the curves are.

RESULTS AND DISCUSSION

Experimental setup calibration.

Reflection and transmission measurements under the same configuration as the one used for the artificial and control samples studied in this work were performed three times for the optical phantom used as calibration standard. The experimental values obtained for the measured reflectance M_R and transmittance M_T are shown in Figure 5.18.

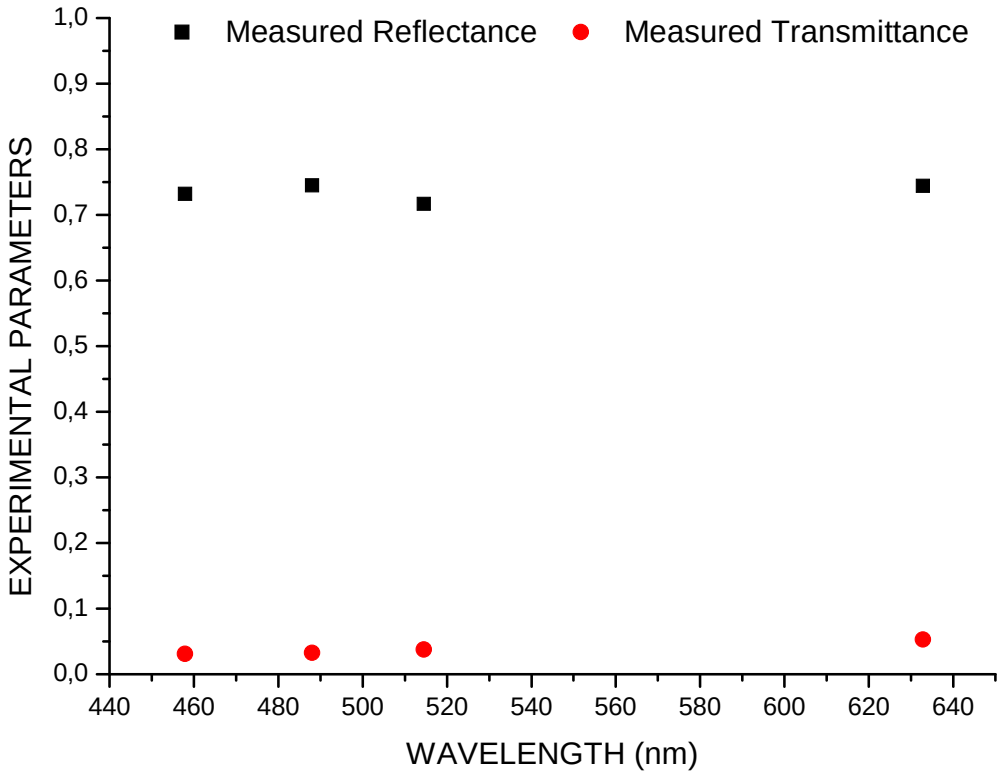

Figure 5.18. Measured reflectance (M_R) and transmittance (M_T) of the optical phantom.

The refractive index of the phantom was 1.5 and its thickness 1.72mm. The average scattering anisotropy coefficient was considered to be 0.6, since this was also the value that the manufacturer used to calculate the true optical values of the phantom. These values together with M_R and M_T were implemented in the ***iad*** program and the absorption (μ_a) and reduced scattering (μ'_s) coefficients were determined. Figure 5.19 shows the comparison between the experimental and true values (given by the manufacturer) of the absorption (μ_a) and reduced scattering (μ'_s) coefficients of the optical phantom. The relative error is displayed in Table 5.3.

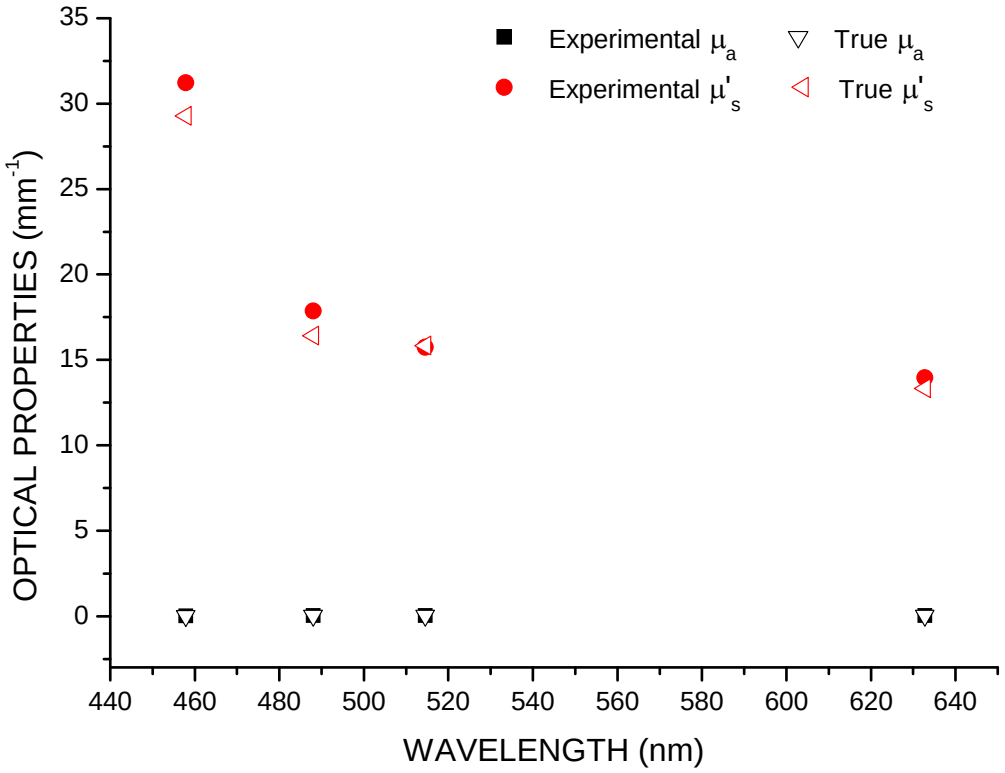

Figure 5.19. Experimental and true values of the absorption (μ_a) and reduced scattering (μ'_s) coefficients of the optical phantom

Relative error	μ_a	μ'_s
457.9nm	**0.83%**	**6.60%**
488nm	**6.40%**	**8.86%**
514.5nm	**4.89%**	**0.53%**
632.8nm	**8.93%**	**4.57%**

Table 5.3. Relative error between the calculated absorption (μ_a) and reduced scattering (μ'_s) coefficients values and the true values of the optical phantom.

The values of the optical properties of the phantom, determined using our single integrating sphere setup are consistent with the true values given by the manufacturer. The maximum error for both absorption and reduced scattering coefficients was less than 9% in all cases. Each of these errors was considered when the optical properties determination of the different samples analyzed in this Thesis were determined.

Microscopic evaluation of the fibrin-agarose corneal construct.

Since no scanning electron microscopy images were taken for the control cornea, used in this work for comparison with the optical properties, the microscopic evaluation of the fibrin-agarose corneal construct was referenced to SEM images of normal native corneas from published papers (Mi et al., 2010).

The SEM analysis of the fibrin-agarose corneal construct showed that the epithelial cells were evenly distributed on the surface of the construct and homogenous in shape and size (Figure 5.20A), similar to the ones of the control cornea (black box in Figure 5.20A).

Also, the fibers within the artificial cornea seemed densely packed and homogeneous (Figure 5.20B) with a morphology similar to the control cornea, although not equally organized (black box in Figure 5.20B)

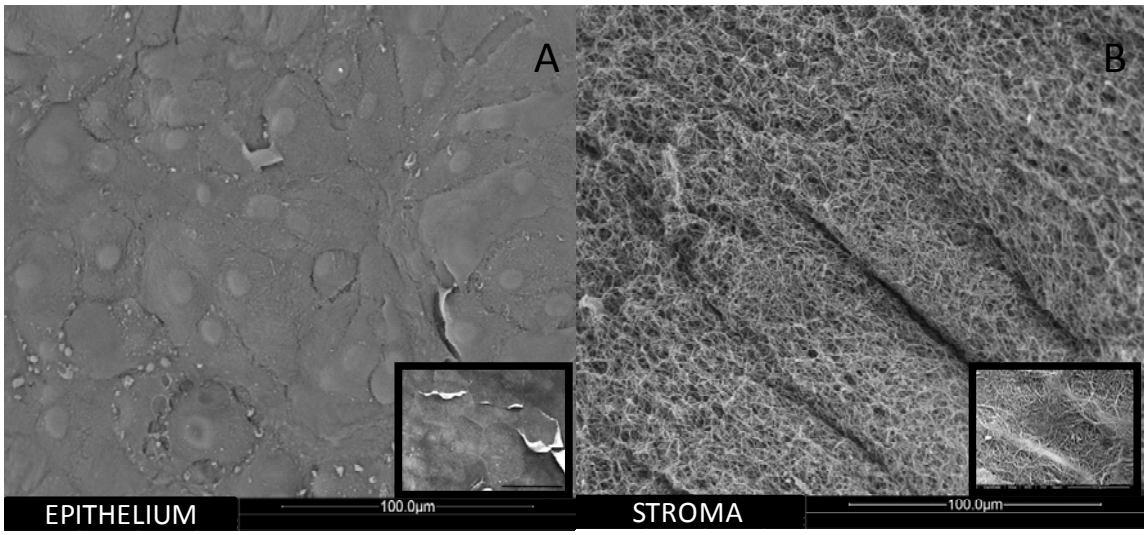

Figure 5.20. Scanning electron micrographs of the artificial fibrin-agarose human cornea: A. Epithelium; B. Stroma. The black boxes show the corresponding corneal layers of a control cornea (Mi et al., 2010)

Optical properties of bioengineered human cornea substitutes.

Measurements of the reflectance and transmittance were repeated three times for each sample of bioengineered human corneas (3 samples/week of analysis) and for each control porcine cornea. These experimental values together with their standard error are presented in Figure 5.21.

The spectral distribution analysis showed that the reflectance values of both artificial and native samples displayed an almost constant behavior for all the wavelengths studied, whereas the transmittance values tended to increase with increasing wavelengths. Statistically significant differences were found when comparing the reflectance and transmittance values for the shorter wavelengths (457.9 and 488nm) with the ones for the larger wavelengths (514.5 and 632.8nm), except for the third week sample (p=0.828 for M_R and p=0.128 for M_T). It can be clearly seen that all artificial samples followed the optical behavior of the control cornea (VAF values higher than 98.63%; Table 5.3), exhibiting for all wavelengths higher transmittance than reflectance, as it would be expected for human cornea substitutes.

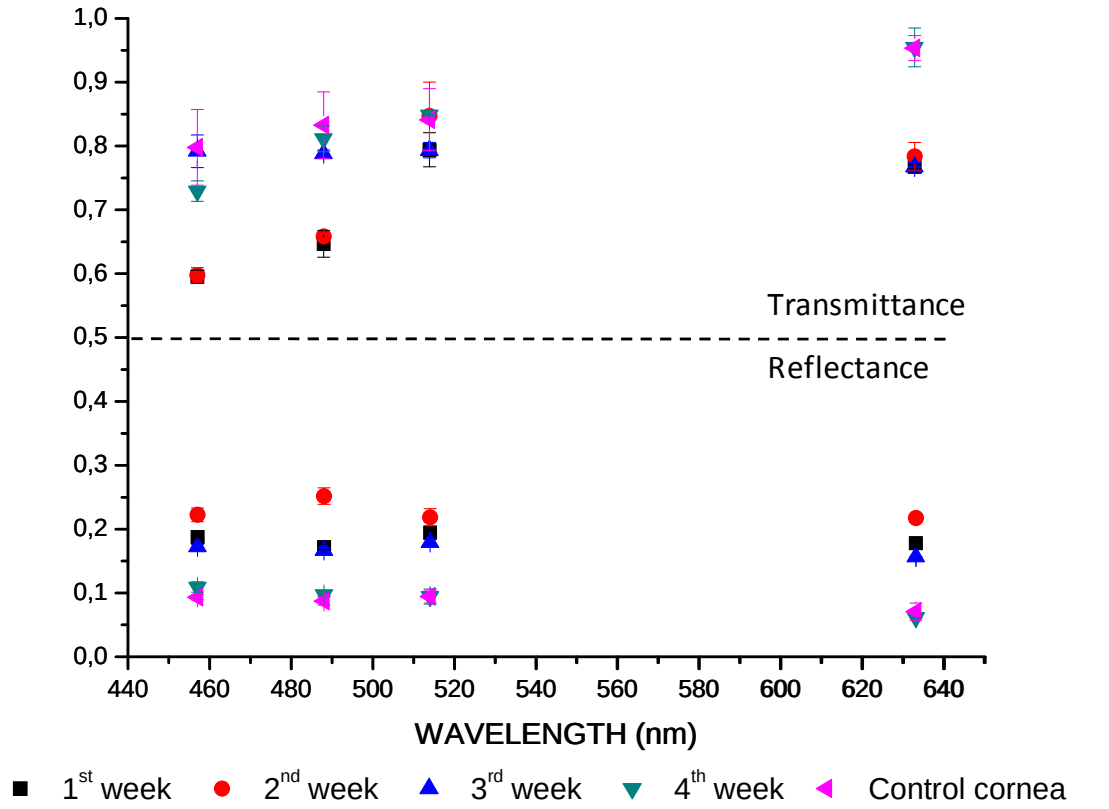

Figure 5.21. Comparison between the values of the measured transmittance and reflectance of all the samples studied in the present Thesis

Comparison between the control cornea and bioengineered cornea after	MR	MT	μ_a	μ'_s
One week	**99.22%** *p<0.001*	**99.20%** *p<0.001*	**86.79%** *p<0.001*	**97.43%** *p<0.001*
Two weeks	**98.63%** *p<0.001*	**98.73%** *p<0.001*	**71.98%** *p=0.105*	**96.45%** *p<0.001*
Three weeks	**99.59%** *p<0.001*	**99.35%** *p<0.001*	**34.52%** *p=0.164*	**95.35%** *p<0.001*
Four weeks	**98.96%** *p=0.016*	**99.87%** *p=0.140*	**95.26%** *p<0.001*	**95.79%** *p<0.001*

Table 5.4. Statistical VAF values for the comparison between control cornea and bioengineered cornea.

Thus, the human artificial corneas are able to transmit the specific wavelengths analyzed in the present study, mimicking the natural optical behavior of the native cornea. In all cases, the bioengineered human corneas had transmittance values higher than the 60% transparency threshold established by Ventura (Ventura et al., 2000) for quality tissues suitable for corneal transplantation.

Time of development in culture was an influencing factor on these experimental results. The reflectance values increased until the second week of development in culture and decreased for the following two weeks analyzed, reaching values similar to those of the control cornea after four weeks in culture. The statistical analysis revealed significant differences for all comparisons performed between the reflectance values of the different artificial samples and also for all comparisons with the control cornea (p<0.001). Whereas transmittance, in the initial stage (first and second weeks), the bioengineered corneas displayed the lowest transmittance values, except for the 514.5nm wavelength. In addition, no significant differences were found between the transmittance values of the first and second week samples (p=148) and the fourth week sample and the control cornea (p=140).

As in the case of reflectance, the values of transmittance obtained for the artificial fibrin-agarose constructs were very similar to the ones obtained for the control cornea, for the last two weeks studied, except the value obtained for the 632.8nm wavelength in the third week. Note that high similarities with the native control cornea were found for both reflectance and transmittance (for all wavelengths), in the fourth week of development in culture. Moreover, the statistical p-value was 0.016 in the case of reflectance and 0.140 for transmittance, showing that the differences between the control cornea and the fourth week artificial sample were not statistically significant in the case of transmittance, contrary to what happened for reflectance.

In order to implement the measured reflectance and transmittance values in the ***iad*** program, the refractive index and thickness of the samples were also determined. The measured refractive index values varied from

1.330 to 1.340 for the artificial human corneas. For each sample, measurements were repeated three times and the obtained values agreed within 5%. For all of the ***iad*** calculations, an average value of 1.335 was assumed for all the artificial samples analyzed. The variation of the refractive index of the porcine cornea was reported to be within the 1.373-1.405 range (Miclea et al., 2011). In our study, an average value of 1.375 was considered. Since only measurements of the diffuse reflection and transmission were made, the average scattering anisotropy coefficient of both artificial and control cornea was assumed to be 0.9, based on the results obtained by previous authors (Sardar et al., 2009; Cheong et al. 1990) who found that the range of the anisotropy coefficient for ocular tissues is 0.85-0.99.

The calculated reduced scattering and absorption coefficients of the artificial and control corneas showed variation across the wavelengths studied (Figure 5.22 A and B).

The absorption coefficient values decreased with increasing wavelength, except for the samples analyzed in the third week of development where a slight increase was observed for the 632.8nm wavelengths. One remarkable characteristic of the human cornea is its ability to protect the deeper corneal structures against the radiation of short wavelengths (Podskochy, 2004). Therefore, any artificial corneal construct generated by tissue engineering to replace this native tissue has to fulfill this requirement. In our case, the highest absorption coefficient values were recorded for the shortest wavelengths (457.9, 488nm). In addition, the statistical comparison between the absorption values obtained for the shorter wavelengths (457.9 and 488nm) and the ones for larger wavelengths (514.5 and 632.8nm) found significant difference for each week studied, except the third one (p=0.509). Since the reflectance and transmittance values were time in culture dependent, their variation is consequently reflected in the scattering and absorption values.

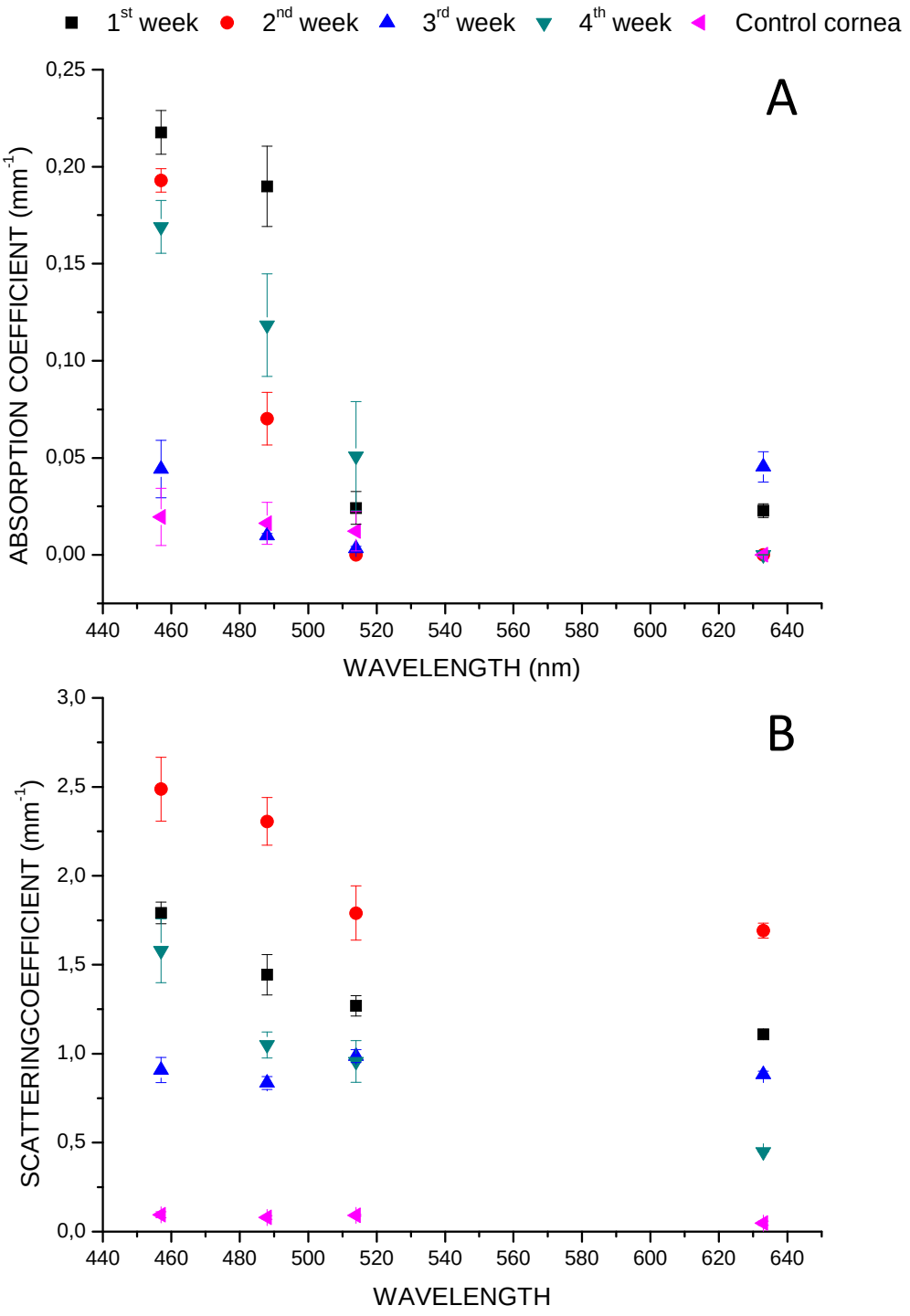

igure 5.22. Optical properties of the bioengineered human cornea and native porcine cornea as determined by the ***iad*** program: A. Absorption coefficient values; B. Scattering coefficient values

The artificial corneas showed absorption coefficients whose values decreased in the third week of culture before slightly increase in the fourth week. The control cornea displayed small absorption values for the specific wavelengths studied with significant differences between the short and the large wavelengths (p=0.005).

Although, similar values were reached by the bioengineered cornea after three weeks in culture with no significant differences (p=0.164), the high value registered for the 632.8nm makes that the overall absorption spectral behavior after three weeks differ from the one of the control porcine cornea (VAF=34.52%-Table 5.4)

The optical analysis of the fibrin-agarose corneal constructs revealed that the spectral behavior of the reduced scattering coefficient was similar to the control cornea although the values were higher in all cases (p<0.001, VAF>95.35%-Table 5.4). The order in the organization of the fibers and cells that constitute the native cornea affects how light interacts with the tissue (Mourant et al., 2000; Meek et al., 2003). In this sense, the high level of organization acquired by native cornea explains the lower scattering values. Nevertheless, the reduced scattering coefficient values decreased with increasing wavelength (except in the third week) and were higher than the absorption values. These results are in agreement with existing literature (Tuchin, 2007; Klose and Larsen, 2006; Cheong et al., 1990;) that states that scattering prevails over absorption in biological tissues. As in the case of absorption, the statistical comparison between the reduced scattering values obtained for the shorter wavelengths (457.9 and 488nm) and the ones for larger wavelengths (514.5 and 632.8nm) found significant difference for each week studied. Time in culture also played an important role in the scattering properties of the artificial human cornea. In general, the highest values were registered in the second week in culture, while the lowest ones after three weeks. Statistically significant differences were found for all comparisons made between all the samples analyzed (p<0.001).

Overall, taking into account the optical properties values obtained in the present study, the artificial fibrin-agarose human corneal substitutes shared many similarities with native control cornea after four weeks of development in culture. Moreover, the fact that no significant differences were found between the transmittance values of the control cornea and the fourth week artificial sample encourages us to recommend a period of four weeks for the development of artificial fibrin-agarose human cornea before it can be considered for several clinical purposes.

6. OPTICAL PROPERTIES OF A BIOMIMETIC MODEL OF HUMAN ORAL MUCOSA BASED ON FIBRIN AND FIBRIN-AGAROSE

BACKGROUND

Understanding the effects of the interaction between light and biological tissues are important not only for those tissues that compose the eye (main organ of vision), but also for those who undergo laser surgery. Laser applications are of particular interest in oral soft tissues surgery due to the many advantages that it may offer compared to conventional instruments (Sulieman, 2005). In particular, laser equipments can be easily used for surgical treatment of vascular lesions such as haemangioma and lymphangioma, thanks to the possibility to control bleeding and avoid the use of suture (Deppe and Horch, 2007). They can be used not only for treatment but also for diagnosis. Goldman (1965) was the first in using the laser technology in dentistry. The distribution and propagation of photons in laser-irradiated tissues are strongly influenced by the fundamental optical properties such as scattering and absorption. Therefore, determining the fundamental properties of tissues has become imperative since establishing a diagnostic or development of imaging devices for oral diseases in the spectral range of interest requires a detailed knowledge of optical parameters to predict performance and effectiveness (Sardar, 2007).

The human oral mucosa is commonly affected by a high number of clinical disorders including congenital abnormalities, infection, periodontal diseases, traumatism, neoplasms, *lichen planus* and *pemphigus vulgaris* (Muñoz-Corcuera et al., 2009; Albandar. 2005; Porter and Leao, 2005) that could result in large tissue defects.

Reconstruction of these defects represents a real challenge since maxillofacial surgeons are often confronted with the lack of oral mucosa to

replace the excised tissues (Song et al., 2004). The oral mucosa acts as a barrier against the external environment. Loss of this barrier function causes dehydration and a high risk of infection. Reconstructions in the oral cavity, as required after tumor resections or cleft palate repair, are often complicated by similar problems. In the last two decades, the field of tissue engineering has provided new solutions to these problems. By using tissue engineering techniques, some researchers have recently proposed different methods for construction of an organotypic substitute of the oral mucosa (Sanchez-Quevedo et al., 2007; Schultze-Mosgau et al., 2004; Song et al., 2004; Lauer and Schimming, 2001). In a recent work on the effects of fibrin and fibrin-agarose on the extracellular matrix profile of bioengineered oral mucosa, San Martin and collaborators (San Martin et al., 2013) showed that the artificial oral substitutes displayed histological and molecular similarities with native human oral mucosa stroma. In addition, they observed that the nature of the biomaterial influenced the behaviour of the oral stromal fibroblasts, thereby modulating their growth, protein synthesis, and collagen fibrillogenesis.

Although some of the histological and morfological properties of tissue-engineered oral mucosa have been described (Moharamzadeh, 2007; Sánchez-Quevedo et al., 2007), to the best of our knowledge a systematic investigation of the propagation of light radiation through artificial human oral mucosa have not been performed. In this sense, the use of lasers can represent an important measurement tool in the investigation of propagation of light throughout the tissue and also a quality control instrument for the adequacy of the artificial specimen compared with the native one.

The aim of the present work is to provide an estimation of the optical properties of artificial human oral mucosa in the visible region, using the inverse adding doubling (IAD) method (Prahl et al., 1993). One integrating sphere is employed to measure the diffuse reflectance and diffuse transmittance for a new nanostructured model of artificial human oral mucosa and, also, for native rabbit oral mucosa, used as control sample.

MATERIALS AND METHODS

Human tissue samples

Twenty small biopsies of oral mucosa were obtained from healthy donors undergoing minor oral surgery during local anesthesia at the School of Dental Sciences at the University of Granada, Spain. They corresponded to normal keratinized oral mucosa located at the retromolar trigonum. Immediately after extraction, all tissues were kept in a transport medium at 4ºC containing Dulbecco's Modified Eagle's Medium (DMEM), 100U/ml penicillin G, 100µl/ml streptomycin and 0.25µg/ml amphotericin B, and processed before 24h. All patients provided informed consent to participate in the study and the study was approved by the local research committee.

Construction of oral mucosa substitutes by tissue engineering

The materials used in the present work were generated employing the same method described in Chapter 3, with the difference that the cells used this time were human oral mucosa fibroblasts. Briefly, primary cultures of oral mucosa fibroblasts were generated as previously described (Sanchez-Quevedo et al., 2007). Stromal samples were isolated from small fragments of oral mucosa, using collagenase I (Invitrogen-Gibco) at 37 ◦C for 6 h. Once the cells had been harvested by centrifugation, stromal fibroblasts were cultured in DMEM supplemented with 10% fetal bovine serum (FBS, Sigma- Aldrich), 4 mM L-glutamine, and 1% antibiotic–antimycotic solution (Invitrogen-Gibco). All cells were incubated at 37ºC in 5% carbon dioxide under standard culture conditions.

Then, 2 types of bioengineered oral mucosa stromal substitute were generated in the laboratory: human fibrin and fibrin with 0.1% agarose

concentration stromas. In both cases, 21 ml of human plasma were added to 1.8 ml of DMEM in which 250,000 cultured fibroblasts had been previously suspended, and 200 µL of tranexamic acid (Amchafibrin, Fides-Ecofarma, Valencia, Spain) were added to avoid spontaneous fibrinolysis. Then, 2 ml of 1% of $CaCl_2$ were added to the solution to precipitate the polymerization reaction of the hydrogel. In the case of the fibrin–agarose gels, previously melted type VII agarose dissolved in PBS (phosphate-buffered saline) was supplemented in the last step. After polymerization, 15 ml of culture medium were added to the surface of the bioengineered oral mucosa substitutes, which were incubated at 37ºC in 5% carbon dioxide. Samples of the different oral mucosa substitutes were studied weekly until four weeks of development in culture.

Acellular fibrin and fibrin-agarose constructs were also generated following the same construction protocol in order to evaluate the influence of the oral fibroblasts on the optical properties of the artificial oral mucosa substitutes.

Once generated before being subjected to the optical measurements all samples were nanostructured, following the method described in Chapter 3 (Hadjipanayi et al., 2011).

The thickness of the samples was determined using a Nikon Eclipse 90i light microscope (Nikon Instruments Inc., USA). All bioengineered oral mucosa tissues were generated and analyzed in triplicates. As controls, 3 fresh rabbit oral mucosa were obtained from adult rabbits immediately after death and were subjected to the same optical tests as the bioengineered artificial oral mucosa constructs.

Determination of the optical properties

Inverse adding doubling was used to find the scattering and absorption of the artificial human oral mucosa and native rabbit oral mucosa using total

reflection and total transmission measurements. The protocol used for these measurements was the same described in Chapter 5 for the artificial human corneas. Figure 6.1 shows the schematic representation of the experimental setup used to perform the reflection and transmission measurements.

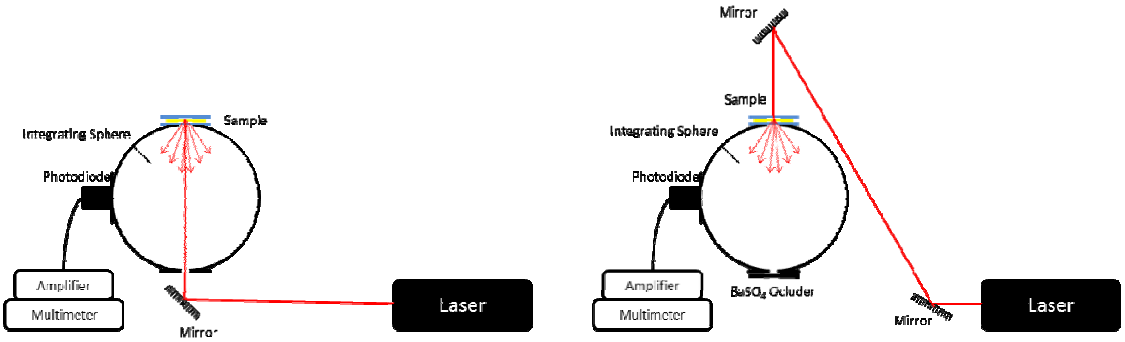

Figure 6.1. Schematic representation of the experimental setup, A) Configuration for Reflection measurements; and B) Configuration for Transmission measurements.

Statistical analysis

As normality (and homogeneity of variance) assumptions were not satisfied, non-parametric tests were used. To test the significance of observed differences between the study groups, the Kruskal-Wallis one-way analysis of variance by ranks (K-W) and the Mann-Whitney U test (M-W) were applied. Considering the Bonferroni's correction, a value of $p \leq 0.001$ was considered to be statistically significant.

RESULTS AND DISCUSSION

Construction of an efficient artificial oral mucosa by tissue engineering represents a major scientific challenge. The use of these kinds of tissue substitutes can help oral and maxillofacial surgeons to improve the outcome of patients in need of large reconstructions involving the oral cavity (Izumi et al., 2003; Lauer and Schimming, 2001; Schlenz et al., 2001; Ueda et al., 1991). In this study, two types of artificial human oral mucosa substitutes (fibrin,

fibrin with 0.1% agarose concentration) were successfully generated in the laboratory and could be used as in vitro models for investigations of experimental pharmacology or toxicology tests, thus avoiding the need for animal research (Alaminos et al., 2006, Sanchez-Quevedo et al., 2007). Previous results by Sanchez-Quevedo and collaborators (Sanchez-Quevedo et al., 2007) on the histological and histochemical evaluation of the human oral mucosa constructs developed by tissue-engineering, using the same method for the generation of the constructs that we used in the present work, proved that the fibrin-agarose complexes satisfy the criteria for biomaterials used in tissue engineering of the human oral mucosa. Nevertheless, the novel technique of nanostructuring that we used for the successful development of human bioengineerd corneas (Ionescu et al., 2011), contributes to provide also useful solutions for the generation of artificial oral tissues by tissue engineering, since reconstructions in the oral cavity, as required after tumor resections, are often complicated. Moreover, Haugh and collaborators (Haugh et al., 2012) showed that the plastic compression (concept the nanostructuring technique is based on) significantly increases the compressive properties of fibrin gels without impairing cellular viability and subsequent extracellular matrix synthesis.

Nowadays, laser-assisted procedures complement conventional treatment in many cases of oral disorders; in some areas laser treatment being now considered the therapy of choice. When applying these therapies, the precise knowledge of the optical properties of examined tissue and also of the surrounding tissues, acquires great importance. For this, the IAD algorithm provides an accurate estimation of the optical properties for biological tissues, such as artificial human oral mucosa and native rabbit oral mucosa tissues studied in the present work, from measurements of the index of refraction, scattering anisotropy coefficient, diffuse total reflectance and diffuse total transmittance.

The measured refractive index values varied from 1.330 to 1.340. For each sample, measurements were repeated three times and the obtained

values agreed to within 5%. For all of the IAD calculations, an average value of 1.335 was assumed for all samples analyzed. Since only measurements of the diffuse reflection and transmission were made, the average scattering anisotropy coefficient of both artificial and control oral mucosa tissues was assumed to be 0.9, based on the results obtained by Cheong et al. (1990) who found that the range of the anisotropy coefficient for biological tissues is 0.73-0.99.

The thickness of the sample was measured weekly and immediately after the nanostructuration process, and values between 0.15 and 1mm were obtained.

The total diffuse reflectance (R_d) and total diffuse transmittance (T_t) measured at 457.9nm, 488nm, 514.5nm from the argon laser and 632.8nm from the He-Ne laser, along with the values of the thickness, refractive index and scattering anisotropy coefficient, were input into the ***iad*** program. The output of the IAD program consisted of the reduced scattering (μ'_s) and absorption (μ_a) coefficients, listed in Table 6.1 and Table 6.2, respectively.

The fibrin oral mucosa samples displayed values of reduced scattering coefficient higher than the ones of the fibrin-0.1% agarose oral mucosa constructs (p<0.001). In general, as expected for biological tissues, the reduced scattering decreased with increasing wavelength. The time of maturation in culture played an important role in the development of the scattering properties of the bioengineered samples. The scattering properties of the fibrin and fibrin with 0.1% agarose artificial tissues increased until the second week in culture, decreased for the third week, to increase again in the fourth week in culture. This increase is more pronounced for the fibrin sample, which showed the highest reduced scattering coefficient values after four weeks of development in culture, than for the fibrin-0.1% agarose sample, which showed the highest reduced scattering coefficient values after only two weeks of development in culture. Nevertheless, these maximum values of the reduced scattering for both fibrin and fibrin with 0.1% agarose bioengineered samples were similar to that of the native rabbit oral mucosa,

with statistically significant differences in the second week of development in culture both for fibrin (p=0.025) and fibrin with 0.1%-agarose (p=0.003)

Reduced Scattering coefficient (mm^{-1})					
Wavelength (nm)	Fibrin oral mucosa sample				Native rabbit
	T1	T2	T3	T4	
457.9	2.402	3.654	2.618	4.394	3.446
488	2.047	3.562	2.255	4.137	3.199
514.5	1.806	3.098	2.646	3.870	2.870
632.8	1.697	2.698	1.721	2.705	2.639
	Fibrin-0.1% agarose oral mucosa sample				Native rabbit
	T1	T2	T3	T4	
457.9	1.527	3.285	1.284	1.468	3.446
488	1.526	2.573	1.220	1.289	3.199
514.5	1.789	2.849	1.133	1.666	2.870
632.8	1.166	2.102	0.993	1.008	2.639

Table 6.1. Reduced scattering coefficient values as calculated using the ***iad*** program.

San Martin et al., (2013) analyzed the number of cells in the fibrin and fibrin-agarose oral mucosa substitutes and found that the fibrin construct displayed a higher number of cells than the fibrin-0.1% agarose ones after two and four weeks of development in culture. Moreover, these cells numbers were similar to the one of human oral mucosa. In addition they revealed a complete degradation of the most of the fibrin in the fibrin constructs after four weeks of development in culture, whereas the fibrin degradation was much slower in the fibrin-0.1% agarose constructs. These findings together with the fact that the majority of light scattering in biological tissue is due to the cells themselves (Mourant et al, 2000) could explain the values of scattering coefficient of the fibrin and fibrin-0.1% agarose human oral mucosa substitutes and their similarity with the native tissue. Besides, the statistical

analysis revealed no significant differences between the artificial constructs and the native rabbit oral mucosa when a general comparison was performed (p=0.098)

When comparing the scattering values of the cellular constructs with the ones of the acellular ones, higher values were obtained for these last substitutes (Figure 6.2) (p<0.001). In addition, similar with what happens for the cellular constructs, the fibrin acellular constructs displayed scattering values higher than the fibrin-agarose constructs (p<0.001). Thus, the small addition of agarose to the fibrin scaffold plays an important role on the scattering properties of the artificial human oral mucosa substitutes, statistically significant differences being found when comparing the different materials (p<0.001). One approach that is used when studying the light scattering by biological tissues states that the scattering depends on the spatial refractive index variation among the different components of the tissues (Mourant et al., 1998). In our case, the lower scattering values of the cellular constructs suggest that artificial tissues suffer a remodeling of the internal organization of tissue components when cells are encapsulated in the scaffolds. This would produce a decrease in the spatial refractive index variation and, therefore a decrease in the scattering coefficient values.

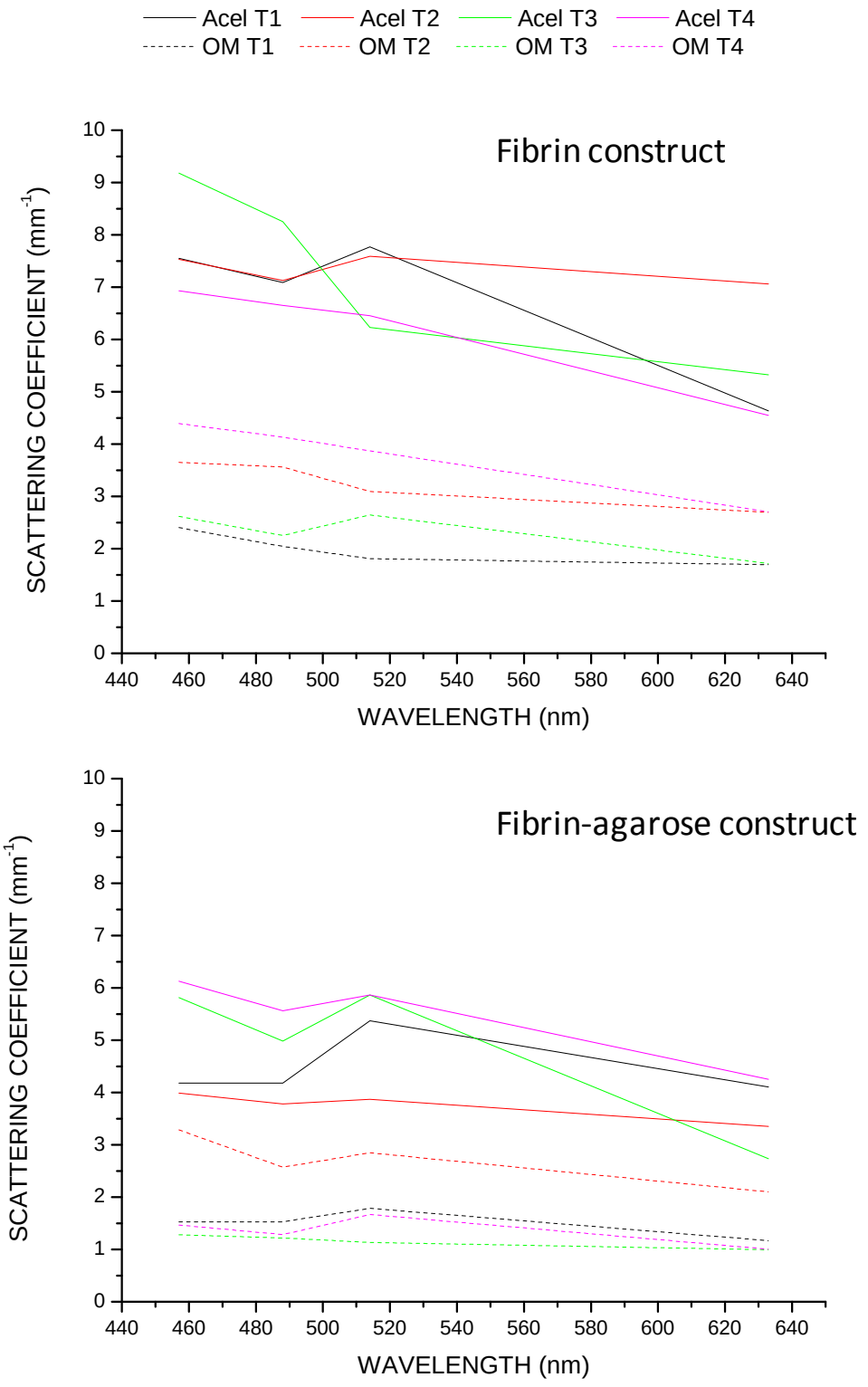

Figure 6.2. Comparison between the scattering coefficient values of acellular (straight line) and cellular (dash line) oral mucosa constructs based on fibrin and fibrin-agarose.

Wavelength (nm)	Absorption coefficient (mm^{-1})				
	Fibrin oral mucosa sample				Native rabbit
	T1	T2	T3	T4	
457.9	0.063	0.068	0.048	0.147	0.237
488	0.069	0.100	0.005	0.177	0.225
514.5	0.014	0.000	0.185	0.024	0.159
632.8	0.000	0.088	0.000	0.081	0.237
	Fibrin-0.1% agarose oral mucosa sample				Native rabbit
	T1	T2	T3	T4	
457.9	0.012	0.175	0.000	0.028	0.237
488	0.006	0.054	0.000	0.032	0.225
514.5	0.037	0.038	0.000	0.023	0.159
632.8	0.014	0.029	0.000	0.040	0.237

Table 6.2. Absorption coefficient values as calculated using the ***iad*** program.

All the artificial constructs of human oral mucosa displayed small or no absorption properties. The values of the absorption coefficient of the control rabbit oral mucosa showed variation across the wavelengths studied decreasing with increasing wavelength. Statistically significant differences were found when comparing the absorption values of the artificial constructs at all times of development in culture with the ones of the control rabbit oral mucosa sample (K-W and M-W $p<0.001$). In biological tissue the responsible cellular components for the absorption are proteins and nucleic acids. Our results suggest that the cells in the artificial fibrin and fibrin-agarose oral mucosa constructs were not committed to the synthesis and secretion of an important amount of absorbing components during the period of time studied in the present work.

Strikingly, when comparing acellular and cellular fibrin constructs during each week of development in culture, it can be seen that the cellular

substitutes had higher absorption values than the acellular ones for the last two weeks studied in the present work, contrary to what happened for the first stage in culture (first and second week). However, no clear behavior was established.

For the fibrin-agarose constructs, no clear influence of the cells on the absorption properties of the oral mucosa substitutes was noticed when performing the comparison between acellular and cellular substitutes, although no statistically significant differences were found (p=0.397). This observation support the statement made before, that no important absorbing components are synthesized or secreted in important quantities in the artificial human oral mucosa.

The results regarding the optical properties of the nanostructured oral mucosa artificial substitutes determined in the present study complete a comprehensive analysis on the morphological, histochemical and rheological characterization of artificial human oral mucosa constructs generated by tissue engineering and based on fibrin and fibrin-agarose. Previous studies by Rodriguez and collaborators (Rodriguez et al., 2012) proved that the addition to fibrin of a small amount of agarose allows the rheological stability of the oral mucosa substitute to be maintained. Moreover, San Martin and collaborators (San Martin et al., 2013) show that these type of bioengineered tissues present histological and molecular similarities with native human oral mucosa stroma. In addition, they observed that the nature of the biomaterial behavior influenced the oral stromal fibroblasts, thereby modulating their growth, protein synthesis, and collagen fibrillogenesis. This feature, together with its viscoelastic and optical behavior could make the fibrin and fibrin-0.1% agarose bioengineered tissues appropriate for clinical use in human oral mucosa applications.

Also, the absorption and scattering properties evaluated represent important tools that can be used to estimate the penetration depth of light in tissues as a function of wavelength, which is a crucial parameter in view of the possible application of optical in vivo imaging in clinical diagnosis

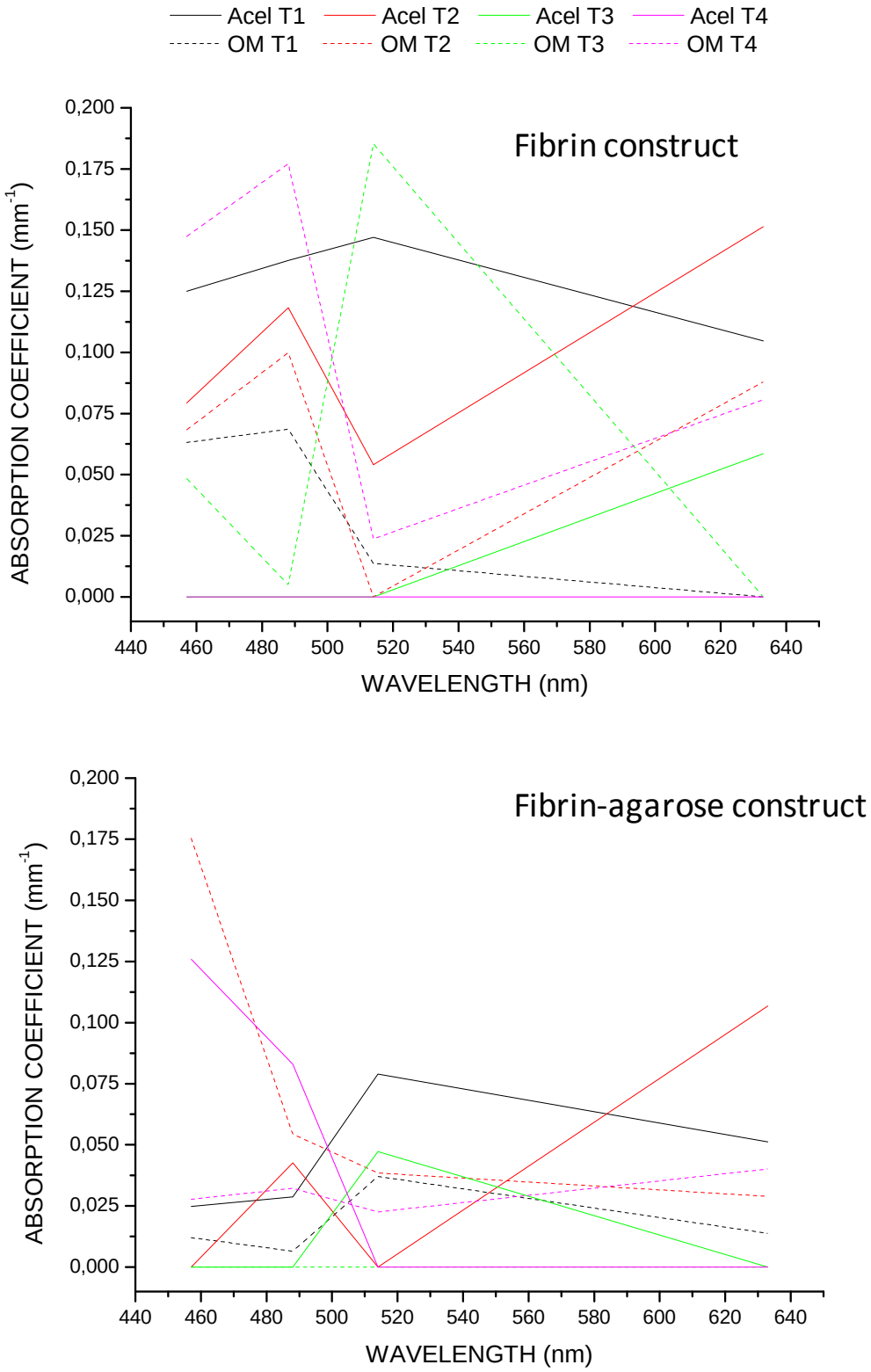

Figure 6.3. Comparison between the absorption coefficient values of acellular (straight line) and cellular (dash line) oral mucosa constructs based on fibrin and fibrin-agarose

Nevertheless, for these bioengineered oral mucosas to be potentially useful from a clinical standpoint, the correlation between the optical properties and the structure and internal features that define the human oral mucosa should be additionally determined.

In summary, the actual values of the absorption and scattering coefficients for the artificial and native tissues reported in the present study provide useful references and data for practical applications requiring the knowledge of the light transport through this type of tissues when using laser therapy. The results of this work suggest that the optical parameters of biological tissues in the diffuse theory model can be determined using the measuring technology of light radiation, and the optical parameters of bioengineered tissues and native tissues can be compared and analyzed. This provides a new method of information analysis for the quality control of the development of the artificial nanostructured oral mucosa substitutes.

7. CONCLUSIONS
CONCLUSIONES

1. El estudio de las propiedades reológicas de sustitutos de estroma corneal basados en fibrina y fibrina-agarosa, nanoestructurados y no nanoestructurados, nos permite afirmar que la técnica de nanoestructuración incrementa significativamente las propiedades viscoelásticas de los constructos de fibrina y fibrina-agarosa. Además, el sustituto corneal nanoestructurado de fibrina con una concentración de 0,1% de agarosa presenta valores de los módulos elástico y viscoso similares a los de la córnea nativa para todos los períodos de tiempo en cultivo analizados. Esto demuestra que el novedoso método de nanoestructuración utilizado en esta Tesis Doctoral proporciona soluciones útiles para la generación de tejidos artificiales con características reológicas adecuadas para aplicaciones en medicina regenerativa.

2. En esta Tesis Doctoral se ha desarrollado un montaje experimental que permite, por medio de un método no invasivo (CTF), evaluar la calidad óptica de constructos de estroma corneal humana generadas en laboratorio sin modificar las condiciones de cultivo. El uso de una pantalla de cristal líquido para presentar los patrones de barras es una técnica versátil que permite la modificación rápida y fácil de la frecuencia espacial de los mismos. La técnica es dinámica y fiable, y puede ser fácilmente implementada en laboratorio como un primer paso para el control de la calidad óptica de sustitutos corneales artificiales. Además, el uso de este método no se limita a constructos corneales, pudiendo proporcionar buenos resultados para la evaluación óptica de cualquier biomaterial translúcido.

La utilización de este método para la evaluación de constructos corneales generados mediante ingeniería tisular a base de fibrina, fibrina-agarosa y colágeno nos permite concluir que, al comparar el mismo tipo de constructos, los sustitutos de fibrina-agarosa después de cuatro semanas de desarrollo en cultivo y los geles de colágeno comprimidos durante tres minutos presentan los mejores valores de CTF. Sin embargo, dadas las desventajas de los geles de colágeno, el modelo corneal de fibrina con una concentración de agarosa del

0,1% podría ser el mejor candidato para el diseño *in vitro* de un modelo córnea humana.

3. El desarrollo de un *setup* experimental utilizando una única esfera integradora y láseres de Argón y Helio-Neón, basado en el método *Inverse Adding-Doubling* y una posterior simulación Monte Carlo ha permitido la evaluación y caracterización óptica de un modelo de córnea lamelar anterior humana generado mediante ingeniería tisular basado en fibrina-agarosa. Este modelo corneal, después de cuatro semanas de desarrollo en cultivo, presenta valores de reflectancia y transmitancia similares a los de la córnea nativa, sin diferencias estadísticamente significativas. El esparcimiento (*scattering*) es la propiedad óptica que afecta en mayor medida la propagación de la luz a través de este tipo de tejidos, prevaleciendo sobre la absorción. Aunque los valores de los coeficientes de esparcimiento y absorción son mayores que los de la córnea nativa, su comportamiento espectral es muy similar. De acuerdo a estos resultados, y teniendo en cuenta sus adecuadas características reológicas, podemos afirmar que el modelo de córnea lamelar anterior propuesto en esta Tesis Doctoral podría ser utilizado para el tratamiento de defectos de la córnea anterior, así como para otras enfermedades de la córnea, y para la realización de pruebas farmacológicas y en investigación biomédica.

4. El método *Inverse Adding-Doubling* junto con una posterior simulación Monte Carlo han sido utilizados para la determinación de las propiedades ópticas de esparcimiento y absorción de un modelo biomimético de mucosa oral humana generada por ingeniería tisular a base de fibrina y fibrina-agarosa. De forma análoga a lo que ocurre en los tejidos nativos, el esparcimiento es el fenómeno más importante que afecta la propagación de la luz en este tipo de tejidos biogenerados. Los sustitutos de mucosa oral presentan valores del coeficiente de absorción que no alcanzan los valores de

la mucosa oral nativa. Esto sugiere que los fibroblastos no sintetizan o no secretan una cantidad considerable de componentes capaces de absorber luz durante el periodo de tiempo en cultivo estudiado en esta Tesis Doctoral. Al comparar constructos celulares y acelulares, se ha demostrado que las células desempeñan un papel importante en el comportamiento de las propiedades ópticas, especialmente en el esparcimiento, siendo éstas capaces de remodelar la estructura interna de los modelos biomiméticos de mucosa oral humana. Ambos tipos de sustitutos de mucosa oral generados en el laboratorio (fibrina y fibrina-agarosa), comparten muchas similitudes con la mucosa oral nativa en términos de esparcimiento. La caracterización óptica de los sustitutos de mucosa oral realizada en esta Tesis Doctoral, podría ser de utilidad para el diseño de modelos de propagación de la luz en la cavidad oral y para predecir daños generados durante la exposición a la luz láser usada con fines terapéuticos.

5. Se han diseñado y aplicado con éxito métodos ópticos y reológicos para la evaluación de distintos tipos de tejidos humanos generados mediante ingeniería tisular. El uso de estos métodos permite determinar propiedades ópticas (reflectancia, transmitancia, esparcimiento, absorción y CTF) y reológicas (elasticidad y viscosidad) tanto de los tejidos artificiales como de los correspondientes tejidos nativos, con el fin de establecer controles de calidad de estos tejidos para posibles aplicaciones clínicas, así como para investigación biomédica básica.

1. The study of rheological properties of fibrin and fibrin-agarose, both nanostructured and non-nanostructured corneal stroma substitutes, shows that the nanostructuring technique significantly increases the viscoelastic properties of the fibrin and fibrin-agarose constructs. In addition, the fibrin with 0.1% agarose concentration nanostructured corneal substitute has elastic and viscous moduli values similar to the ones of native corneas for all analyzed periods of time in culture, proving that the novel nanostructuring method used in this study provides useful solutions for the generation of artificial tissues with proper rheological characteristics for applications in regenerative medicine.

2. An experimental non-invasive set-up that allows the optical quality evaluation of bioengineered constructs without modifying the culture conditions (method CTF) has been developed. The use of a LCD screen to present the bar patterns is a versatile technique, enabling quick and easy modification of the spatial frequency of the bar patterns. The technique is fast and reliable and it can be easily implemented in laboratories as a first step for the optical quality control of bioengineered corneal substitutes. Noteworthy, the use of this method is not limited to corneal constructs, and it is expected to provide good results in the optical evaluation of any translucent biomaterial.

The application of this method for the evaluation of bioengineered corneas based on fibrin, fibrin-agarose and collagen, allows us to conclude that, when comparing the same type of constructs, the fibrin-agarose substitutes corresponding to four weeks of development in culture and the collagen gels compressed for three minutes, have the best CTF values. However, due to the disadvantages that the collagen gels display, the fibrin with 0.1% agarose concentration could be a better candidate for the design of an *in vitro* human cornea model.

3. The development of an experimental setup using a single integrating sphere and Argon and Helium-Neon Lasers, based on the Inverse Adding Doubling method and a subsequent Monte Carlo simulation has allowed the optical evaluation and characterization of the human anterior lamellar cornea model generated by tissue engineering based on fibrin-agarose. After four weeks of development in culture, the values of reflectance and transmittance of this bioengineered cornea are similar to those of the native cornea, with no statistically significant differences. Scattering is the optical property that mainly affects the light propagation through this type of tissues, prevailing over absorption. Although the values of the scattering and absorption coefficients of the bioengineered constructs were higher than the ones of the native cornea, their spectral behavior was very similar. According to these results and the appropriate rheological characteristics, we can state that the fibrin–0.1% agarose anterior cornea model proposed in this Thesis could serve as a bioengineered tissue generated to repair defects of the anterior cornea, as a treatment for different kinds of corneal diseases and also for conducting pharmaceutical testing and biomedical research.

4. The Inverse Adding-Doubling method together with a subsequent Monte Carlo simulation have been used to determine the scattering and absorption properties of the biomimetic fibrin and fibrin-agarose model of human oral mucosa generated by tissue engineering . Analogously to what happens in native tissues, scattering dominates the light propagation in the bioengineered tissues. The absorption properties of the bioengineered oral mucosa did not reach the native oral mucosa values, suggesting that the fibroblasts were not able to synthesize and secrete considerable amounts of absorbing components during the culture period of time studied in this Thesis. When comparing the cellular and acellular constructs, we found that cells play an important role in the optical properties behavior, especially in scattering, since cells could be able to remodel the internal structure of the biomimetic human oral mucosa models. Both fibrin and fibrin-agarose oral

mucosa substitutes generated in the laboratory by tissue engineering shared many similarities with native human oral mucosa stroma in terms of scattering properties. The optical characterization of the bioengineered oral mucosa samples reported in this Thesis could be useful for the design of light propagation models for the oral cavity and to predict damage during exposure to laser light used for therapeutic purposes.

5. Optical and rheological methods have been successfully developed and applied for the evaluation of different types of human tissues generated by tissue engineering. The use of these methods allows to determine optical (reflectance, transmittance, scattering, absorption and CTF) and rheological (elasticity and viscosity) properties of both bioengineered and corresponding native tissues, as part of the required quality control for potential clinical applications as well as for use in basic biomedical investigation.

8. REFERENCES

Aghamohammadzadeh H, Newton RH, Meek KM. X-ray scattering used to map the preferred collagen orientation in the human cornea and limbus. Structure 2004;12:249–256.

Ahearne M, Buckley CT, Kelly DJ. A growth factor delivery system for chondrogenic induction of infrapatellar fat pad-derived stem cells in fibrin hydrogels. Biotechnology and Applied Biochemistry 2011;58:345–352.

Ahmed TA, Dare EV, Hincke M. Fibrin: a versatile scaffold for tissue engineering applications. Tissue Eng Part B Rev 2008;14:199-215.

Alaminos M, Sanchez-Quevedo MC, Munoz-Avila JI, Serrano D, Medialdea S, Carreras I, Campor A. Construction of a complete rabbit cornea substitute using a fibrin-agarose scaffold. Investigative Ophthalmology and Visual Science 2006;47:3311-3317.

Albandar JM. Epidemiology and risk factors of periodontal diseases. Dental Clinics of North America 2005;49: 517–532.

Albes JM, Klenzner T, Kotzerke J, Thiedemann KU, Schafers HJ, Borst, HG. Improvement of tracheal autograft revascularization by means of fibroblast growth factor. Annals of Thoracic Surgery 1994;57:444 – 449.

Alldredge OC, Krachmer JH. Clinical types of corneal rejection: their manifestations, frequencies, preoperative correlates, and treatment. Archives of Ophthlamology 1981;99:599-604.

Alper MG. The anesthetic eye: an investigation of changes in the anterior ocular segment of the monkey caused by interrupting the trigeminal nerve at various levels along its course. Transactions of the American Ophthalmological Society. 1975;73: 323–365.

Amrani DL, Diorio JP, Delmotte Y. Wound healing: role of commercial fibrin sealants. Annals of New York Academy of Science 2001;936:566–579.

Andreassen TT, Simonsen AH, Oxlund H. Biomechanical properties of keratoconus and normal corneas. Experimental Eye Research 1980;31:435–441.

Andrews LC, Philips RL. Laser beam propagation through random media 2nd Edition. SPIE Press 2005.

Ansari M, Mohajerani E. Mechanisms of laser-tissue interaction: optical properties of tissue. Journal of Lasers in Medical Sciences 2011;2(3): 119-125.

Anseth A.. Studies on corneal polysaccharides. III. Topographic and comparative biochemistry. Experimental Eye Research. 1961;1:106–115.

Arenholt-Bindslev D, Jepsen A, MacCallum DK, Lillie JH. The growth and structure of human oral keratinocytes in culture. Journal of Investigative Dermatology 1987;88:314-319.

Atkins JT. Optical properties of turbid materials. In The biological effects of ultraviolet radiation (with emphasis on the skin). Urbach F, ed. Oxford: Pergamon, 1969:141-150.

Atkinson ME, Jowett A, White FH. Principles of anatomy and oral anatomy for dental students. Taddington: Cava Cadavers 2000.

Atula S, Grenman R, Syrjanen S. Fibroblasts can modulate the phenotype of malignant epithelial cells in vitro. Experimental Cell Research 997;235:180-187.

Auger FA, Lopez Valle CA, Guignard R, Tremblay N, Noel B, Goulet F, Germain L. Skin equivalent produced with human collagen. In Vitro Cellular & Developmental Biology. 1995;31:432-439.

Axelsson I, Heinegard D. Fractionation of proteoglycans from bovine corneal stroma. Biochemical Journal 1975;145:491–500.

Bakri A, Farooqui N, Myung D, Koh WG, Noolandi J, Carrasco M et al. Biocompatibility of a Hydrogel Corneal inlay in vivo. Investigative Ophthalmology and Visual Science (Arvo Annual Meeting) 2006; 47 [e-pub ahead of print; abstract no. abstract 3592].

Barandan-Rafii A, Karimian F, Javadi MA, Jafarinasab MR, Nowroozpour K, Hosseini M, Anisian A. Corneal graft rejection: incidence and risk factors. Journal of Ophthalmic and Vision Research 2007;2(1):7-14.

Barnes HA. A review of the slip (wall depletion) of polymer solutions, emulsions and particle suspensions in viscometers: its cause, character, and cure. Journal of Non-Newtonian Fluid Mechanics 1995;56:221–251.

Bashkatov AN, Genina EA, KOchubey VI, Tuchin V. Optical properties of human skin, subcutaneous and mucous tissues in the wavelength range from 400 to 2000nm. Journal of Physics D: Applied Physics 2005;38:2543-2555.

Bashkatov AN, Genina EA, Tuchin V. Optical properties of skin, subcutaneous, and muscle tissues: a review. Journal of Innovative Optical Health Sciences 2011;4(1): 9-38.

Baumann I, Greschniok A, Bootz F and Kaiserling E. Free transplanted, microvascularreanastomosed forearm flap for reconstruction of the mouth cavity and oropharynx. Clinical and morphologic findings with special reference to reinnervation. HNO. 1996;44: 616–623

Beer A. Bestimmung der Absorption des rothen Lichts in farbigen Flüssigketiten. Annual Review of Physical Chemistry 1852;86(5):78–88.

Bell E, Ivarsson B, Merrill C. Production of a tissue-like structure by contraction of collagen lattices by human fibroblasts of different proliferative potential in vitro. Proceedings of the National Academy of Science USA 1979;76(3):1274-1278.

Benedek GB. Theory of the transparency of the eye. Applied Optics. 1971;10:459–473.

Bennett ES, Weissman BA. Clinical Contact Lens Practice. Philadelphia, PA: Lippincott Williams & Wilkins; 2004.

Bensaid W, Triffitt JT, Blanchat C, Oudina K, Sedel L, Petite H. A biodegradable fibrin scaffold for mesenchymal stem cell transplantation. Biomaterials 2003;24:2497-2502.

Berthod F, Hayek D, Damour O, Collombel C. Collagen synthesis by fibroblasts cultured within a collagen sponge. Biomaterials 1993;14:749-754.

Bhang SH, Lee YE, Cho SW, Shim JW, Lee SH, Choi CY, Chang JW, Kim BS. Basic fibroblast growth factor promotes bone marrow stromal cell transplantation-mediated neural regeneration in traumatic brain injury. Biochemical and Biophysical Research Communications 2007;359:40–45.

Bhargava S, Chapple CR, Bullock AJ, Layton C, MacNeil S. Tissue engineered buccal mucosa for substitution urethroplasty. BJU International 2004;93:807-811.

Birla, R.K., G.H. Borschel, R.G. Dennis, D.L. Brown (2005) Myocardial engineering in vivo: formation and characterization of contractile, vascularized three-dimensional cardiac tissue. Tissue Eng 11: 803–813.

Bonanno JA. Identity and regulation of ion transport mechanisms in the corneal endothelium. Progress in Retinal and Eye Research.2003; 22: 69–94.

Boot JP, van Best JA, Stolwijk TR, Sterk CC. Epithelial permeability in corneal grafts by fluorophotometry. Graefe's Archive for Clinical and Experimental Ophthalmology. 1991;229, 533–535.

Borene ML, Barocas VH, Hubel A. Mechanical and cellular changes during compaction of a collagen-sponge-based corneal stromal equivalent. Annals of Biomedical Engineering 2004; 32:274–283.

Bouguer, P. Essai d'optique sur la gradation de la lumière. Section II. De la transparence et de l'opacité. II. De la proportion selon laquelle la lumière diminué en traversant les milieux. 1729.

Boulnois JL. Photophysical processes in recent medical laser developments: a review. Lasers in Medical Science 1986;1:47-66.

Breen A, O'Brien T, Pandit A. Fibrin as a delivery system for therapeutic drugs and biomolecules. Tissue Engineering Part B 2009;15:201-214.

Brown RA, Wiseman M, Chuo CB, Cheema U, Nazhat SN. Ultrarapid engineering of biomimetic materials and tissues: fabrication of nano- and microstructures by plastic compression. Advanced Functional Materials 2005;15;1762-1770.

Cardona JC, Ionescu AM, Gomez-Sotomayor R, Gonzalez- Andrades M, Campos A, Alaminos M, Perez MM.. Transparency in a fibrin and fibrin–agarose corneal stroma substitute generated by tissue engineering. Cornea 2011;30(12):1428-1435.

Carrier P, Deschambeault A, Talbot M, Giasson CJ, Auger FA, Guerin SL et al. Characterization of wound reepithelialization using a new human tissue-engineered corneal wound-healing model. Investigative Ophthalmology and Visual Science 2008; 49: 1376–1385.

Castano AP, Mroz P, Hamblin MR. Photodynamic therapy and antitumour immunity. Nature Reviews Cancer 2006;6:535–545.

Chen J, Li Q, Xu J, Huang Y, Ding Y, Deng H, Zhao S, Chen R. Study on biocompatibility of complexes of collagen-chitosan-sodium hyaluronate and cornea. Artificial Organs 2005;29(2):104–113.

Cheong W .Appendix to chapter 8: summary of optical properties. In: Welch AJ, van Gemert MJC (eds) Optical-thermal response of laser-irradiated tissue. Plenum, New York, 1995; pp 275–303

Cheong WF, Prahl SA, Welch AJ. A review of the optical properties of biological tissues. IEEE Journal of Quantum Electronics 1990;26(12):2166-

Cho KH, Ahn HT, Park KC, Chung JH, Kim SW, Sung MW, Kim KH, Chung PH, Eun HC, Youn JI. Reconstruction of human hard-palate mucosal epithelium on deepidermized dermis. Journal of Dermatological Science 2000;22:117-124.

Choi YS, Hong SR, Lee YM, Song KW, Park MH, Nam YS. Studies on gelatin-containing artificial skin: II. Preparation and characterization of cross-linked gelatin-hyaluronate sponge. Journal of Biomedical Materials Research 1999b; 48:631-639

Choi YS, Hong SR, Lee YM, Song KW, Park MH, Nam YS. Study on gelatin-containing artificial skin: I. Preparation and characteristics of novel gelatin-alginate sponge. Biomaterials 1999a; 20:409-417.

Cima LG, Langer R, Vacanti JP. Polymers for tissue and organ culture. Journal of Bioactive and Compatible Polymers. 1991;6:232-239.

Cox JL, Farrell RA, Hart RW, Langham ME. The transparency of the mammalian cornea. Journal of Physiology. 1970;210:601–616.

Cox S, Cole M, Tawil B. Behavior of human dermal fibroblasts in three-dimensional fibrin clots: dependence on fibrinogen and thrombin concentration. Tissue Engineering 2004;10:942–954

Crabb RA, Chau EP, Decoteau DM, Hubel A. Microstructural characteristics of extracellular matrix produced by stromal fibroblasts. Annals of Biomedical Engineering. 2006a; 34:1615–1627.

Crabb RA, Chau EP, Evans MC, Barocas VH, Hubel A. Biomechanical and microstructural characteristics of a collagen film-based corneal stroma equivalent. Tissue Engineering. 2006b; 12, 1565–1575.

Crabb RAB. Collagen processing for tissue-engineered corneas: influence on optical and biomechanical properties. ProQuest, USA 2007.

Dam JS, Dalgaard T, Fabricius PE, Andersson-Engels S. Multiple polynomial regression method for determination of biomedical optical properties from integrating sphere measurements. Applied Optics 2000;39(7): 202-9

Deppe H, Horch HH. Laser applications in oral surgery and implant dentistry. Lasers in Medical Science 2007;22:217-221.

Doiron DR, Svaasand LO, and Profio AE. Light dosimetry in tissue applications to photoradiation therapy. In: Porphyrin Photosensitization, D. Kessel and T. J. Dougherty, Eds. New York:Plenum, 1983:63-75.

Douwes J. (1-->3)-Beta-D-glucans and respiratory health: a review of the scientific evidence. Indoor Air 2005;15:160-169.

Du Y, Funderburgh ML, Mann MM, SundarRaj N, Funderburgh JL. Multipotent stem cells in human corneal stroma. Stem Cells 2005; 23: 1266–1275.

Du Y, Sundarraj N, Funderburgh ML, Harvey SA, Birk DE, Funderburgh JL. Secretion and organization of a cornea-like tissue in vitro by stem cells from human corneal stroma. Investigative Ophthalmology and Visual Science 2007; 48: 5038–5045.

El-Ghalbzouri A, Lamme EN, van Blitterswijk C, Koopman J, Ponec M. The use of PEGT/PBT as a dermal scaffold for skin tissue engineering. Biomaterials 2004;25:2987-2996.

Engelmann K, Bednarz J, Valtink, M. Prospects for endothelial transplantation. Experimental Eye Research. 2004;78: 573–578.

Engelmann K, Drexler D, Bohnke M. Transplantation of adult human or porcine corneal endothelial cells onto human recipients in vitro. Part I: cell culturing and transplantation procedure. Cornea. 1999;18:199–206.

Engler A, Bacakova L, Newman C, Hategan A, Griffin M, Discher D. Substrate compliance versus ligand density in cell on gel responses. Biophysical Journal 2004;86:617–628.

Engler AJ, Sen S, Sweeney HL, Discher DE. Matrix elasticity directs stemcell lineage specification. Cell 2006;126:677–689.

Enrione J, Osorio F, Lopez P, Weinstein-Oppenheimer C, Fuentes MA, Ceriani R, Brown DI et al. Characterization of a gelatin/chitosan/ hyaluronan scaffold-polymer. Electronic Journal of Biotechnology 2010;13(5):20-21.

Ethier CR, Johnson M, Ruberti J. Ocular biomechanics and biotransport. Annual Review of Biomedical Engineering.2004;6:249–273.

Eyrich D, Brandl F, Appel B, Wiese H, Maier G, Wenzel M, Staudenmaier R, Goepferich A, Blunk T. Long-term stable fibrin gels for cartilage engineering. Biomaterials 2007;28: 55–65.

Farhat WA, Chen J, Sherman C, Cartwright L, Bahoric A, Yeger H. Impact of fibrin glue and urinary bladder cell spraying on the in-vivo acellular matrix cellularization: a porcine pilot study. The Canadian Journal of Urology 2006;13:3000–3008.

Farrell RA, McCally RL, Tatham PER. Wavelength dependencies of light scattering in normal and cold swollen rabbit corneas and their structural implications. Journal of Physiology 1973;233:589–612.

Fernald RD. Evolution of eyes. Current Opinion in Neurobiology. 2000;10:444–450.

Fernandez-Oliveras A, Rubiño M, Pérez MM. Scattering anisotropy measurements in dental tissues and biomaterials. Journal of the European Optical Society-Rapid Publications 2012;7:12016.1-12016.8.

Freund DE, McCally RL, Farrell RA, Cristol SM, L'Hernault NL, Edelhauser HF. Ultrastructure in anterior and posterior stroma of perfused human and rabbit corneas: relation to transparency. Investigative Ophthalmology and Visual Science 1995;36:1508–1523.

Freund DE, McCally RL, Farrell RA. Direct summation of fields for light scattering by fibrils with applications to normal corneas. Applied Optics 1986;25:2739–2746.

Freund DE, McCally RL, Farrell RA. Light scattering tests of structure in normal and swollen rabbit corneas. Johns Hopkins APL Tech Dig 1991; 12: 137–143.

Friedman MH.. A quantitative description of equilibrium and homeostatic thickness regulation in the in vivo cornea. I. Normal cornea. Biophysical Journal. 1972;12:648–665.

Fu Y, Fan X, Chen P, Shao C, Lu W. reconstruction of a tissue-engineered cornea with porcine corneal acellular matrix as the scaffold. Cell Tissues Organs 2010;191:193-202.

Fusenig NE. Epithelial-mesenchymal interactions regulate keratinocyte growth and differentiation in vitro. In: The keratinocyte handbook. Leigh IM, Lane EB, Watt FM, editors. Cambridge: University Press, 1994; pp. 71-94.

Garcia de Abajo FJ. Colloquium: Light scattering by particle and hole arrays Reviews of Modern Physics 2007;(79): 1267–1290.

Garzón I, Sánchez-Quevedo MC, Moreu G, González-Jaranay M, González-Andrades M, Montalvo A, Campos A, Alaminos M. In vitro and in vivo cytokeratin patterns of expression in bioengineered human periodontal mucosa. Journal of Periodontal Research 2009;44 (5): 588–597.

Gaudreault M, Carrier P, Larouche K, Leclerc S, Giasson M, Germain L, Guerin SL. Influence of sp1/sp3 expression on corneal epithelial cells proliferation and differentiation properties in reconstructed tissues. Investigative Ophthalmology and Visual Science 2003; 44:1447–1457.

Germain L, Auger FA, Grandbois E, Guignard R, Giasson M, Boisjoly H, Guerin SL. Reconstructed human cornea produced in vitro by tissue engineering. Pathobiology 1999;67:140–147.

Germain L, Carrier P, Deschambeault A, Talbot M, Guerin SL, Auger FA. Fibroblasts Modulate Differentiation and Stratification of Epithelial Cells on Reconstructed Human Cornea through the Production of Soluble Factors. ARVO, Fort Lauderdale, 2004.

Goldman JN, Benedek GB, Dohlman CH, Kravitt B. Structural alterations affecting transparency in swollen human corneas. Investigative Ophthalmology and Visual Science. 1968;7:501–519.

Goldman JN, Benedek GB. The relationship between morphology and transparency in the nonswelling corneal stroma of the shark. Investigative Ophthalmology. 1967;6:574–600.

Goldman L, Gray JA, Goldman B, Meyer R. Effect of laser beam impacts on teeth. Journal of the American Dental Association 1965;70:601-606.

Gonzalez-Andrades M, Cardona JC, Ionescu AM; Campos A, Perez MM, Alaminos M. Generation of bioengineered corneas with decellularized xenografts and human keratocytes. Investigative Ophthalmology and Visual Science 2009;52(1):215-222.

Goodfellow JM, Elliott GF, Woolgar AE. X-ray diffraction studies of the corneal stroma. Journal of Molecular Biology 1978; 119: 237–252.

Griffith M, Hakim M, Shimmura S, Watsky MA, Li F, Carlsson D, Doillon CJ, Nakamura M, Suuronen E, Shinozaki N, Nakata K, Sheardown H.. Artificial human corneas: scaffolds for transplantation and host regeneration. Cornea 2002;21:S54–61.

Griffith M, Jackson WB, Lagali N, Merrett K, Li F, Fagerholm P. Artificial corneas: a regenerative medicine approach. Eye 2009;23:1985-1989.

Griffith M, Osborne R, Munger R, Xiong X, Doillon CJ, Laycock NL, Hakim M, Song Y, Watsky MA. Functional human corneal equivalents constructed from cell lines. Science 1999;286:2169–2172.

Grobe G, Reichl S. Examining the suitability of Riboflavin/UVA treatment for strengthening the stromal bioequivalent of a human cornea construct. Current Eye Research 2011;36:217–231.

Gruber HE, Fisher EC, Desai B, Stasky AA, Hoelscher G, Hanley ENJr.: Human intervertebral disc cells from the annulus: three-dimensional culture in agarose or alginate and responsiveness to TGF-beta1. Experimental Cell Research 1997;235:13–21.

Gruber HE, Hoelscher GL, Leslie K, Ingram JA, Hanley ENJr. Three-dimensional culture of human disc cells within agarose or a collagen sponge: assessment of proteoglycan production. Biomaterials 2006;27:371–376.

Guo X, Hutcheon AE, Melotti SA, Zieske JD, Trinkaus-Randall V, Ruberti JW. Morphologic characterization of organized extracellular matrix deposition by ascorbic acid stimulated human corneal fibroblasts. Investigative Ophthalmology and Visual Science 2007; 48: 4050–4060.

Hadjipanayi E, Ananta M, Binkowski M, Streeter I, Lu Z, Cui ZF, Brown RA, Mudera V. Mechanisms of structure generation during plastic compression on nanofibrillar collagen hydrogel scaffolds: towards engineering of collagen. Journal of Tissue Engineering and Regenerative Medicine. 2011;5:505–519.

Hale GM, Querry MR. Optical constants of water in 200 nm to 200 μm wavelength region. Applied Optics 1973;12:555-563

Hamada R, Giraud JP, Graf B, Pouliquen Y. Etude analytique et statistique des lamelles, des keratocytes, des fibrilles del collagene de la region centrale de la cornee humaine normale. Archives of Ophthalmology 1972;32:563–570.

Han B, Schwab IR, Madsen TK and Isseroff RR. A fibrin-based bioengineered ocular surface with human corneal epithelial stem cells. Cornea 2002; 21(5):505-510.

Hanna C, O'Brien JE. Cell production and migration in the epithelial layer of the cornea. Archives of Ophtalmology 1960; 64:536-539.

Hart RW, Farrell RA. Light scattering in the cornea. Journal of the Optical Society of America. 1969;59:766–774.

Haugh MG, Murphy CM, Mckiernan RC, Altenbuchner C, O'Brien FJ. Crosslinking and mechanical properties significantly influence cell attachment, proliferation, and migration within collagen glycosaminoglycan scaffolds. Tissue Engineering Part A 2011;17:1201–1208.

Haugh MG, Thorpe SD, Vinardell T, Buckley CT, Kelly DJ. The application of plastic compression to modulate fibrin hydrogel mechanical properties. Journal of the Mechanical Behavior of Biomedical Materials 2012;16:66-72.

Hedbys BO, Mishima S, Maurice DM. The imbibition pressure of the corneal stroma. Experimental Eye Research. 1963;2:99–111.

Hedbys BO. The role of polysaccharides in corneal swelling. Experimental Eye Research. 1961;1: 81.

Hennighausen H, Feldman ST, Bille JF, McCulloch AD. Anterior–posterior strain variation in normally hydrated and swollen rabbit cornea. Investigative Ophthalmology and Visual Science. 1998;39: 253–262.

Heureux NL, Paquet S, Labbe R, Germain L, Auger FA. A completely biological tissue-engineered human blood vessel. FASEB Journal. 1998;12:47-56.

Hjortdal JO, Koch-Jensen P. *In situ* mechanical behavior of the human cornea as evaluated by simultaneous measurements of corneal strain, corneal surface contour, and corneal thickness. Investigative Ophthalmology and Visual Science 1992;33 (Suppl.):1022.

Hjortdal JO. Regional elastic performance of the human cornea. Journal of Biomechanics 1996;29(7):931-942.

Hoeltzel DA, Altman P, Buzard K, Choe K. Strip extensiometry for comparison of the mechanical response of bovine, rabbit, and human corneas. Journal of Biomechanical Enngineering 1992;114:202–215.

Hollis VS. Non-Invasive Monitoring of Brain Tissue Temperature by Near-Infrared Spectroscopy. PhD Thesis. University College of London 2002.

Honda N, Ishii K, Kimura A, Sakai M, Awazu K. Determination of optical property changes by laser treatments using inverse adding-doubling method. Proceedings of SPIE 7175, Optical Interactions with Tissue and Cells XX, 71750Q, 2009.

Hong SR, Lee SJ, Shim JW, Choi YS, Lee YM, Song KW, Park MH, Nam YS, Lee Si. Study on gelatin-containing artificial skin IV: a comparative study on the effect of antibiotic and EGF on cell proliferation during epidermal healing. Biomaterials 2001;22:2777-2783.

Hu X, Lui W, Cui L, Wang M, Cao Y. Tissue engineering of nearly transparent corneal stroma. Tissue Engineering 2005;11:1710–1717.

Huang Y, Meek KM. Swelling studies on the cornea and sclera: the effects of pH and ionic strength. Biophysical Journal 1999;77:1655–1665.

Hull E, Ediger M, Unione A, Deemer E, Stroman M, Baynes J. Noninvasive, optical detection of diabetes: model studies with porcine skin. Optics Express 2004;2:4497–4510.

Ionescu AM, Alaminos M, Cardona JC, García-López Durán JD, Gonzalez-Andrades M, Ghinea R, Campos A, Hita E, Perez MM. Investigating a novel nanostructured fibrin-agarose biomaterial for huam cornea tissue engineering: rheological properties. Journal of the Mechanical Behavior of Biomedical Materials 2011;4:1963-1973.

Ionescu AM, Cardona JC, González-Andrades M, Alaminos M, Campos A, Hita E, Pérez MM. UV Absorbance of a bioengineered corneal stroma substitute in the 240–400 nm range. Cornea 2010;29:895–898.

Irvine WM. Multiple scattering in planetary atmospheres. Icarus 1975;25(2)175-204.

Ishii K, Kimura A, Awazu K. Optical properties of tissues after laser treatments in the wavelength range of 350 - 1000 nm. Proceedings of SPIE 6991, Biophotonics: Photonic Solutions for Better Health Care, 69912F, 2008.

Ishimaru A. Wave propagation and scattering in random media. New York: Academic Press 1978.

Izumi K, Feinberg SE, Iida A, Yoshizawa M. Intraoral grafting of an ex vivo produced oral mucosa equivalent: a preliminary report. International Journal of Oral and Maxillofacial Surgery 2003;32:188-197.

Jacob JT, Rochefort JR, Bi J, Gebhardt BM. Corneal epithelial cell growth over tethered-protein/peptide surface-modified hydrogels. Journal of Biomedical Materials Research Part B: Applied Biomaterials 2005;72:198–205.

Jacques SL and Prahl SA. Modeling optical and thermal distributions in tissue during laser irradiation. Lasers in Surgery and Medicine.1987; 6: 494-503.

Jacques SL, Prahl SA. Modeling optical and thermal distributions in tissue during laser irradiation. Lasers in Surgery and Medicine 1987;6:494-503.

Jain A., Kim YT, McKeon RJ, Bellamkonda RV. In situ gelling hydrogels for conformal repair of spinal cord defects, and local delivery of BDNF after spinal cord injury. Biomaterials 2006;27:497–504.

Jester JV, Moller-Pedersen T, Huang J, Sax CM, Kays T, Cavangh HD, petrol WM, Piatigorsky J. The cellular basis of corneal transparency: evidence for 'corneal crystallins'. Journal of Cell Science 1999a;122:613-622.

Jester JV, Petroll WM, Cavanagh HD. Corneal stromal wound healing in refractive surgery: the role of myofibroblasts. Progress in Retinal and Eye Research. 1999b;18:311–356.

Joyce NC, Zhu CC. Human corneal endothelial cell proliferation: potential for use in regenerative medicine. Cornea. 2004;23:S8–S19.

Jue B, Maurice DM. The mechanical properties of the rabbit and human cornea. Journal of Biomechanics 1986;19(10):847–853.

Kaiser HW, Stark GB, Kopp J, Balcerkiewicz A, Spilker G, Kreysel HW. Cultured autologous keratinocytes in fibrin glue suspension, exclusively and combined with STS-allograft (preliminary clinical and histological report of a new technique). Burns 1994;20:23-29.

Karring H, Thogersen IB, Klintworth GK, Enghild JJ, Moller-Pedersen T. Proteomic analysis of the soluble fraction from human corneal fibroblasts with reference to ocular transparency. Molecular & Cellular Proteomics 2004;3:660–674.

Khorramizadeh MR, Tredget EE, Telasky C, Shen Q, Ghahary A. Aging differentially modulates the expression of collagen and collagenase in dermal fibroblasts. Molecular and Cellular Biochemistry 1999;194:99-108.

Kienle A, Patterson MS. Determination of the optical properties of turbid media from a single Monte Carlo simulation. Physics in Medicine and Biology 1996;(41):2221–2227.

Klose AD, Larsen EW. Light transport in biological tissue based on the simplified spherical harmonics equations. Journal of Computational Physics 2006;220:441-470.

Ko HC, Milthorpe BK, McFarland CD. Engineering thick tissues – the vascularisation problem. European Cells & Materials Journal 2007;14:1–19.

Kobayashi AS, Staberg LG, Schlegel WA. Viscoelastic properties of human corneas. Experimental Mechanics 19873;13(12):497–503.

Kostyuk O, Nalovina O, Mubard TM, Regini JW, Meek KM, Quantock A, Elliott GF, Hodson SA. Transparency of the bovine corneal stroma at physiological hydration and its dependence on concentration of the ambient anion. Journal of Physiology. 2002;543:633–642.

Kottler F. Turbid media with plane-parallel surfaces. Journal of the Optical Society of America 1960;50:483-490.

Lambert, J H.. Photometria, sive de mensura et gradibus luminis, colorum et umbrae. Augsburg. 1760.

Land MF, Fernald RD. The evolution of eyes. Annual Review of Neuroscience 1992;15:1–29.

Langer R, Vacanti JP. Tissue engineering. Science 1993;260:920–926.

Lauer G, Schimming R. Tissue-engineered mucosa graft for reconstruction of the intraoral lining after freeing of the tongue: a clinical and immunohistologic study. Journal of Oral and Maxillofacial Surgery 2001;59:169-175.

Lauer G. Autografting of feeder-cell free cultured gingival epithelium. Method and clinical application. Journal of Craniomaxillofacial Surgery 1994;22:18-22.

Leber T.. Studien uber den Flussigkeitswechsel im Auge. Graefe's Archives of Ophthalmology. 1873;19: 87.

Lee SB, Jeon HW, Lee YW, Lee YM, Song KW, Park MH, Nam YS, Ahn HC. Bio-artificial skin composed of gelatin and (1-->3), (1-->6)-betaglucan. Biomaterials 2003;24:2503-2511.

Leonard DW. The ultrastructure of the corneal stroma and its implications for transparency. PhD thesis, The Open University, Milton Keynes, UK, 1996.

Levis HJ, Brown RA, Daniels JT. Plastic compressed collagen as a biomimetic substrate for human limbal epithelial cell culture. Biomaterials 2010;31(30):7726 – 7773.

Levis HJ, Peh GSL, Toh K-P, Poh R, Shortt AJ, Drake RAL, Mehta JS, Daniels JT. Plastic compressed collagen as a novel carrier for expanded human corneal endothelial cells for transplantation. PLoS ONE 2012;7(11):e50993.

Li F, Carlsson D, Lohmann C, Suuronen E, Vascotto S, Kobuch K, Sheardown H, Munger R, Nakamura M and Griffith M. Cellular and nerve regeneration within a biosynthetic extracellular matrix for corneal transplantation. Proceedings National Academy of Science U.S.A. 2003;100:15346–15351.

Li F, Griffith M, Li Z, Tanodekaew S, Sheardown H, Hakim M, Carlsson DJ. Recruitment of multiple cell lines by collagen-synthetic copolymer matrices in corneal regeneration. Biomaterials 2005;26:3093–3104

Liu J, Li L. SDS-aided immobilization and controlledrelease of camptothecin from agarose hydrogel. European Journal of Pharmaceutical Sciences. 2005;25:237–244.

Liu Q, Ruprecht E. Radiative transfer model: matrix operator method. Applied Optics 1996;35(21):4229-4237.

Liu Q, Weng F. Advanced doubling adding method for radiative transfer in planetary atmospheres. Jounal of Atmospheric Sciences 2006;63(12):3459-3465.

Liu W, Merrett K, Griffith M, Fagerholm P, Dravida S, Heyne B et al. Recombinant human collagen for tissue engineered corneal substitutes. Biomaterials 2008; 29:1147–1158.

Ma L, Gao C, Mao Z, Zhou J, Shen J, Hu X, Han C. Collagen/chitosan porous scaffolds with improved biostability for skin tissue engineering. Biomaterials 2003;24:4833-4841.

Ma PX. Scaffolds for tissue fabrication. Materials Today 2004;7(5): 30–40.

MacCallum DK, Lillie JH. Evidence for autoregulation of cell division and cell transit in keratinocytes grown on collagen at an air liquid interface. Skin Pharmacology and Physiology 1990;3:86-96.

Macosko CW. Rheology: Principles, Measurements, and Applications. VCH, New York, 1994

Madsen SJ, Wilson BC. Optical properties of brain tissue. In: Madsen SJ (ed.) Optical methods and instrumentation in brain imaging and therapy. New York: Springer; 2013. pp. 1-22.

Mao JS, Liu HF, Yin YJ, Yao KD. The properties of chitosan-gelatin membranes and scaffolds modified with hyaluronic acid by different methods. Biomaterials 2003; 24:1621-1629.

Marchesini R, Pignoli E, Tomatis S, Fumagalli S, Sichirollo AE, Palma SD, Fante MD, Spinelli P, Croce AC Bottiroli G. Ex vivo optical properties of human colon tissue. Lasers in Surgery and Medicine 1994;(15):351–357.

Marieb, E N.. Human Anatomy and Physiology. Third ed. Redwood City, California: Benjamin/Cummings 1995.

Martin SS, Alaminos M, Zorn TM, Sánchez-Quevedo MC, Garzón I, Rodriguez IA, Campos A. The effects of fibrin and fibrin-agarose on the extracellular matrix profile of bioengineered oral mucosa. Journal of Tissue Engineering and Regenerative Medicine 2013;7(1):10-19

Marynka-Kalmani K, Treves S, Yafee M, Rachima H, Gafni Y, Cohen MA, Pitaru S. The lamina propria of adult human oral mucosa harbours a novel stem cell population. Stem Cells. 2010;28(5):984-995.

Masuda I. An in vitro oral mucosal model reconstructed from human normal gingival cells. Kokubyo Gakkai Zasshi 1996;63:334-353 [article in Japanese].

Maurice DM. The location of the fluid pump in the cornea. Journal of Physiology. 1972;221:43–54.

Maurice DM. The structure and transparency of the corneal stroma. Journal of Physiology. 1957;136:263–286.

McAlister JC, Joyce NC, Harris DL, Ali RR and Larkin DF. Induction of replication in human corneal endothelial cells by E2F2 transcription factor cDNA transfer. Investigative Ophthalmology and Visual Science. 2005;46:3597–3603.

McIntosh Ambrose W, Schein O, Elisseeff J. A tale of two tissues: stem cells in cartilage and corneal tissue engineering. Current Stem Cell Research & Therapy. 2010;5(1):37-48.

McPhee TJ, Bourne WM, Brubaker RF. Location of the stress-bearing layers of the cornea. Investigative Ophthalmology and Visual Science. 1985;26: 869–872.

Meador WE, Weaver WR. Diffusion approximation for large absorption in radiative transfer. Applied Optics 1979;18:1204-1208.

Meek KM, Boote C. The organization of collagen in the corneal stroma. Experimental Eye Research. 2004;78:503–512.

Meek KM, Leonard DW, Connon CJ, Dennis S, Khan S. Transparency, swelling and scarring in the corneal stroma. Eye 2003;17:927-936.

Meek KM, Leonard DW. Ultrastructure of the corneal stroma: a comparative study. Biophysical Journal 1993;64:273–280.

Merne M, Syrjanen S. The mesenchymal substrate influences the epithelial phenotype in a three-dimensional cell culture. Archives of Dermatological Research 2003;295:190-198.

Merrett K, Fagerholm P, McLaughlin CR, Dravida S, Lagali NS, Shinozaki N et al. Tissue engineered recombinant human collagen-based corneal substitutes for implantation: performance of type I versus type III collagen. Investigative Ophthalmology and Visual Science 2008; 49:3887–3894.

Mi S, Chen B, Wright B, Connon CJ. Ex vivo construction of an artificial ocular surface by combination of corneal limbal epithelial cells and a compressed collagen scaffold containing keratocytes. Tissue Engineering Part A. 2010a;16(6):2091:2100.

Mi S, Chen B, Wright B, Connon CJ. Plastic compression of a collagen gel forms a much improved scaffold for ocular surface tissue engineering over conventional collagen gels. Journal of Biomedical Materials Research A 2010b;95A(2):447-453.

Miclea M, Skrzypczak U, Fankhauser F, Faust S, Graener H, Seifert G. Applanation-free femtosecond laser processing of the cornea. Biomedical Optics Express 2011;2(3):534-542.

Minami Y, Sugihara H, Oono S. Reconstruction of cornea in three dimensional collagen gel matrix culture. Investigative Ophthalmology and Visual Science 1993;34:2316–2324.

Moan J, Peng Q. An outline of the hundred-year history of PDT. Anticancer Research 2003;(3):3591–3600.

Moffitt T, Chen YC, Prahl SA. Preparation and characterization of polyurethane optical phantoms. Journal of Biomedical Optics 2006;11(4):041103.1-041103.10.

Moharamzadeh M, Brook IM, Van Noort, R, Scut t AM, Thornhill. Tissue-engineered oral mucosa: a review of the scientific literature. Journal of Dental Research 2007;86(2):115-124.

Moller-Perdersen T, Cavanagh HD, Petrol WM, Jester JV. Stroma wound healing explains refractive instability and haze development after photorefractive keratectomy: 1-year confocal microscopy study. Ophthalmology 2000;107:1235–1245.

Moriyama T, Asahina I, Ishii M, Oda M, Ishii Y, Enomoto S. Development of composite cultured oral mucosa utilizing collagen sponge matrix and contracted collagen gel: a preliminary study for clinical applications. Tissue Engineering 2001;7:415-427.

Mourant JR, Bigio IJ, Boyer J, Conn RL, Johnson T, Shimada T. Spectroscopic diagnosis of bladder cancer with elastic light scattering. Lasers in Surgery and Medicine 1995;17(4):350-357.

Mourant JR, Canpolat M, Brocker C, Esponda-ramos O, Johnson TM, Matanock A, Stetter K, Freyer JP. Light scattering from cells: the contributions of the nucleus and the effects of proliferative status. Journal of Biomedical Optics 2000;5:131–137.

Mourant JR, Freyer JP, Hielscher AH, Eick AA, Shen D, Johnson TM.. Mechanisms to light scattering from biological cells relevant to noninvasive optical-tissue diagnostics. Applied Optics 1998;37(16):3586–3593.

Mourant JR, Hielscher AH, Eick AA, Johnson TM, Freyer JP. Evidence of intrinsic differences in the light scattering properties of tumorigenic and nontumorigenic cells. Cancer 1998;84:366-374.

Muñoz-Corcuera M, Esparza-Gómez G, González-Moles MA, Bascones-Martinez A. Oral ulcers: clinical aspects. A tool for dermatologists. Part II. Chronic ulcers. Clinical and Experimental Dermatology 2009;34: 456–461.

Murphy CM, Matsiko A, Haugh MG, Gleeson JP, O'Brien FJ. Mesenchymal stem cell fate is regulated by the composition and mechanical properties of collagen – glycosaminoglycan scaffolds. Journal of the Mechanical Behavior of Biomedical Materials 2012;11:53-62

Myung D, Koh W, Ko J, Noolandi J, Carrasco M, Smith A, Frank C, Ta C. Characterization of poly(ethylene glycol)-poly(acrylic acid) (PEG-PAA) double networks designed for corneal implant applications. Investigative Ophthalmology and Visual Science 2005; 46:E-Abstract 5003.

Nakamura T, Inatomi T, Sotozono C, Ang LP, Koizumi N, Yokoi N et al. Transplantation of autologous serum-derived cultivated corneal epithelial equivalents for the treatment of severe ocular surface disease. Ophthalmology 2006; 113:1765–1772.

Nash IS, Greene PR, Foster CS. Comparison of mechanical properties of keratoconus and normal corneas. Experimental Eye Research 1982;35:413–423.

Nerem R. The challenge of imitating nature. In: Principles of Tissue Engineering. 2nd Ed. Lanza RP, Langer R, Vacanti J. Elsevier, USA 2000.

Nerem RM, Sambanis A. Tissue engineering: From biology to biological substitutes. Tissue Eng. 1995;1:3-13.

Nerem RM. Tissue engineering: the hope, the hype, and the future. Tissue Engineering. 2006;12:1143–1150.

Newsome DA, Gross J, Hassell JR. Human corneal stroma contains three distinct collagens. Investigative Ophthalmology and Visual Science 1982;22(3):376-381.

Ng KW, Tham W, Lim TC, Werner Hutmacher D. Assimilating cell sheets and hybrid scaffolds for dermal tissue engineering. Journal of Biomedical Materials Reaseach Part A 2005;75:425-438.

Niemz MH. Laser-tissue interactions. Fundamentals and applications. 3rd Edition, Springer, 2007

Nieto-Aguilar R, Serrato D, Garzón I, Campos A, Alaminos M. Pluripotential differentiation capability of human adipose-derived stem cells in a novel fibrin–agarose scaffold. Journal of Biomaterials Applications 2011;25 (7):743–768.

Nimni ME. Collagen: molecular structure and biomaterial properties. In: Encyclopedic handbook of biomaterials and bioengineering. Part A: Materials. Wise DL, editor. New York: Marcel Dekker Inc., 1995; pp. 1229-1243.

Nishida K. Tissue engineering of the cornea. Cornea 2003;22:S28-S34.

Normand V, Lootens DL, Amici E, Plucknett KP, Aymard P. New insight into agarose gel mechanicalproperties. Biomacromolecules 2000;1:730–738.

Nyquist GW. Reology of the cornea: experimental techniques and results. Experimental Eye Research 1968;7:183–188.

Okazaki M, Yoshimura K, Suzuki Y, Harii K (). Effects of subepithelial fibroblasts on epithelial differentiation in human skin and oral mucosa: heterotypically recombined organotypic culture model. Plastic and Reconstructive Surgery 2003;112:784-792.

Orlando G, Wood KJ, De Coppi P, Baptista PM, Binder KW, Bitar KN, Breuer C, Burnett L et al. Regenerative medicine as applied to general surgery. Annals of Surgery 2012;255:867-880.

Orwin EJ, Borene ML, Hubel A. Biomechanical and optical characteristics of a corneal stromal equivalent. Journal of Biomechanical Engineering 2003;125:439–444.

Orwin EJ, Hubel A. In vitro culture characteristics of corneal epithelial, endothelial, and keratocyte cells in a native collagen matrix. Tissue Engineering 2000;6:307–319.

Palade GE. Mitochondria. Baltimore: University Park Press. Chap. An electron microscopy study of the mitochondrial structure, 1972; pp. 35–58.

Palmer GM, Ramanujam N. Monte Carlo-based inverse model for calculating tissue optical properties. Part I: Theory and validation on synthetic phantoms. Applied Optics 2006a;(45):1062-1071.

Palmer GM, Zhu C, Breslin TM , Xu F, Gilchrist KW, Ramanujam N. Monte Carlo-based inverse model for calculating tissue optical properties. Part II: Application to breast cancer diagnosis. Applied Optics 2006b;(45):1072-1078.

Patterson MS, Wilson BC, Wyman DR. The propagation of optical radiation in tissue I. Models of radiation transport and their application. Lasers in Medical Science 1991;6(2):155-168.

Pelaez D, Huang CY, Cheung HS. Cyclic compression maintains viability and induces chondrogenesis of human mesenchymal stem cells in fibrin gel scaffolds. Stem Cells and Development 2009;18:93–102.

Plass GN, Kattawar GW, Catchings FE. Matrix operator theory of radiative transfer. 1: Rayleigh scattering. Applied Optics 1973;12:314-329.

Podskochy A. Protective role of corneal epithelium against ultraviolet radiation damage. Acta Ophthalmologica Scandinavica 2004;82:714–717.

Porter SR, Leao JC. Review article: oral ulcers and its relevance to systemic disorders. Alimentary Pharmacology and Therapeutics 2005;21:295–306.

Prahl SA http://omlc.ogi.edu/software/iad/index.html 2012

Prahl SA, van Gemert MJC, Welch AJ. Determining the optical properties of turbid media by using the adding-doubling method. Applied Optics 1993;32:559-568.

Prahl SA, van Gemert MJC, Welch AJ. Determining the optical properties of turbid media by using the adding-doubling method. Applied Optics 1993;32(4): 559-568.

Prahl SA. Light Transport in Tissue. PhD thesis. University of Texas at Austin, 1988.

Prahl SA. The adding-doubling method. In: Welch AJ and van Gemert MJC (eds.) Optical-thermal response to laser irradiated tissue. New York: Plenum Press; 1995.

Preuss LE, Bolin FP, and Cain BW. Tissue as a medium for laser light transport-Implications for photoradiation therapy. Proceedings SPIE 1982; vol. 357, Lasers in Surgery and Medicine, M. Berns, Ed.: 77-84.

Proulx S, Uwamaliya JA, Carrier P, Deschanbeault A, Audet C, Giasson CJ, Guérin SL, Auger FA, Germain L. Reconstruction of a human cornea by the self-assembly approach of tissue engineering using the three native cell types. Molecular Vision 2010;16:2192-2201.

Qazi Y, Wong G, Monson B, Stringham J, Ambati BK. Corneal transparency:genesis, maintenance and dusfunction. Brain Research Bulletin 2010;81(2-3):198-210.

Radner W, Mallinger R. Interlacing of collagen lamellae in the midstroma of the human cornea. Cornea 2002;21:598–601.

Radner W, Zehetmayer M, Aufreiter R, Mallinger R. Interlacing and cross-angle distribution of collagen lamellae in the human cornea. Cornea 1998;17:537–543.

Rama P, Bonini S, Lambiase A, Golisano O, Paterna P, De Luca M et al. Autologous fibrin-cultured limbal stem cells permanently restore the corneal surface of patients with total limbal stem cell deficiency. Transplantation 2001; 72:1478–1485.

Rawe IM, Leonard DW, Meek KM, Zabel RW. X-ray diffraction and transmission electron microscopy of Morquio Syndrome Type A cornea: a structural analysis. Cornea 1997;16:369–376.

Reichl S, Muller-Goymann CC. The use of a porcine organotypic cornea construct for permeation studies from formulations containing befunolol hydrochloride. International Journal of Pharmaceutics 2003;250:191-201.

Rheinwald JG,Green H. Serial cultivation of strains of human epidermal keratinocytes: the formation of keratinizing colonies from single cells. Cell.1975;Nov;6(3):331-43.

Rodríguez IA, López-López MT, Oliveira AC, Sánchez-Quevedo MC, Campos A, Alaminos M, Durán JD. Rheological characterization of human fibrin and fibrin-agarose oral mucosa substitutes generated by tissue engineering. Tissue Engineering and Regenerative Medicine 2012;6(8):636-644.

Rogers JD, Çapoğlu IR, Backman V. Nonscalar elastic light scattering from continuous random media in the Born approximation. Optics Letters 2009;(34):1891-1893.

Rosso F, Marino G, Giordano A, Barbarisi M, Parmeggiani D, Barbarisi A. Smart materials as scaffolds for tissue engineering. Journal of Cellular Physiology 2005;203:465–470.

Ruberti J, Zieske J, Trinkaus-Randall V. Corneal tissue replacement. In: Lanza, R., Langer, R., Vacanti, J. (Eds.), Principles of Tissue Engineering. Elsevier/ Academic Press (Chapter 68) 2007.

Ruberti J, Klyce SD. Physiological system models of the cornea. In:Hung, G.K., Ciuffreda, K.J. (Eds.), Models of the Visual System. Kluwer Academic/Plenum Publishers, New York, 2002, pp. 3–55.

Ruberti JW, Zieske JD. Prelude to corneal tissue engineering – Gaining control of collagen organization. Progress in Retinal and Eye Research 2008;27:549-577.

Ruszymah BH. Autologous human fibrin as the biomaterial for tissue engineering. Medical Journal of Malaysia 2004;59(Suppl B):30-31.

Saintigny G, Bonnard M, Damour O, Collombel C. Reconstruction of epidermis on a chitosan cross-linked collagen-GAG lattice: effect of fibroblasts. Acta Dermato-Venereologica 1993;73:175-180.

Sakai S, Hashimoto I, Kawakami K. Synthesis of an agarose-gelatin conjugate for use as a tissue engineering scaffold. Journal of Bioscience and Bioengineering 2007;103(1):22-26.

Sakai S, Kawabata K, Ono T, Ijima H, Kawakami K. Development of mammalian cell-enclosing subsieve-size agarose capsules (<100 μm) for cell therapy. Biomaterials 2005;26:4786–4792.

Sanchez-Quevedo MC, Alaminos M, Capitan LM, Moreu G, Garzon I, Crespo PV, Campos A. Histological and histochemical evaluation of human oral mucosa constructs developed by tissue engineering. Histology and Histopathology 2007;22(6):631–640.

Sangwan VS, Ramamurthy B, Shah U, Garg P, Sridhar MS, Rao GN. Outcome of corneal transplant rejection, a 10 year study. Clinical and Experimental Ophthalmology 2005;33:623-627.

Sardar DK, Levy LB. Optical properties of whole blood. Lasers in Medical Science 1998;13(2):106-111.

Sardar DK, Swanland GY, Yow RM, Thomas RJ, Tsin ATC. Optical properties of ocular tissues in the near infrared region. Lasers in Medical Science 2007;22:46-52.

Sardar DK, Yust BG, Barrera F, Minum LC, Tsin ATC. Optical absorption and scattering of bovine cornea, lens and retina in the visible region. Lasers in Medical Science 2009;24:839-847.

Schermer A, Galvin S and Sun TT. Differentiation-related expression of a major 64K corneal keratin in vivo and in culture suggests limbal location of epithelial stem cells. Journal of Cell Biology 1986;103:49-62.

Schlenz I, Korak KJ, Kunstfeld R, Vinzenz K, Plenk HJ Holle J. The dermis-prelaminated scapula flap for reconstructions of the hard palate and the alveolar ridge: a clinical and histologic evaluation. Plastic and Reconstructive Surgery 2001;108:1519-1524.

Schmoekel HG, Weber FE, Schense JC, Gratz KW, Schawalder P, Hubbell JA. Bone repair with a form of BMP-2 engineered for incorporation into fibrin cell ingrowth matrices. Biotechnology and Bioengineering 2005;89:253–262.

Schneider AI, Mauer-Reif K, Graeve T. Constructing an in vitro cornea from cultures of the three specific corneal cell types. In Vitro Cellular and Developmental Biology-Animal 1999;35:515-526.

Schultze-Mosgau S, Lee BK, Ries J, Amann K, Wiltfang J. In vitro cultured autologous pre-confluent oral keratinocytes for experimental prefabrication of oral mucosa. International Journal of Oral and Maxillofacial Surgery. 2004;33:476-485.

Scott JE. Proteoglycan: collagen interactions and corneal ultrastructure. Biochemical Society Transactions. 1991;19:877–881.

Seliktar D, Black RA and Nerem RM. Use of a cyclic strain bioreactor to precondition a tissue-engineered blood vessel substitute. Annals of Biomedical Engineering. 1998;26(suppl.1):S.137.

Shin JE, Cornillion P, Salim L.. The effect of centrifugation on agar/sucrose gels. Food Hydrocolloids 2002;16:89–94

Sierra DH. Fibrin sealant adhesive systems: a review of their chemistry, material properties and clinical applications. Journal of Biomaterials Applications 1993;7:309-352.

Singh A, Karsten AE, Dam JS. 2008. Determination of optical properties of tissue and other bio-materials. Science real and relevant: 2nd CSIR Biennial Conference, CSIR International Convention Centre Pretoria, 17 & 18 November 2008, pp 8-15 - http://hdl.handle.net/10204/2631

Smelser GK. Corneal hydration. Comparative physiology of fish and mammals. Investigative Ophthalmology and Visual Science. 1962;1:11–32.

Smola H, Stark HJ, Thiekotter G, Mirancea N, Krieg T, Fusenig NE. Dynamics of basement membrane formation by keratinocyte-fibroblast interactions in organotypic skin culture. Experimental Cell Research 1998; 239:399-410.

Solter D, Gearhart J. Putting stem cells to work. Science. 1999;283:1468-1470.

Song J, Izumi K, Lanigan T and Feinberg SE. Development and characterization of a canine oral mucosa equivalent in a serum free environment. Journal of Biomedical Materials Research 2004;71: 143-53.

Star WM. Comparing the P3-approximation with diffusion theory and with Monte Carlo calculations of light propagation in a slab geometry. Proceedings of SPIE 1989; vol. IS5, Dosimetry of Laser Radiation in Medicine and Biology, G. J. Muller and D. H. Sliney, Eds.: 146- 154.

Steward AJ, Thorpe SD, Buckley CT, Wagner DR, Kelly DJ. Cell–matrix interactions regulate mesenchymal stem cell response to hydrostatic pressure. Acta Biomaterialia 2012;8:2153–2159.

Stolik S, Delgado JA, Pérez A, Anasagasti L. Measurement of the penetration depths of red and near infrared light in human “ex vivo” tissues, Journal of Photochemistry and Photobiology B: Biology. 2000;57(2–3): 90-93.

Sugrue SP, Zieske JD. ZO1 in corneal epithelium: association to the zonula occludens and adherens junctions. Experimental Eye Research 1997;64:11–20.

Sulieman M. An overview of the use of lasers in general dental practice: 2. Laser wavelengths, soft and hard tissue clinical applications. Dental Update Publication 2005;32:286-296.

Svaasand LO, Doiron DR, and Profio AE. Light distribution in tissue during photoradiation therapy. USC Instit. Phys. Imaging Sci., USC-IPIS 1981: 900-902.

Sweeney DF, Xie RZ, Evans MD, Vannas A, Tout SD, Griesser HJ, Johnson G, Steele JG.. A comparison of biological coatings for the promotion of corneal epithelialization of synthetic surface in vivo. Investigative Ophthalmology and Visual Science. 2003;44:3301–3309.

Sweeney DF, Xie RZ, O'Leary DJ, Vannas A, Odell R, Schindhelm K, Cheng HY, Steele JG, Holden BA. Nutritional requirements of the corneal epithelium and anterior stroma: clinical findings. Investigative Ophthalmology and Visual Science 1998;39:284–291.

Takeda K, Gosiewska A, Peterkofsky B. Similar, but not identical, modulation of expression of extracellular matrix components during in vitro and in vivo aging of human skin fibroblasts. Journal of Cellular Physiology 1992; 153:450-459.

Talbot M, Carrier P, Giasson CJ, Deschambeault A, Guerin SL, Auger FA, Bazin R, Germain L. Autologous transplantation of rabbit limbal epithelia cultured on fibrin gels for ocular surface reconstruction. Molecular Vision 2006;12:65–75.

Terán E, Méndez ER, Enríquez S, Iglesias-Prieto R. Multiple light scattering and absorption in reef-building corals. Applied. Optics 2010;49:5032-5042.

Toftet K, Keller GS and Blackwell KE. Ectopic hair growth after flap reconstruction of the head and neck. Archives of Facial Plastic Surgery. 2000;2:148-150.

Torbet J, Malbouyres M, Builles N, Justin V, Roulet M, Damour O, Oldberg A, Ruggiero F, Hulmes DJ Orthogonal scaffold of magnetically aligned collagen lamellae for corneal stroma reconstruction. Biomaterials. 2007;28:4268–4276.

Trentin D, Hall H, Wechsler S, Hubbell JA. Peptide-matrix-mediated gene transfer of an oxygen-insensitive hypoxia-inducible factor-1 variant for local induction of angiogenesis. Proceedings of the National Academy of Science USA 2006;103:2506–2511.

Troilo D, Wallman J. The regulation of eye growth and refractive state: an experimental study of emmetropization. Vision Research 1991;31:1237–1250.

Troilo D. Neonatal eye growth and emmetropisation – a literature review. Eye 1992;6(2):154–160.

Tuchin V. Tissue Optics: Light Scattering Methods and Instruments for Medical Diagnosis SPIE Press 2007

Ueda M, Ebata K, Kaneda T. *In Vitro* fabrication of bioartificial mucosa for reconstruction of oral mucosa: Basic research and clinical application. Annals of Plastic Surgery 1991;27:540-549.

Vacanti CA. History of tissue engineering and a glimpse into its future. Tissue Eng. 2006;12:1137–1142.

Van de Hulst HC. Multiple light scattering tables, formulas and applications. New York: Academic Press, 1980

Van de Hulst HC. Multiple Light Scattering Vol I Academic Press, 1980.

Van de Hulst. A new look at multiple scattering. Unnumbered mimeographed report, NASA Institute for Space Science, New York, 1963.

Van den Berg TJTP, Tan KEWP. Light transmittance of the human cornea from 320 to 700 nm for different ages. Vision Research 1994;34:1453–1456.

Van Gemert MJC, Welch AJ, Star WM, Motamedi M, Cheong WF. Tissue optics for a slab geometry in the diffusion approximation. Lasers in Medical Science 1987;2:295-302.

Ventura L, Sousa SJ, Messias AM, Bispo JM. System for measuring the transmission spectrum of _in vitro_ corneas. Physiological Measurement 2000;21:197–207.

Viola J, Bhavya L, Oren G. Emergence of Tissue Engineering as a Research Field.Abt Associates Inc. for National Science Foundation, Cambridge, MA.2003; 3–129.

Vogel G. Harnessing the power of stem cells. Science. 1999;283:1432-1434.

Wang H, Prendiville PL, McDonnell PJ, Chang WV. An ultrasonic technique for the measurement of the elastic moduli of human cornea. Journal of Biomechanics 1996;29(12):1633-1636.

Wang Z, Wang L, Zhang YT, Chen XD. Monte Carlo simulation of light propagation in human tissue. IEEE Bioinformatics and Biomedical Engineering ICBBE 2009. 3rd International Conference on, 978-1-4244-2902, 2009;1-4.

Weinberg CB, Bell E. A blood vessel model constructed from collagen and cultured vascular cells. Science. 1986;231:397-399.

Welch AJ, Gardner C. Optical and thermal response of tissue to laser radiation. In: Waynant RW (ed.) Lasers in medicine. Boca Raton: CRC Press; 2002. pp. 27-45.

West-Mays JA, Dwivedi DJ. The keratocyte: corneal stromal cell with variable repair phenotypes. International Journal of Biochemistry & Cell Biology. 2006;38:1625–1631.

Willerth SM, Arendas KJ, Gottlieb DI, Sakiyama-Elbert SE. Optimization of fibrin scaffolds for differentiation of murine embryonic stem cells into neural lineage cells. Biomaterials 2006;27:5990–6003.

Willerth SM, Faxel TE, Gottlieb DI, Sakiyama-Elbert SE. The effects of soluble growth factors on embryonic stem cell differentiation inside of fibrin scaffolds. Stem Cells 2007;25:2235–2244.

Wilson BC, Patterson MS, Burns DM. Effect of photosensitizer concentration in tissue on the penetration depth of photoactivating light," Lasers in Medical Science 1986; 1:235-244.

Wilson BC, Patterson MS. The physics, biophysics and technology of photodynamic therapy Physics in Medicine and Biology 2008;. 53:R61–R109.

Xu YG, Xu TS, Huang C, Feng Y, Li Y, Wang W. Development of a rabbit corneal equivalent using an acellular corneal matrix of a porcine substrate. Molecular Vision 2008;14:2180-2189.

Yamada Y, Boo JS, Ozawa R, Nagasaka T, Okazaki Y, Hata K, Ueda M. Bone regeneration following injection of mesenchymal stem cells and fibrin glue with a biodegradable scaffold. Journal of Craniomaxillofacial Surgery 2003;31: 27–33.

Yang H, Iwata H, Shimizu H, Takagi T, Tsuji T, Ito F. Comparative studies of in vitro and in vivo function of three different shaped bioartificial pancreases made of agarose hydrogel. Biomaterials 1994;15:113–118.

Yang S, Leong KF, Du Z, Chua CK. The design of scaffolds for use in tissue engineering.Part I. Traditional factors. Tissue Eng. 2001;7(6): 679–689.

Ye Q, Zund P Benedikt S, Jockenhoevel S, Hoerstrup SP, Sakyama S, Hubbell JA, Turina M. Fibrin gel as a three dimensional matrix in cardiovascular tissue engineering. European Journal of Cardio-Thoracic Surgery 2000;17:587–591.

Yeung T, Georges PC, Flanagan LA, Marg B, Ortiz M, Funaki M, Zahir N, Ming W, Weaver V, Janmey PA. Effects of substrate stiffness on cell morphology, cytoskeletal structure, and adhesion. Cell Motility and the Cytoskeleton 2005;60:24–34.

Yoon G, Prahl SA, Welch AJ. Accuracies of the diffusion approximation and its similarity relations for laser irradiated biological media. Applied Optics 1989; 28: 2250-2255.

Yoshizawa M, Feinberg SE, Marcelo CL, Elner VM. Ex vivo produced human conjunctiva and oral mucosa equivalents grown in a serum-free culture system. Journal of Oral and Maxillofacial Surgery 2004;62:980-988.

Yust BG, Mimun LC, Sardar DK. Optical absorption and scattering of bovine cornea, lens, and retina in the near-infrared región. Lasers in Medical Science 2012;27:413-422.

Zacchi V, Soranzo C, Cortivo R, Radice M, Brun P, Abatangelo G. In vitro engineering of human skin-like tissue. Journal of Biomedical Materials Research1998; 40:187-194.

Zerbe BL, Belin MW, Ciolino J. Results from the multicentre Boston type 1 keratoprothesis study. Ophthalmology. 2006;113 (10):1779.e1-7.

Zieske JD, Mason VS, Wasson ME, Meunier SF, Nolte CJ, Fukai N, Olsen BR and Parenteau NL. Basement membrane assembly and differentiation of cultures cells: importance of culture environment and endothelial cell interaction. Experimental Cell Research 1994;214:621-633.

9. PUBLICATIONS

PUBLICATIONS RELATED TO THIS PhD THESIS:

Ionescu AM, Cardona JC, Alaminos M, García-López Duran JD, González-Andrades M, Ghinea R, Campos A, Hita E, Pérez MM. *Investigating a novel nanostuctured fibrin-agarose biomaterial for human cornea tissue engineering: rheological properties* Journal of Mechanical Behavior of Biomedical Materials 2011;4:1963-1973.

Cardona JC, ***Ionescu AM***, Gómez-Sotomayor R, González-Andrades M, Campos A, Alaminos M, Pérez MM. *Transparency in a fibrin and fibrin-agarose corneal-stroma substitute generated by tissue engineering*. Cornea 2011;30:1428-1435.

González-Andrades M, Cardona JC, ***Ionescu AM***, Campos A, Pérez MM, Alaminos M. *Generation of bioengineered corneas with decellularized xenografts and human keratocytes*. Investigative Ophthalmology and Visual Science 2011;52:215-222.

Ionescu AM, Cardona JC, González-Andrades, Alaminos M, Campos A, Hita E, Pérez MM. *UV Absorbance of a bioengineered corneal stroma substitute in the 240-400nm range*. Cornea 2010;29:895-898.

Gonzalez-Andrades M, Garzon I, Cardona JC, ***Ionescu AM***, Pérez-Roca F, Campos A, Alaminos M. *New approaches to corneal regeneration based on fibrin-agarose scaffolds and acellular xenografts.*: Abstract booklet of the International Symposium on Ocular Pharmacology and Therapeutics 2011;pp.91.

Ionescu AM, Cardona JC, Ghinea R, Durán JD, Alaminos M, Pérez MM. *Nanostructured fibrin-agarose corneal construct: rheological properties for potential clinical application*. Histology and Histopathology 2011;26(1):301.

Ghinea R, Cardona JC, Pozo AM, ***Ionescu AM***, Rubiño AM, Alaminos M, Pérez MM. *Contrast transfer function for evaluating the optical quality of bioengineered human corneal stroma.* Histology and Histopathology 2011;26(1):304.

Pérez MM, ***Ionescu AM***, Cardona JC, Ghinea R, Campos A, Hita E, Alaminos M. *Influence on transparency of a nanostructuring technique for the generation of artificial corneas*. Histology and Histopathology 2011;26(1):309.

Cardona JC, Pérez MM, ***Ionescu AM***, Díaz C, Muñoz-Avila JI, Alaminos M, Campos A. *Optical quality control of corneas developed by tissue engineering: retinal image quality*. Tissue Engineering and Regenerative Medicine 2009;6(12):S112.

Ionescu AM, Cardona JC, Pérez Ocón F, González-Andrades M, Alaminos M, Campos A, Pérez MM. *Refractive index of the fibrin and fibrin-agarose corneal substitutes*. Histology and Histopathology 2009;24(S1):S94-S95.

Ionescu AM, Cardona JC, Ghinea R, González-Andrades M, Alaminos M, Pérez MM. *UV Absorbance of the corneal stroma constructs in the 240 to 400-nm range*. Histology and Histopathology 2009;24(S1):S109.

Cardona JC, ***Ionescu AM***, Ghinea R, Muñoz-Ávila JI, González-Andrades M, Alaminos M, Pérez MM. *Optical properties of nanostructured corneal stroma constructs as determined by the adding-doubling method*. Histology and Histopathology 2009;24(S1):S110.

Gómez-Sotomayor R, Alaminos M, Pérez MM, ***Ionescu AM***, Cardona JC, Campos A. *Influence of thickness on the transmittance in fibrin-agarose corneal constructs*. Tissue Engineering Part A 2008;14(5):869.

Gómez-Sotomayor R, Pérez MM, Muñoz-Ávila JI, Alaminos M, ***Ionescu AM***, Cardona JC, Campos A. *Optical characterization of fibrin and fibrin-agarose corneal constructs: the coefficients of absorption, scattering and extinction*. Tissue Engineering Part A 2008;14(5): 891-892.

PUBLICATIONS RELATED TO OTHER RESEARCH LINES

Pecho OE, Ghinea R, ***Ionescu AM***, Cardona JD, Paravina RD, Pérez MD. *Colour and translucency of zirconia ceramics, human dentine and bovine dentine* .Journal of Dentistry 2012;40(S2):e34-e40.

Pérez MM, Ghinea R, Herrera LJ, ***Ionescu AM***, Pomares H, Pulgar R, Paravina RD. *Dental Ceramics: A CIEDE2000 acceptability thresholds for lightness, croma and hue differences*. Journal of Dentistry 2011;39(3):e37-e44.

Pérez MM, Ghinea R, ***Ionescu AM***, Cardona JC. *Changes in scattering and absorption during curing of dental resin composites: silorane and nanocomposite*. Proceedings of SPIE 2011;8001:321-326.

Ghinea R, Cardona JC, ***Ionescu AM***, Pérez MM, Herrera LJ. *Using Takagi Sugeno-Kang approximation fuzzy logic for evaluating the performance of color difference formulas in dentistry*. Proceedings of the 11th Conference of ISDA 2011;pp.247-252.

Pecho OE, Ghinea R, ***Ionescu AM***, González-López S, Pérez MM. *Optical characterization in different bovine dentin zones*. Histology and Histopathology 2011;26(1):306.

Ghinea R, Ugarte-Alvan L, ***Ionescu AM***, Cardona JC, Perez MM. *Optical characterization of dental- resin composites based on image analysis*. Proceedings of IADR General Session 2010;pp.97.

Pecho OE, Ghinea R, ***Ionescu AM,*** González-López S, Perez MM. *Optical properties in bovine dentin*. Proceedings of IADR General Session 2010;pp.214.